

# **Numerical Study on Halting Crack Growth using Crack Stop Hole and Carbon Fibre Reinforced Polymer (CFRP) Laminates**

Kolanu Shashidar Reddy

A Thesis Submitted to  
Indian Institute of Technology Hyderabad  
In Partial Fulfilment of the Requirements for  
The Degree of Master of Technology



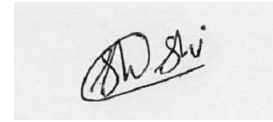
भारतीय प्रौद्योगिकी संस्थान हैदराबाद  
Indian Institute of Technology Hyderabad

Department of Civil Engineering

July, 2014

## Declaration

I declare that this written submission represents my ideas in my own words, and where others' ideas or words have been included, I have adequately cited and adhered to all principles of academic honesty and integrity and have not misrepresented or fabricated or falsified any idea/data/fact/source in my submission. I understand that any violation of the above will be a cause for disciplinary action by the Institute and can also evoke penal action from the sources that have thus not been properly cited, or from whom proper permission has not been taken when needed.



---

(Signature)

---

(Kolanu Shashidar Reddy)

---

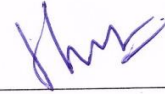
(CE13M1004)

This thesis entitled “**Numerical Study on Halting Crack Growth using Crack-Stop Hole and Carbon Fibre Reinforced Polymer (CFRP) Laminate**” by Kolanu Shashidar Reddy is approved for the degree of Master of Technology from IIT Hyderabad.



Dr. Mahendrakumar Madhavan

Adviser



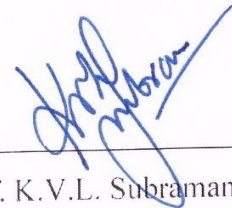
Dr. S. Suriya Prakash

Internal Examiner



Dr. Viswanath Chinthapenta

External Examiner



Prof. K.V.L. Subramaniam

Chairman

## **Acknowledgements**

I would like to thank Ministry of Human resources Development (MHRD), Government of India for providing financial support during my stay at IIT, Hyderabad. During last one year time, the guidance and assistance given by my thesis advisor Dr. Mahendrakumar Madhavan is highly acknowledged. I would like to thank Prof. K.V.L. Subramaniam, Dr. S.SuriyaPrakash and Dr. Viswanath Chinthapenta for reviewing the progress of my work. I am thankful for computational facilities provided by the department of civil engineering; IIT Hyderabad. I would like to thank my friends Mr. Jaswanthsai, Mr. Vinod, Mr. Akhil and Mr. Siva Ganesh for their time and valuable suggestions. I am thankful to my family, who helped me to pursue my Masters. I would like to thank all my friends for their support during my stay at IIT Hyderabad.

## Abstract

It is well known that drilling a hole ahead of crack tip is one of the most common techniques to prevent crack propagation in structures subjected to fatigue load. An adequate size crack stop hole is necessary to convert a sharp crack into a blunt notch there by preventing crack propagation. However, fatigue cracks typically occur at locations where drilling a crack-stop hole of required dimensions may not be possible due to geometrical constraints. In such situations, the crack may initiate again from the hole within its service life. Hence, there is a need to strengthen undersized crack-stop holes. In the present study, a combination of crack-stop hole and carbon fiber reinforced polymer (CFRP) overlays under static loads are studied numerically using finite element analysis (FEA) to evaluate its potential as a viable repair technique. A steel plate with an initial central crack subjected to static tensile loading is considered. A hole is modelled ahead of a crack tip and CFRP patches are applied on either side of the crack. The numerical analysis is performed using general purpose FEA ANSYS to evaluate the stress intensity factor at notch tip (NSIF). The material behaviour is assumed to be elastic in case of linear analysis and as a multi linear isotropic hardening material type for nonlinear analysis.

Chapter 1 deals with the effect of crack stop hole and symmetrically bonded CFRP patch in halting a crack propagation in mode-I. A comparison between CSIF and NSIF is carried out in Chapter 1. The parameters that are varied in study are crack length, crack stop hole radius, load and CFRP layers. The results from linear analysis are used to compare Crack Stress Intensity Factor (CSIF,  $K_I / \sqrt{\rho}$ ) and Notch Stress Intensity Factor (NSIF,  $K_I / \rho^\alpha$ ). The results indicate the need to include the stress gradient  $\alpha$  in arriving at adequate crack stop hole radius for both bare steel and CFRP patched specimens. Nonlinear FEA, which takes into account the post yield material behaviour, is carried out to propose a modified NSIF expression by including a Reduction Factor (RF) that is a function of the ratio of the radius of crack stop hole to crack length ( $\rho / 2a$ ), the ratio of stiffness of CFRP to steel (SR) and the ratio of applied stress to yield stress ( $\sigma_{applied} / \sigma_{ys}$ ). A numerical example is provided to demonstrate the applicability of the proposed equation.

Chapter 2 deals with the effect of crack stop hole and asymmetrically bonded CFRP patch in halting a crack propagation in mode-I. The parameters that are varied in study are crack length, crack stop hole radius, load and CFRP layers. The patch is applied only on one side, this done to simulate condition where there is no access to apply patch on other side. This results in bending due to eccentricity in loading caused due to difference in stiffness ratios of steel and CFRP. Nonlinear FEA, which takes into account the post yield material behaviour, is carried out to propose a modified NSIF expression by including a Reduction Factor (RF) that is a function of the crack stop hole radius ( $\rho$ ), crack length ( $2a$ ), the ratio of stiffness of CFRP to steel (SR) and applied stress ( $\sigma_{applied}$ ). A numerical example is provided to demonstrate the applicability of the proposed equation.

Chapter 3 deals with the effect of crack stop hole and CFRP patch in halting a crack propagation when it is inclined with respect to loading. The parameters that are varied in study are crack inclination, crack stop hole radius, load and CFRP layers. The effect of patch when it bonded symmetrically and asymmetrically is also studied in this chapter. Nonlinear FEA, which takes into account the post yield material behaviour, is carried out to propose a modified NSIF expression by including a Reduction Factor (RF) that is a function of the crack stop hole radius ( $\rho$ ), crack inclination ( $2a$ ), the ratio of stiffness of CFRP to steel (SR) and applied stress ( $\sigma_{applied}$ ). A numerical example is provided to demonstrate the applicability of the proposed equation.

## Nomenclature

CFRP	Carbon fibre reinforced polymer
CSIF	Crack stress intensity factor
$E_{CFRP}$	Young's modulus of CFRP
$E_{Steel}$	Young's modulus of steel
NSIF	Notch stress intensity factor
RF	Reduction factor
SR	Stiffness ratio
$X_c$	Characteristic distance up to which stress is constant a head of crack stop hole
$\alpha$	Gradient of stress distribution a head of crack stop hole
$\rho$	Crack stop hole radii
$\sigma_{ys}$	Yield strength of steel
$\sigma_{y \max}$	Maximum stress in Y-direction
$\sigma_{\text{applied}}$	Applied stress
$\sigma_{yy}$	Stress in Y-direction
$2a$	Crack length

# Contents

Declaration.....	ii
Approval Sheet .....	iii
Acknowledgements.....	iv
Abstract.....	v
<b>Nomenclature .....</b>	<b>vii</b>
<b>1 Numerical Study on Halting Crack growth using Crack Stop Hole and symmetrically bonded CFRP Laminate .....</b>	<b>1</b>
1.1 Introduction.....	1
1.2 Background.....	2
1.2.1 Crack stop hole expression.....	3
1.2.2 CFRP and steel application .....	3
1.3 Geometry and FE modelling.....	5
1.3.1 Validation of FE model .....	6
1.4 Results and discussion .....	6
1.4.1 CSIF calculation.....	6
1.4.2 NSIF calculation.....	7
1.4.3 Effect of SR and $\rho$ on $K_I/\rho^\alpha$ .....	8
1.4.4 Reduction factor .....	9
1.4.5 Effect of SR and load on peel stress.....	10
1.4.6 Numerical example and verification using FEA .....	10
1.5 Conclusions.....	11
References.....	12
Figures.....	14-26
Tables.....	27-34
<b>2 Numerical Study on Halting Crack growth using Crack Stop Hole and asymmetrically bonded CFRP Patch .....</b>	<b>35</b>
2.1 Introduction.....	35
2.2 Geometry and FE modelling.....	37
2.3 Results and discussion .....	38
2.3.1 NSIF calculation.....	38
2.3.2 Effect of SR and $\rho$ on $K_I/\rho^\alpha$ .....	39



2.3.3	Reduction factor .....	40
2.3.4	Effect of SR and load on peel stress.....	41
2.4	Numerical examples illustrating the usage of proposed equation.....	42
2.4.1	Example 1.....	42
2.4.2	Example 2.....	43
2.5	Conclusions.....	44
	References .....	45
	Figures.....	48-61
	Tables .....	62-68
<b>3</b>	<b>Numerical Study on Halting Inclined Crack growth using Crack Stop Hole and CFRP Patch .....</b>	<b>69</b>
3.1	Introduction.....	69
3.2	Geometry and FE modelling.....	72
3.3	Results and discussion .....	73
3.3.1	NSIF calculation.....	73
3.3.2	Effect of SR and $\rho$ on $K_I/\rho^\alpha$ in case of symmetrically repaired panel .....	74
3.3.3	Effect of SR and load on peel stress in case of symmetrically repaired panel ..	74
3.3.4	Effect of SR and $\rho$ on $K_I/\rho^\alpha$ in case of asymmetrically repaired panel ....	74
3.3.5	Effect of SR and load on peel stress in case of asymmetrically repaired panel	76
3.3.6	Comparison of $K_I/\rho^\alpha$ and peel stress for different crack inclinations .....	76
3.3.7	Reduction factor .....	77
3.4	Numerical examples illustrating the usage of proposed equation.....	78
3.4.1	Example 1.....	78
3.4.2	Example 2.....	79
3.5	Conclusions.....	80
	References .....	81
	Figures.....	83-116
	Tables .....	117-128
<b>4</b>	<b>Further Study .....</b>	<b>129</b>

# CHAPTER 1

## Numerical Study on Halting Crack Growth using Crack Stop Hole and Symmetrically Bonded CFRP Laminate

### 1.1 Introduction

Steel bridge girders are subjected to fatigue loading due to continuous vehicular traffic. The girders that are not designed as per fatigue detailing may develop cracks due to fatigue load. In most cases, cracks initiate at potential weld sites, where there is a material discontinuity (see Fig.1). If the crack continues to grow and is left unrepaired for a long time, it may lead to catastrophic failure, which is undesirable. Hence, cracks need to be arrested by using appropriate retrofitting techniques. The success of any retrofitting technique depends on identifying the location of the crack and the nature of loading. These retrofitting techniques are classified broadly into two groups [1]: (a) Local retrofitting techniques which include crack stop holes, peening, gas tungsten arc (GTA) welding that modify the local stress state and (b) Global retrofitting techniques that include strengthening with steel plate or composite laminates. Experimental studies by Fisher et al. [2] indicate that of the repair methods discussed above, drilling a crack stop hole ahead of a crack tip is one of the effective methods to arrest the crack propagation. The basic principle behind the use of crack stop hole is to convert the sharp crack into a blunt notch thereby converting it into a problem of evaluating Notch Stress Intensity Factor (NSIF) than the Crack Stress Intensity Factor (CSIF). A comparison between CSIF and NSIF is shown in Table 1.

The success of using a crack-stop hole as a means to arrest crack growth depends on the length of the crack, type of the loading and location of the crack. In some cases, it is not possible to drill a hole with a radius as obtained from analytical expressions, due to lack of space in complex structural steel connections. In such situations, a practicing structural engineer may be required to drill an undersized crack stop hole (less than design diameter) as a temporary measure. This approach may lead to re-initiation of crack stop hole after few loading cycles. Crack stop hole is fully effective only if the radius of the hole satisfy design requirements [3]. In addition, crack stop hole technique is not feasible, if the crack propagates to a substantial size. In such cases a

global retrofitting technique such as external strengthening needs to be adopted. The usual practice was to weld an additional plate on the top of the damaged portions. However, the literature indicates that in most cases, the cracks emanated from the edges of the attached plate. In addition, these plates were causing an increase in dead load which was undesirable. Recently, carbon fiber reinforced polymer (CFRP) patches have been used to replace these steel plates for external strengthening owing to its better properties such as light weight and better fatigue performance [4]. These techniques are more efficient and are applied in strengthening old bridges. In the current study, both these techniques i.e. drilling holes and application of adhesive patches are studied together as repair techniques. The literature indicates that limited research has been conducted on the combined behavior of crack stop hole and CFRP as a repair technique for retarding crack growth and is important to develop one [1].

## 1.2 Background

Prior to studying the combined behavior of crack stop hole and CFRP reinforced steel plates, it is essential to study the individual behavior of cracked steel plates and crack stop hole without CFRP. As discussed previously, the objective of drilling a crack stop hole is to convert a sharp crack to a blunt crack. Unlike sharp cracks where the crack initiation life ( $N_i$ ) is negligible, blunt cracks have significant  $N_i$  and cannot be neglected. In this study, Linear Elastic Fracture Mechanics (LEFM) approach is adopted to explain the crack initiation from blunt cracks. Experimental studies carried out by Barsom and Nicol [5] and Jack and Price [6] express the crack initiation life ( $N_i$ ) of the blunt crack, as a function of ratio of stress intensity factor ( $K_I$ ) to the square root of notch radius ( $\rho$ ) as shown in Eq. 1. The relationship between two terms,  $K_I / \sqrt{\rho}$  and maximum stress at the edge of the hole ( $\sigma_{y \max}$ ) was given by Creagor and Paris [7] using LEFM concepts that is obtained by substituting  $r=\rho/2$  and  $\Theta=0$  in Eq. 3. The expressions (Eqs.2, 3 & 4) represent the stress state at the edge of the notch obtained by shifting the origin to a distance half of the radius ( $\rho/2$ ) behind the crack front as shown in Table 1, and is accurate when radius of the hole is small compared to the length of the crack ( $\rho \ll a$ ).

$$\sigma_{y \max} = \frac{2K_I}{\sqrt{\pi\rho}} \quad (1)$$

$$\sigma_x = \frac{K_I}{\sqrt{2\pi r}} \cos \frac{\theta}{2} \left( 1 - \sin \frac{\theta}{2} \sin \frac{3\theta}{2} \right) - \frac{K_I}{\sqrt{2\pi r}} \frac{\rho}{2r} \cos \frac{3\theta}{2} \quad (2)$$

$$\sigma_y = \frac{K_I}{\sqrt{2\pi r}} \cos \frac{\theta}{2} \left( 1 - \sin \frac{\theta}{2} \sin \frac{3\theta}{2} \right) + \frac{K_I}{\sqrt{2\pi r}} \frac{\rho}{2r} \cos \frac{3\theta}{2} \quad (3)$$

$$\tau_{xy} = \frac{K_I}{\sqrt{2\pi r}} \cos \frac{\theta}{2} \left( \sin \frac{\theta}{2} \sin \frac{3\theta}{2} \right) - \frac{K_I}{\sqrt{2\pi r}} \frac{\rho}{2r} \sin \frac{3\theta}{2} \quad (4)$$

### 1.2.1 Crack stop hole expressions

There are two major crack stop hole expressions that exist in the literature. One is by Barsom [8] and the other is by Fisher et al. [2]. Both researchers adopted LEFM approach to explain their experimental studies on notches with different acuities. However, these two studies are different in terms of scale of testing and grade of steels used. Barsom [8] studied the notch effects on the fatigue crack initiation behavior of different grade steels from 250 MPa (36 ksi) to 800 MPa (110 ksi) were studied at a stress ratio of 0.1 in three point bending. Test results indicate that the fatigue crack initiation threshold ( $K_I/\sqrt{\rho}$ ) increases with the increase in grade of steel. The same test carried out at different stress ratios -1.0 and 0.5 indicate that the fatigue crack initiation threshold ( $K_I/\sqrt{\rho}$ ) is independent of stress ratio and is given as:

$$\frac{K_I}{\sqrt{\rho}} = 10\sqrt{\sigma_{ys}} \quad (5)$$

Equation 5 is unit sensitive and all units must be in ksi and inches.

Fisher et al. [2] studied several retrofitting techniques and compared them experimentally. These retrofitting techniques include peening, gas tungsten arc (GTA) welding and crack stop holes. A comparison was made between different retrofitting techniques in terms of increase in fatigue life. For long cracks, a crack stop hole of 13 mm (1/2 inch) and 25 mm (1 inch) diameter was drilled at the crack tips. After drilling the crack stop hole, the radius of crack tip becomes the radius of the hole. Based on experimental study, a threshold ratio of  $K_I/\sqrt{\rho}$  was proposed (Eq. 6). Tests were conducted at different stress ranges from 41.2 MPa (3 ksi) to 103.4 MPa (12 ksi).

$$\frac{K_I}{\sqrt{\rho}} = 4\sqrt{\sigma_{ys}} \quad (6)$$

Equation 6 is also unit sensitive and all units must be in ksi and inches.

### 1.2.2 CFRP and steel applications

The use of CFRP as a repair material was initially used in the aerospace industry for arresting the crack growth in fastener holes due to fatigue load in addition to static cold working. Heller et al. [9] carried out an experimental study to evaluate the combined effect of adhesive patches and

static cold working. The experimental program concluded that strengthening with bonded adhesives in addition to bonded sleeve increases fatigue life twice. Jones and Civjan [10] carried out an experimental program to find the effect of different parameters ranging from surface preparation, development length, single sided, double sided patch applications on the efficiency of the patch system. It was concluded that application of CFRP overlays is beneficial both as a preventive and as a repair technique and were effective in arresting the cracks that originated from the notches. Tavakkolizadeh and Saadatmanesh [11] conducted experiments on notched steel beams repaired with CFRP under four point bending load. CFRP patches were applied to tension flanges. The results showed that the CFRP patch not only tends to extend the fatigue life of the component but also decreases the crack growth.

Achour et al. [12] performed finite element analysis to understand the effect of composite patches in retarding the crack from semicircular notches. The stress concentration factor was decreased by 30% due to the patch. The studies also indicate that the properties of patch system such as patch thickness and adhesive properties need to be optimized for the effectiveness of the repair. A review of work done in strengthening of steel structures with composites was presented in [13]. This study indicated that bond behavior, bond strength and fatigue crack propagation modeling are important study areas in this repair technique. Liu et al. [14] proposed an analytical model to predict the fatigue crack propagation for cracks emanating from CFRP strengthened circular notches. Alemдар et al. [15] conducted a detailed experimental program combined with finite element study to determine the influence of different variables like stiffness ratio, Young's modulus of composite, thickness of adhesive and number of layers. It was concluded that stiffness ratio greater than one (CFRP stiffer than parent material steel) leads to diminishing results. Hmidan et al. [16] has conducted a numerical study by varying different parameters like flange to web area ratios, crack depth to height ratios, CFRP to steel area ratios, CFRP to steel modular ratios and CFRP bond widths. The results were used to propose a correction factor for the SIF ( $K_I$ ) of CFRP strengthened steel girders.

From the existing literature it can be observed that most of the research work is focused on the use of CFRP alone as a repair technique except Jones and Civjan [10] and Achour et al. [12] who have induced a notch at the crack tip in addition to adhesive patch. Since the potential for using crack stop hole combined with CFRP as an effective technique to prevent crack propagation is

large, there is a need to study the same. In the present work, a numerical study using FEA is considered to study this combined action.

### 1.3 Geometry and FE modelling

In this research work, both linear and nonlinear finite element analysis (FEA) is carried out. Linear elastic analysis is necessary to evaluate CSIF since the expression for crack stop hole present in the literature in terms of CSIF, is based on linear elastic assumption. However, this assumption is valid in most cases due to the fact that bridge girders are typically loaded well below their yield strength. Nonlinear FEA is necessary as it considers the post yield material behavior of steel which in the present study is Multi Linear Isotropic hardening (MISO) and its stress strain values are given in Table 2. FEA is conducted in this study using ANSYS 12.0 software. The components (i.e. steel plate, adhesive, and CFRP patch) were modeled using Solid 186 element that has mid side nodes and perform better in stress singularity regions. The connection between adhesive and CFRP patch and adhesive and steel plate are modeled using bonded contact. In bonded contact, contacting surfaces are assumed to be glued together throughout the analysis by using multi point constraint (MPC) algorithm.

The CFRP laminate is modeled as an orthotropic material whose material properties (Table 3) are taken from [17]. In this study, the fibers are oriented in the direction of load to achieve maximum capacity. Static tensile loading is applied for all the analysis. The magnitudes of loads applied are 41.2 MPa (6 ksi), 62 MPa (9 ksi), 82.7 MPa (12 ksi), 103.4 MPa (15 ksi) which are reported as loads that the bridge girders are generally subjected to [2]. Incremental meshing is employed around the hole to capture the sharp stress gradient because the value of stress at the edge of the hole is sensitive to the element size. The number of elements used around the hole is 6 elements in the thickness direction, 20 elements in radial direction and 48 elements in angular direction [18]. Figure 2 shows the typical central crack that is used in FEA along with a crack stop hole and CFRP, the dimensions of which are given in Table 4. A typical FE mesh is shown in Fig. 3a and circular meshing around crack stop hole is shown in Fig. 3b. The parameters studied include the ratio of the radius of crack stop hole to crack length ( $\rho/2a$ ), the ratio of stiffness of CFRP to steel (SR) and the ratio of applied load to yield stress ( $\sigma_{applied}/\sigma_{ys}$ ). A total of 1008 nonlinear FEA analyses were carried out by varying different parameters as shown in the Table 5. These analyses was carried out to understand the effect of crack length, crack stop hole radius and the number of patches on the stress at the edge of the hole.

### 1.3.1 Validation of FE model

The finite element model that is developed in this work is validated by comparing the SIF ( $K_I$ ) value obtained from ANSYS and analytical expression (Eq. 7) for a bare steel specimen having 25.4 mm (1 inch) crack length. The SIF ( $K_I$ ) from ANSYS is obtained by evaluating the J-integral, which is obtained using the domain integral method in ANSYS software (2012). The relationship between SIF ( $K_I$ ) and J-integral is given in Eq. 8. The comparison between the values obtained from ANSYS and analytical expression is shown in Fig. 4. From the figure it can be observed that the results obtained from ANSYS is in close comparison with the results obtained from analytical expression with an average error of approximately 3%.

$$K_I = \sigma_{applied} * \sqrt{\pi a} \quad (7)$$

$$K_I = \sqrt{E * J} \quad (8)$$

## 1.4 Results and discussion

This numerical study is aimed at studying the combined action of crack stop hole and the CFRP patch in arriving at the appropriate crack stop hole radius when subjected to static tensile load. Prior to the combined effect, the effect of bare steel specimen was studied to understand the effect of hole radius in crack retardation. It was observed that the existing equations for crack stress intensity factor was un-conservative due to the fact that it does not take into account the characteristic distance ( $X_c$ ) from the hole edge up to which the stress remains constant and the linear decrease in stress at a gradient ( $\alpha$ ) thereafter. To overcome the above problem, the stress intensity factor was calculated using NSIF which includes the effect of  $X_c$  and  $\alpha$ . As will be described in the next sections, it was observed that the use of NSIF resulted in a larger radius hole compared to CSIF which indicates that the use of CSIF results in a un-conservative prediction. Henceforth, the stress analysis carried out for the combined action of crack stop hole and CFRP patch were based on NSIF. The resulting stress reduction factors were curve fit using simple regression models to arrive at a reduction equation in terms of  $\rho/2a$ , SR and  $(\sigma_{applied}/\sigma_{ys})$ . The applicability of the proposed equation is demonstrated using a design example. In addition to NSIF, the variation of peel stress at CFRP edge is also studied.

### 1.4.1 CSIF calculation

Prior to proceeding with NSIF, a study was carried out to determine the crack stop hole diameter using Eq. 9 which is based on CSIF.

$$\frac{K_I}{\sqrt{\rho}} = \frac{\sigma_{y \max} * \sqrt{\pi}}{2} \quad (9)$$

The value of maximum stress at the edge of the hole in the loaded direction ( $\sigma_{y \max}$ ) is obtained from FEA. According to the threshold radius (Eq. 5) by Barsom [8] for given loading conditions and crack length, a crack stop hole of 1 mm (0.039 inch) is necessary to prevent crack growth (see Fig. 5), which can be considered as equivalent to sharp crack due to very small radius with respect to crack initiation life. Therefore, as per the threshold limit given by Barsom [8] the crack does not propagate for an applied stress of 41.2 MPa and for a crack length of 50.8 mm (2 inch) (kept constant for all values of radius). The required radius of crack stop hole is so small that it obviates the need to drill a crack stop hole. This might be due to the use of a constant exponent of 0.5 for  $\rho$  in the existing formulation (Eq. 9) irrespective of hole dimension and may lead to un-conservative prediction. To determine the accurate stress intensity value and stress gradient, NSIF is calculated.

#### 1.4.2 NSIF calculation

The literature review indicates that the crack initiation life ( $N_i$ ) of a notch is typically expressed as a function of  $K_I / \sqrt{\rho}$  which is based on LEFM. In LEFM frame work, the stress gradient is expressed as a function of  $1 / \sqrt{r}$  singularity which indicates that when the radius approaches zero, it behaves like a sharp crack. However, the LEFM assumption is not valid if loading, crack geometry and the specimen thickness leads to yielding at notch tip. In the present study, initially NSIF based on linear FEA is calculated to compare with CSIF. The results indicate that CSIF is un-conservative than NSIF. Later, nonlinear FEA is carried out to propose the modified NSIF expression. The output from FEA is used to determine  $X_c$  and  $\alpha$  needed to evaluate NSIF using Eq. 10, which is given by Boukharouba et al. [19].

$$K_\rho = \sigma_{yy}(X_c) * \sqrt{2\pi} \left( X_c + \frac{\rho}{2} \right)^\alpha \quad (10)$$

where,  $\sigma_{yy}$ = Stress at characteristic distance  $X_c$ ,  $\rho$ = Radius of the notch and  $\alpha$ = Stress gradient. Figure 6 shows a typical variation in stress ahead of a crack stop hole in a log-log plot for one particular case [2 inch crack length, 82.7 MPa loading, 9.525 mm (3/8 inch) hole radius, without CFRP].



It is found that the crack stop hole radius calculation based on NSIF approach gives a radius value 10 mm (Fig. 5) which is much greater than 1 mm obtained from  $K_I/\sqrt{\rho}$  for a load value of 41.2 MPa. To further demonstrate the importance of NSIF, a comparison was made between  $K_I/\sqrt{\rho}$  and  $K_I/\rho^\alpha$  for a crack length of 50.8 mm (2 inch) and seven different radii. Four different loads were applied to the specimen as shown in Table 6. From the table it is clear that  $K_I/\sqrt{\rho}$  approach is unconservative (smaller design hole radius) compared to  $K_I/\rho^\alpha$  approach and the percentage difference in predicted values varies from 50% at 9.53 mm radius to 70% at 0.79 mm radius for each load case. This indicates that the optimum crack stop hole radius should be based on  $K_I/\rho^\alpha$  approach. Having established the importance of NSIF for bare steel specimen, henceforth,  $K_I/\rho^\alpha$  should be calculated based on Eq. 10. Similarly, the combined action of CFRP patch and crack stop hole is studied numerically by carrying out nonlinear FEA and the results are expressed in terms of  $K_I/\rho^\alpha$ . Prior studies on CFRP–steel application indicate that CFRP patches are effective in arresting the cracks initiating from the notches. The results were expressed as a variation of  $K_I/\rho^\alpha$  with stiffness ratio and crack stop hole radius.

#### 1.4.3 Effect of stiffness ratio (SR) and crack stop hole radii ( $\rho$ ) on $K_I/\rho^\alpha$

Stiffness ratio (SR) is defined as the ratio of axial stiffness of composite plate to axial stiffness of steel plate (Eq.11). It is assumed that the axial load is transferred in the ratio of their stiffness.

$$SR = \frac{t_{CFRP}E_{CFRP}}{t_{Steel}E_{Steel}} \quad (11)$$

Figure 7 shows the variation of  $K_I/\rho^\alpha$  with stiffness ratio (includes specimen w/o patch) for a crack length of 25.4 mm (1 inch) and for applied load of 41.2 MPa, 62 MPa, 82.7 MPa and 103.4 MPa. In general, it can be observed that there is a decrease in  $K_I/\rho^\alpha$  with an increase in stiffness ratio. The effect of the first two to three layers are significant as can be seen from the steepness of the curves whereas with increase in the number of layers (stiffness ratio), the percentage reduction in  $K_I/\rho^\alpha$  decreases as shown by the flattening of the curve.

Figure 8 shows the variation of  $K_I/\rho^\alpha$  with crack stop hole radii for a crack length of 25.4 mm (1 inch) and for applied load of 41.2 MPa, 62 MPa, 82.7 MPa and 103.4 MPa. Akin to stiffness ratio, it can be observed that there is a steep decrease in the  $K_I/\rho^\alpha$  values for the hole radii up to 5 mm after which the percentage reduction in  $K_I/\rho^\alpha$  decreases as shown by the flattening of the curve. Similar variation of  $K_I/\rho^\alpha$  with SR and crack stop hole is observed for crack lengths 1.5, 2.0 and 2.5 inches, the results of which are not shown here for brevity.

#### 1.4.4 Reduction Factor (RF)

To account for the effect of CFRP patch in stress reduction, a reduction factor (RF) is introduced.

$$\text{Reduction factor} = \frac{(K_I / \rho^\alpha) \text{with CFRP}}{(K_I / \rho^\alpha) \text{w/o CFRP}} \quad (12)$$

The RF for different loads, SR and  $\rho$  of a 1 inch crack length are plotted in Fig. 9. From Fig. 9a to 9c it is clear that as the SR is increasing RF is decreasing, which means that there is a decrease in NSIF with increase in the number of CFRP layers. In Fig. 9d (103.4 MPa) it can be observed that there is a slight kink in RF curves for stiffness ratio less than 0.1. The kink in RF curves indicates that for higher applied stress of 103.4 MPa, lesser number of layers is not sufficient to cause a reduction in  $K_I / \rho^\alpha$ . Whereas when the stiffness ratio crosses beyond 0.1, the stiffness of CFRP is sufficient enough to cause a reduction in  $K_I / \rho^\alpha$ . It can also be observed that an SR of 0.96 can reduce the  $K_I / \rho^\alpha$  value on an average to 14%, 20%, 24%, and 28% of the bare steel specimen corresponding to applied loads of 41.2 MPa, 62 MPa, 82.7 MPa and 103.4 MPa respectively. The RF value for different crack lengths (1.5, 2, 2.5 inches) and for different applied loads are given in Table 7 through 9. This factor is a function of stiffness ratio (SR), ratio of applied load to yield stress ( $\sigma_{applied} / \sigma_{yield}$ ), and ratio of crack stop hole radius to crack length ( $\rho / 2a$ ). This factor could be incorporated in Eq. 10 given by Boukharouba et al. [19] as shown below:

$$K_\rho = (\sigma_{yy}(X_c) * \sqrt{2\pi} \left( X_c + \frac{\rho}{2} \right)^\alpha) * RF \quad (13)$$

For  $0 \leq SR \leq 0.96$

$$RF = a (SR^5) + b (SR^4) + c (SR^3) + d (SR^2) + e (SR) + 1 \quad (14)$$

Where, RF = Reduction Factor and SR = Stiffness Ratio

Eq. 14 is formulated such that the RF becomes unity when the SR becomes zero. This means that with no CFRP patches, Eq.13 merges with the original equation (Eq.10) provided by Boukharouba et al. [19]. The variables  $a$ ,  $b$ ,  $c$ ,  $d$  and  $e$  are the coefficients of Eq. 14 that are dependent on  $\sigma_{applied} / \sigma_{ys}$  and  $\rho / 2a$  as given in Eq. 15.

$$\begin{aligned} & p0 + p1 * x + p2 * y + p3 * x^2 + p4 * y^2 + p5 * x * y + p6 * x^2 * y + p7 * x * \\ & y^2 + p8 * y^3 \end{aligned} \quad (15)$$

Note: In Eq.15 the variables  $x$  and  $y$  represent  $\sigma_{applied}/\sigma_{ys}$  and  $\rho/2a$  respectively. The coefficients of Eq. 15 vary with  $a, b, c, d$  and  $e$  as shown in Table 10. It should be noted that Eq.14 is empirical and the units of load, radius and crack length are in MPa, mm and mm respectively.

#### 1.4.5 Effect of SR and load on peel stress

Peel stress ( $\sigma_{zz}$ ) at the CFRP edge causes debonding of CFRP from the specimen, due to the large stiffness difference between adhesive and CFRP. In this paper a study on peel stress for different loads and CFRP thicknesses (SR) has been carried out. The variation of peel stress has been studied along the X-X and Y-Y lines as shown in Fig. 10. Figure 11 shows the variation of peel stress on CFRP edge along the line x-x for 4 different loads and 8 different SR's. From Fig. 11 it can be observed that as the number of CFRP layers increases, the magnitude of peel stress also increases. Similar observation can be made for Fig. 12 where the peel stress is plotted for 4 different loads with lower (SR = 0.08) and higher (SR = 0.96) SR. In addition, the peel stress variation along the line Y-Y is shown in Fig.13. From the plot it can be observed that there is a spike in peel stress at the CFRP edge due to sudden change in stiffness and with an increase in SR, the magnitude of peel stress also increases. It should be noted that the variation in peel stress shown in Figs 11-13 were based on a crack length of 25.4 mm (1 inch) and 6.35 mm (0.25 inch) crack stop hole radius.

#### 1.4.6 Numerical example and verification using FEA

Consider a load of 34.4 MPa (5 ksi) acting on a specimen with center crack of length 50.8 mm (2 inch). The steel and CFRP properties and dimensions are the same as considered in this paper. The site conditions are such that the maximum radius of hole that can be drilled is 4 mm. Determine the number of CFRP layers required to arrest the crack.

*Solution:* The solution to the problem is carried out in a step by step format as shown below: 1. Calculate  $K_I/\rho^a$  of a bare steel specimen and plot the variation of the same with respect to various crack stop hole radii (0.375 inch to 1/32 inch) as shown in Fig. 14.

2. Plot the threshold line given by Barsom [8] (Eq. 5) in the same plot of  $K_I/\rho^a$  versus crack stop hole radii to determine the threshold radius. The threshold radius in this case is 6 mm which is greater than the 4 mm hole that can be drilled on site necessitating the need to reinforce the crack with CFRP patch to prevent crack re-initiation.

3. Now, as a start assume that 1 layer of CFRP patch is required with a crack stop hole radii of 3 mm and calculate the parameters  $\rho/2a$  (3/50.8) and  $\sigma_{applied}/\sigma_{ys}$  (34.4/303) to input in Eq.15.
4. Input the parameters obtained from Step 3 in Eq.15 and determine coefficients  $a$  through  $e$  by using corresponding  $p0$  through  $p8$  for each coefficient using Table 10.
5. Using the coefficients  $a$  through  $e$  obtained from Step 4 and  $SR$  from Eq. 11, calculate  $RF$  using Eq. 14. The  $RF$  value comes to around 0.4564.
6. From Fig. 14, the value of  $K_I/\rho^a$  of a bare steel specimen with crack stop hole radius of 3 mm is approximately 600 MPa. The corresponding value of specimen reinforced with 1 CFRP layer will be 274 MPa (0.4564\*600).
7. The reduced  $K_I/\rho^a$  value (274 MPa) is now compared with  $10\sqrt{\sigma_{ys}}$  (477 MPa). This value (477 MPa) is greater than reduced  $K_I/\rho^a$  value (274 MPa) which indicates that 1 layer of CFRP with 3 mm radius will not result in crack re-initiation. Since the site conditions in the problem permit up to 4 mm crack stop hole radius, the assumed 1 layer of CFRP reinforcement with 3 mm crack stop hole radius (undersized) is valid.

A nonlinear FEA was carried out for the above conditions ( $2a= 50.8$  mm,  $\rho= 3$  mm,  $SR = 0, 0.08$ , load = 34.4 MPa) and the results were used to calculate  $K_I/\rho^a$  for bare steel specimen and patched specimen with 1 layer respectively. The results indicate that the  $RF$  value is 1 (591 MPa) for bare steel specimen and 0.442 (261 MPa) for a patched specimen with 1 layer. It can be observed that the difference is 3.2% between proposed equation and FEA indicating the accuracy of the proposed equation.

## 1.5 Conclusions

This numerical study focuses on fracture mechanics approach to evaluate the effectiveness of the combined action of crack stop hole and CFRP patch. The studies to determine the appropriate crack stop hole radius for bare steel specimen indicated the need to adopt NSIF equation rather than CSIF due to the un-conservative nature of the latter. In the present study, crack stop hole serves as a notch and it is assumed that the crack originates from the edge of the hole. The application of CFRP will retard the crack re-initiation by reducing the stress value. The effect of patch thickness on the reduction of stress is calculated in terms of stiffness ratio and it is observed that stress is reduced by 80% and 20% at a stiffness ratio of 0.96 and 0.16 respectively. A parametric study was carried out for various crack stop hole radii, stiffness ratio and magnitude

of loads. A total of 1008 nonlinear FEA (Table 5) was carried out and the results of this study were curve fit to arrive at a reduction factor. This reduction factor in terms of  $\rho/2a$ , SR and  $\sigma_{applied}/\sigma_{ys}$  to include the effect of CFRP patch was used to modify the equation proposed by Boukharouba et al. [19]. The applicability of the developed reduction factor is demonstrated using a numerical example and validated by FEA. The peel stress studies carried out indicates that the magnitude of peel stress increases with stiffness ratio and magnitude of load.

It should be recognized that the current formulation of perfect bonding between steel and CFRP layers may not reflect reality. However, the significant improvement in stress reduction when evaluated against the bare steel specimen simulated with the same geometry (crack length and crack stop hole radius) and material properties of steel shows the potential of the proposed retrofit and the suitability of NSIF in predicting its effectiveness.

## REFERENCES

- [1] Shield C, Hajjar J, Nozaka K. Repair of fatigued steel bridge girders with carbon fiber strips. Report no-MN/RC-2002-04, Minnesota Department of Transportation, 2004.
- [2] Fisher JW, Barthelemy BM, Mertz DR, Edinger JA. Fatigue behaviour of full scale welded bridge attachments. NCHR 12-15(3), March 1980 (80-29), Fritz Laboratory Reports, 1980.
- [3] Crain J. Fatigue enhancement of undersized, drilled crack-stop holes. Masters thesis, Kansas state university, (<http://hdl.handle.net/1808/6288>), 2010.
- [4] Miller C, Chajes MJ, Mertz DR, Hastings JN. Strengthening of a steel bridge girder using CFRP Plates. Journal of Bridge Engineering 2001; 6(6): 514-522.
- [5] Barsom JM, McNicol RC. Effect of stress concentration on fatigue-crack initiation in HY-130 Steel. Fracture Toughness and Slow-Stable Cracking 1974; 4STM STP 559, 402 American Society for Testing and Materials: 183-204.
- [6] Jack AR, Price AT. The Initiation of fatigue cracks from notches in mild steel plates. International Journal of Fracture Mechanics 1970; 6(4): 401-409.
- [7] Creager M, and Paris PC. Elastic field equations for blunt cracks with reference to stress corrosion cracking. International Journal of Fracture Mechanics 1967; 3(4): 247-252.
- [8] Barsom JM, Fracture Mechanics – Fatigue and Fracture 1985. Metals Handbook – Desk 398 Edition, American Society for Metals, Metals Park, Ohio.

- [9] Heller M, Hill TG, Williams JF, Jones R. Increasing the fatigue life of cracked fastener holes using bonded repairs. *Theoretical and Applied Fracture Mechanics* 1989; 11 (1): 1-8.
- [10] Jones SC, and Civjan SA, Application of fiber reinforced polymer overlays to extend steel fatigue life. *Journal of Composites for Construction* 2003; 7(4): 331-338.
- [11] Tavakkolizadeh M, Saadatmanesh H. Fatigue strength of steel girders strengthened with carbon fiber reinforced polymer patch. *Journal of Structural Engineering* 2003; 129 (2): 186-196.
- [12] Achour T, Bachir BB, Serier B. Numerical analysis of the performance of the bonded composite patch in reducing stress concentration and repairing crack at notch. *Computational Material Science* 2003; 28 (1): 41–48.
- [13] Zhao XL, Zhang L. State-of-the-art review on FRP strengthened steel structures. *Engineering Structures* 2007; 29 (8): 1808–1823.
- [14] Liu H, Xiao Z, Zhao XL, Al-Mahaidi R. Prediction of fatigue life for CFRP-strengthened steel plates. *Thin-Walled Structures* 2009; 47 (10): 1069–1077.
- [15] Alemdar F, Gangel R, Matamoros A, Bennett C, Barrett-Gonzalez R, Rolfe ST, Liu H. Use of CFRP overlays to repair fatigue damage in steel plates under tension loading. *Journal of Composites for Construction* 2013; 18 (4): 04013052
- [16] Hmidan A, Kim Y, Yazdani S. Stress intensity factors for cracked steel girders strengthened with CFRP sheets. *Journal of Composites for Construction* 2014; 10.1061/ (ASCE) CC.1943-5614.0000552: 04013052.
- [17] Ramji M, Srilakshmi R, Bhanu Prakash M. Towards optimization of patch shape on the performance of bonded composite repair using FEM. *Composites: Part B* 2012; 45(1): 710–720.
- [18] Nakmura T, Parks DM. Antisymmetrical 3D stress field near the crack front of a thin elastic plate. *International Journal of Solids and Structures* 1989; 25 (12): 1411-1426.
- [19] Boukharouba T, Tamine T, Niu L, Chehimi C, Pluvinage G. The use of notch stress intensity factor as a fatigue crack initiation parameter. *Engineering Fracture Mechanics* 1995; 52(3): 503-512.

- Figure 1.1:** A pictorial view of a girder with cracks
- Figure 1.2:** Schematic representation of the specimen
- Figure 1.3a:** Typical FE mesh of specimen
- Figure 1.3b:** Circular meshing around the crack stop hole
- Figure 1.4:** Comparison between  $K_I$  obtained from ANSYS and analytical expression for an bare steel specimen with 1” crack length.
- Figure 1.5:** Comparison between  $K_I / \sqrt{\rho}$  and  $K_I / \rho^\alpha$  (41.2 MPa load)
- Figure 1.6:** Stress distribution ahead of crack stop hole
- Figure 1.7:**  $K_I / \rho^\alpha$  versus SR for 1.0” Crack Length at different loads (a) 41.2 MPa, (b) 62 MPa, (c) 82.7 MPa and (d) 103.4 MPa
- Figure 1.8:**  $K_I / \rho^\alpha$  versus Radius for 1.0” Crack Length at different loads (a) 41.2 MPa, (b) 62 MPa, (c) 82.7 MPa and (d) 103.4 MPa
- Figure 1.9:** RF versus SR for 1.0” Crack Length at different loads (a) 41.2 MPa, (b) 62 MPa, (c) 82.7 MPa and (d) 103.4 MPa
- Figure 1.10:** Schematic representation of the lines considered for peel stress distribution
- Figure 1.11:** Variation of peel stress in X-X direction for 1” Crack Length at different loads (a) 41.2 MPa, (b) 62 MPa, (c) 82.7 MPa and (d) 103.4 MPa
- Figure 1.12:** Variation of peel stress in X-X direction for 1” Crack Length at different SR (a) 0.08 and (b) 0.96
- Figure 1.13:** Variation of peel stress along Y-Y direction for 1” Crack Length at different loads (a) 41.2 MPa, (b) 62 MPa, (c) 82.7 MPa and (d) 103.4 MPa
- Figure 1.14:**  $K_I / \rho^\alpha$  versus crack stop hole radius of bare steel specimen having a crack of 2” for 34.4 MPa load

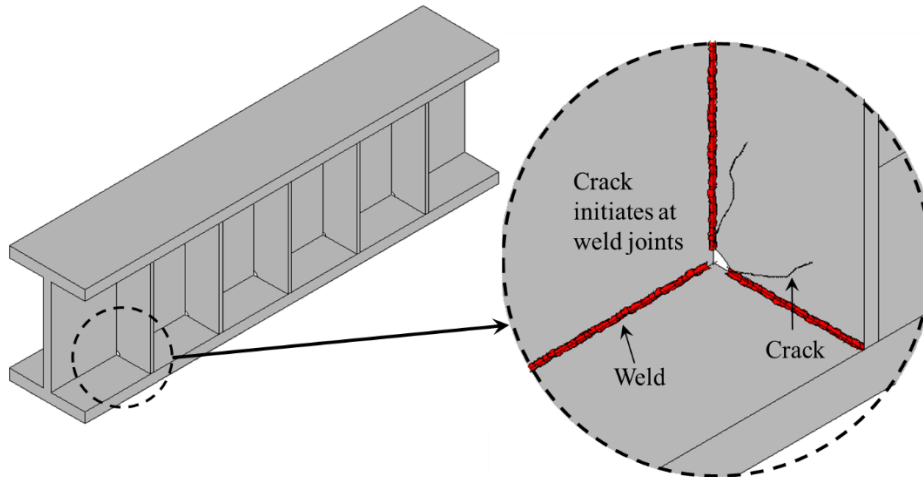


**Figure 1.1: A pictorial view of a girder with cracks**

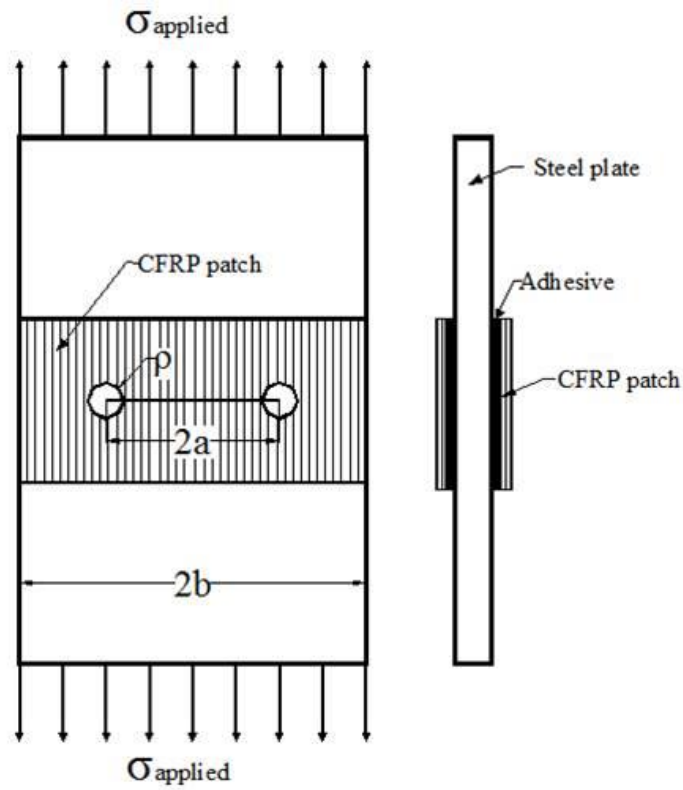


**Figure 1.2: Schematic representation of the specimen**



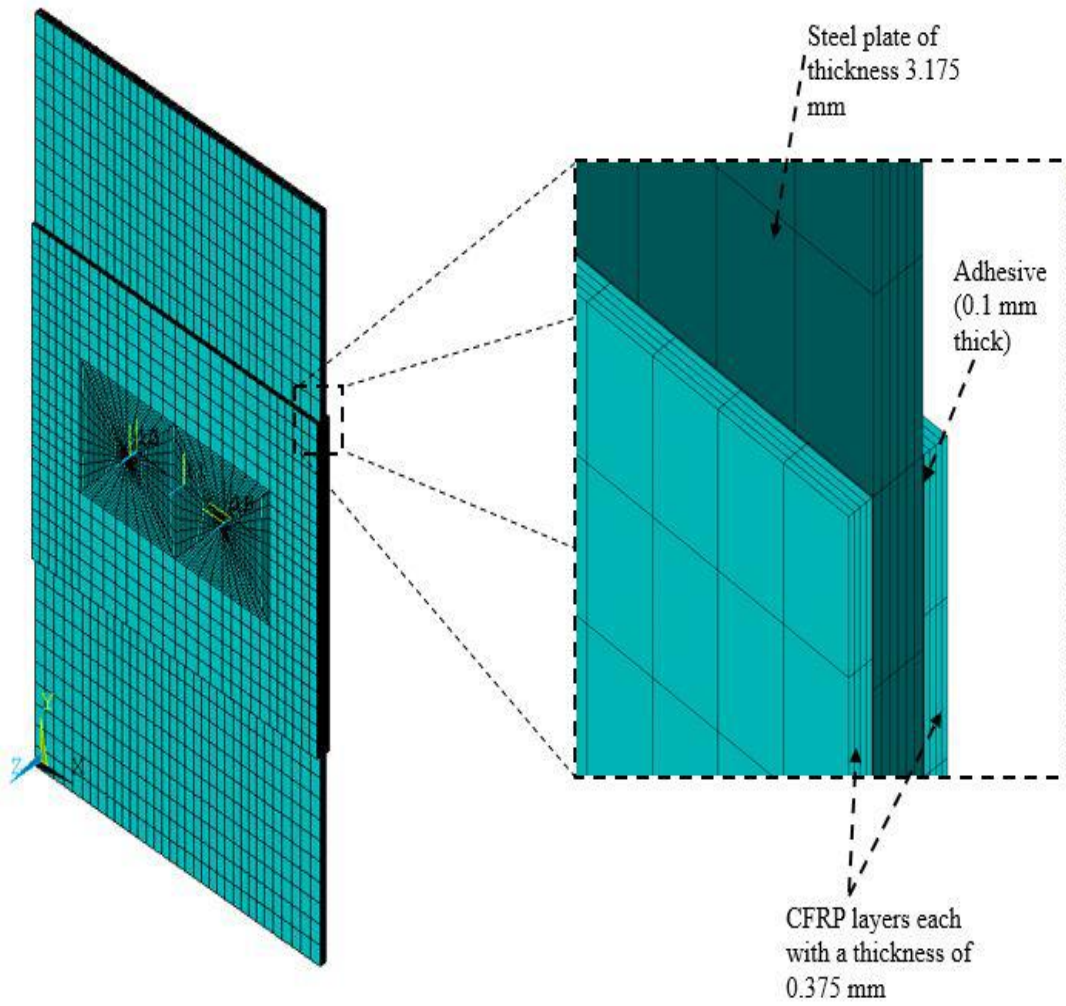


**Figure 1.3a: Typical FE mesh of specimen**

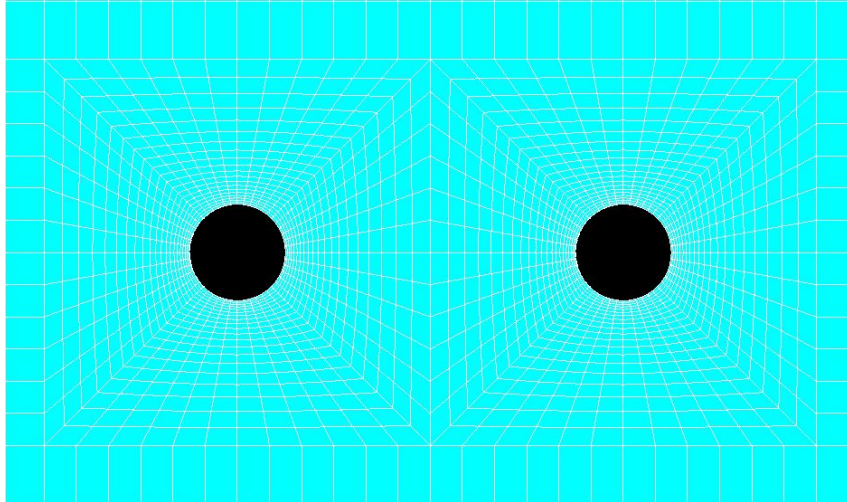


**Figure 1.3b: Circular meshing around the crack stop hole**

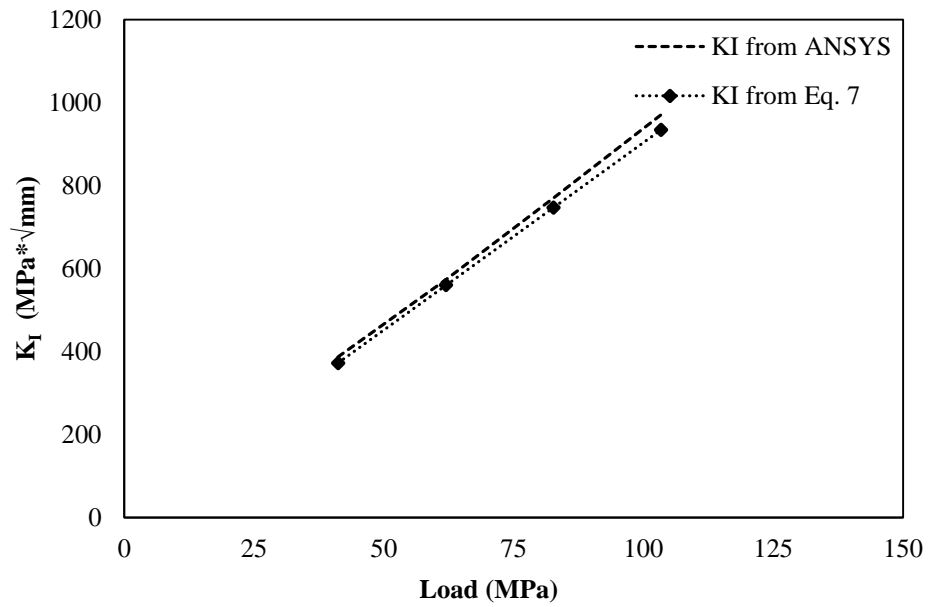


**Figure 1.4: Comparison between  $K_I$  obtained from ANSYS and analytical expression for a bare steel specimen with 1" crack length.**

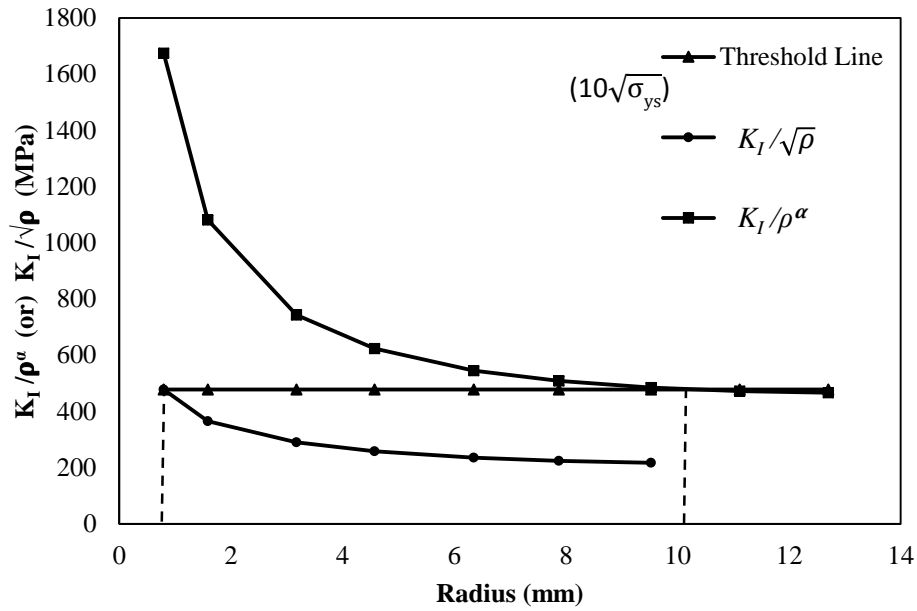


Figure 1.5: Comparison between  $K_I/\sqrt{\rho}$  and  $K_I/\rho^\alpha$  (41.2 MPa load, 2 inch crack)

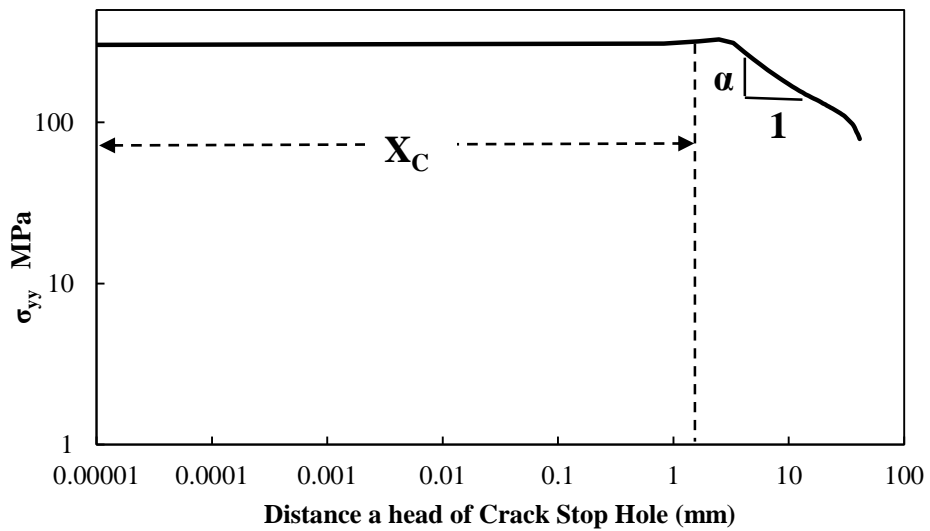
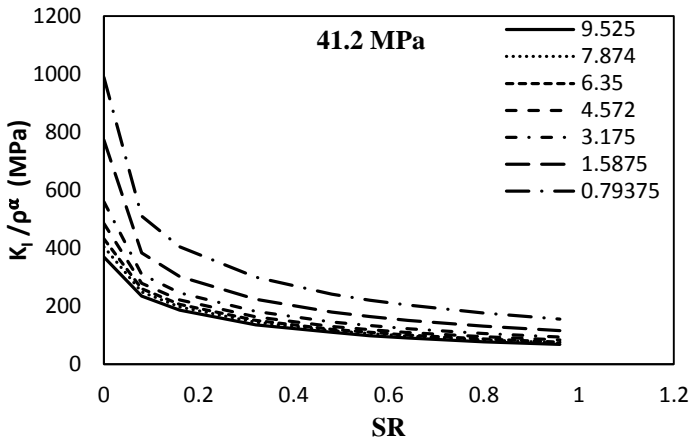
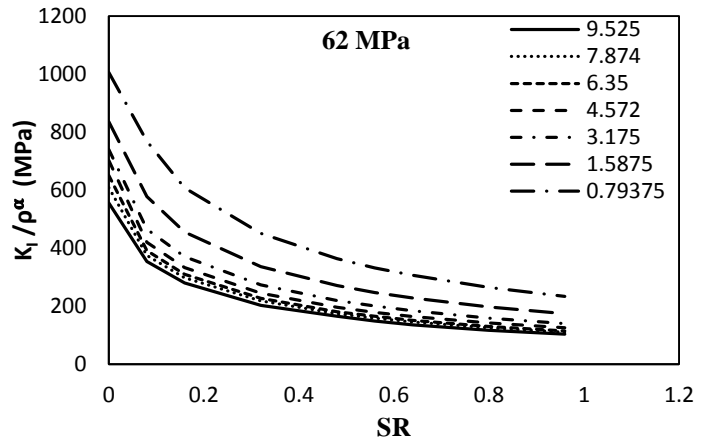


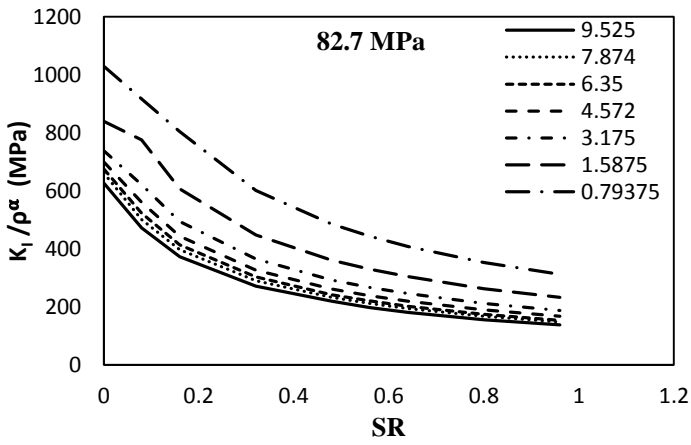
Figure 1.6: Stress distribution ahead of crack stop hole



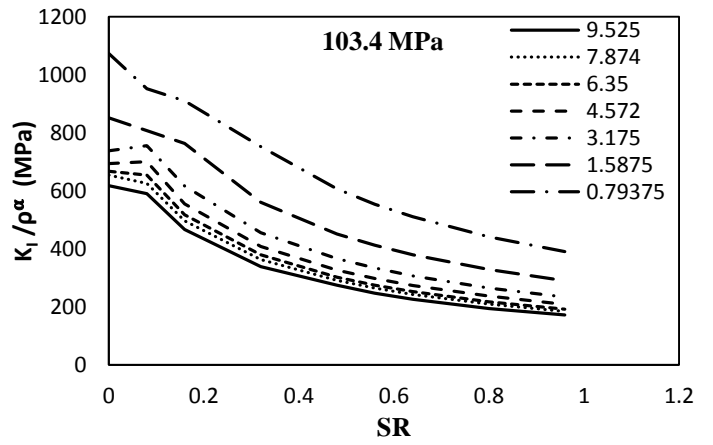
(a)



(b)

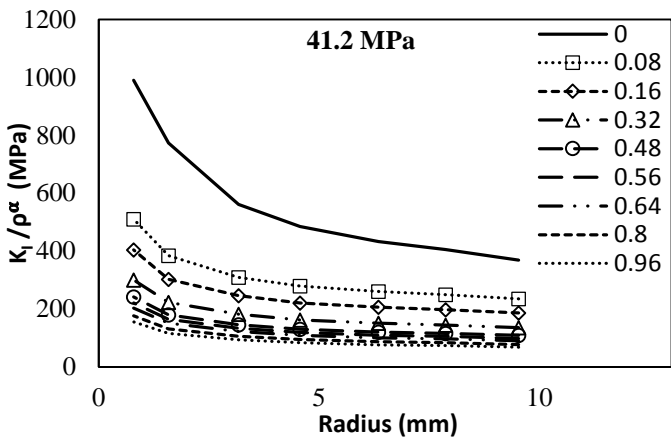


(c)

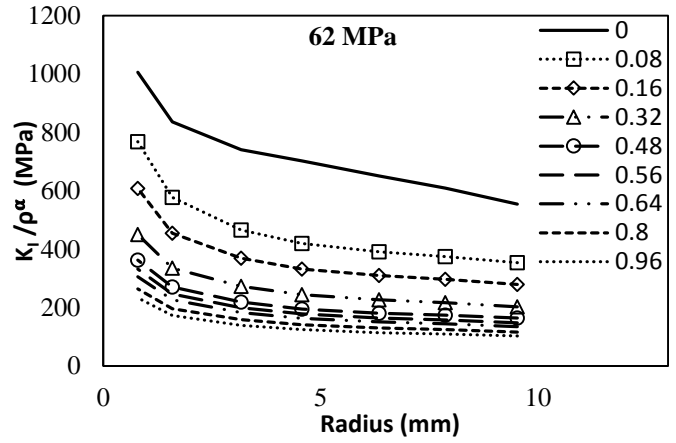


(d)

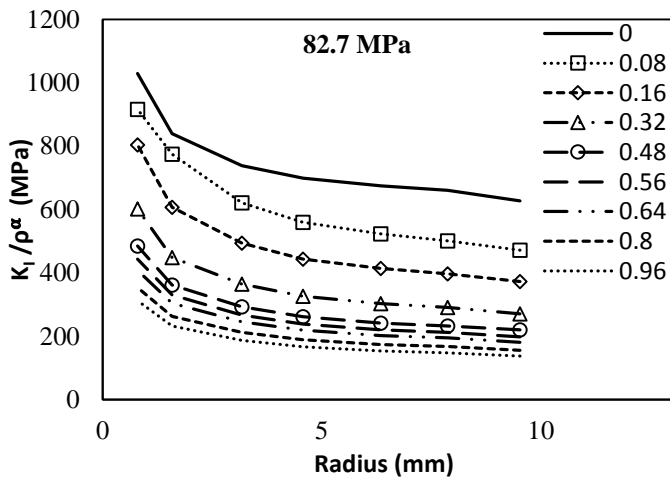
Figure 1.7:  $K_I/\rho^\alpha$  versus SR for 1" Crack Length at different loads (a) 41.2 MPa, (b) 62 MPa, (c) 82.7 MPa and (d) 103.4 MPa



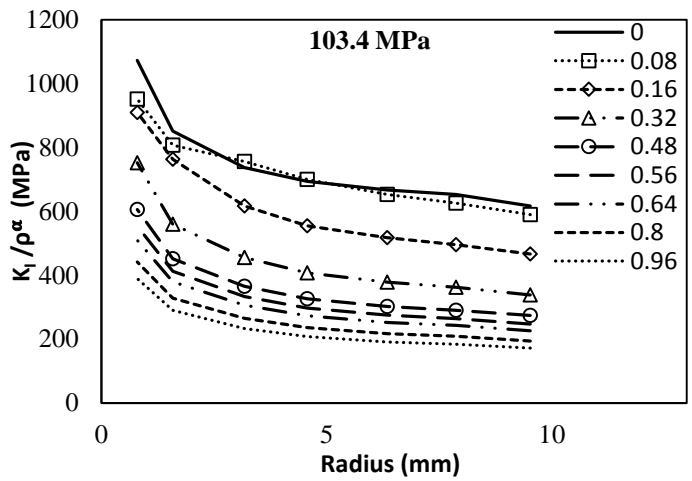
(a)



(b)

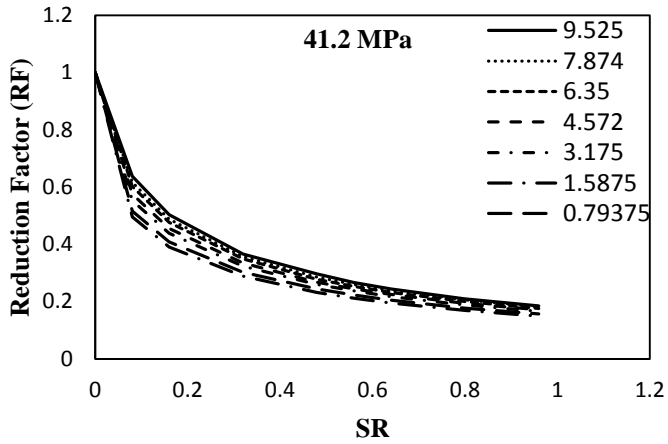


(c)

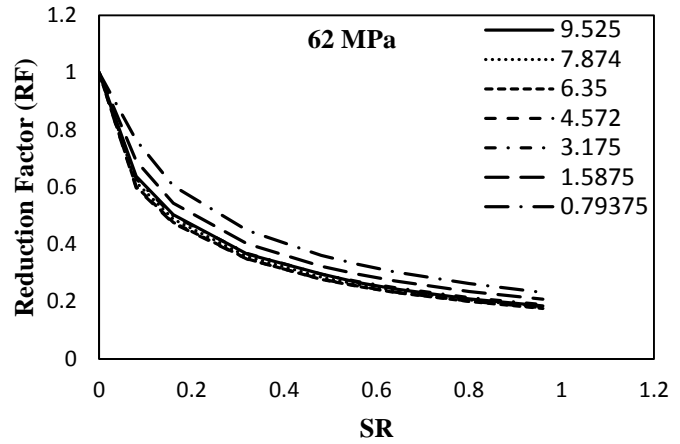


(d)

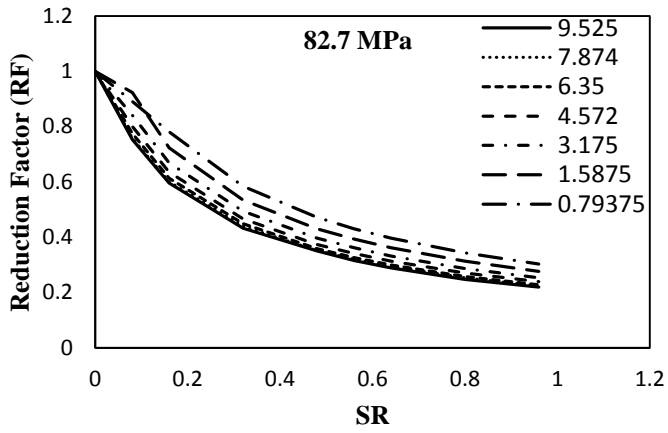
Figure 1.8:  $K_I/\rho^\alpha$  versus Radius for 1" Crack Length at different loads (a) 41.2 MPa, (b) 62 MPa, (c) 82.7 MPa and (d) 103.4 MPa



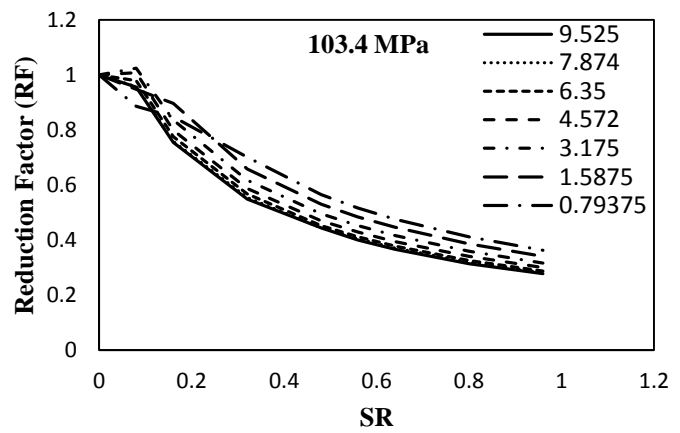
(a)



(b)



(c)



(d)

Figure 1.9: RF versus SR for 1" Crack Length at different loads (a) 41.2 MPa, (b) 62 MPa, (c) 82.7 MPa and (d) 103.4 MPa

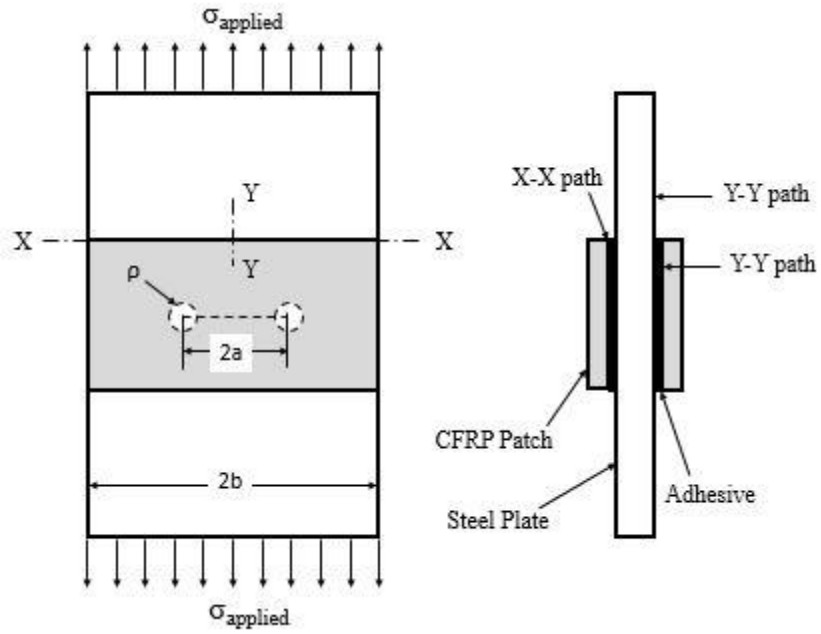
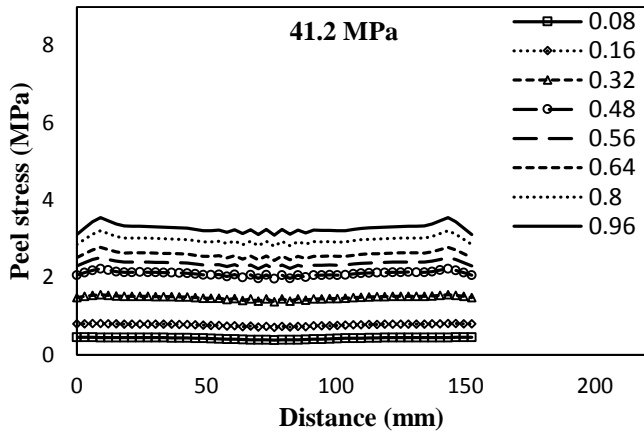
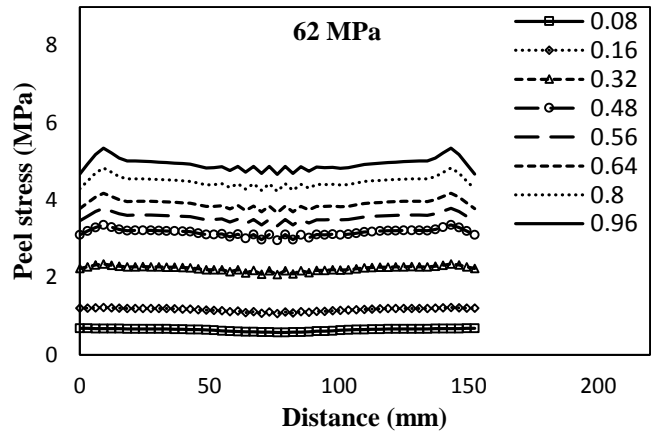


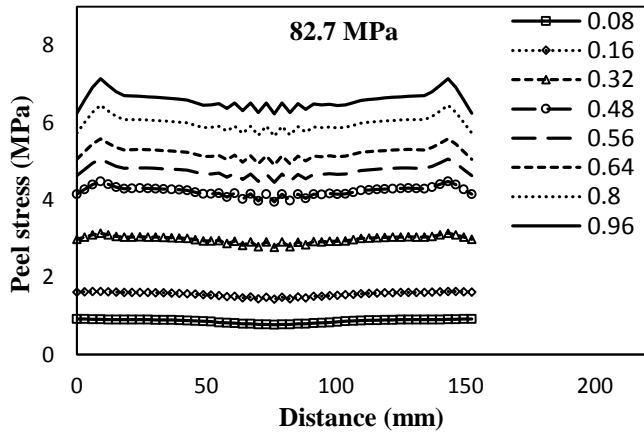
**Figure 1.10: Schematic representation of the lines considered for peel stress distribution**



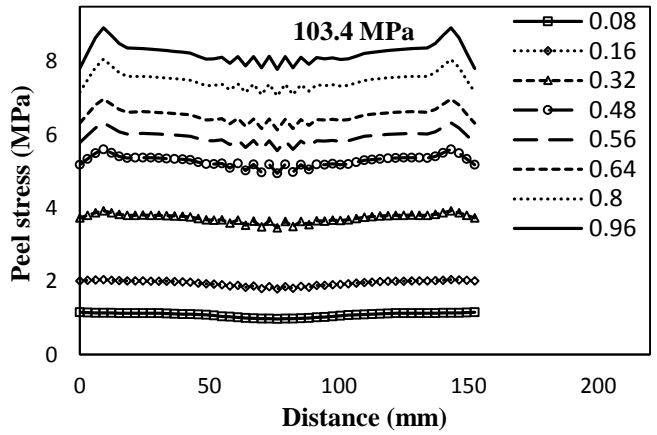
(a)



(b)



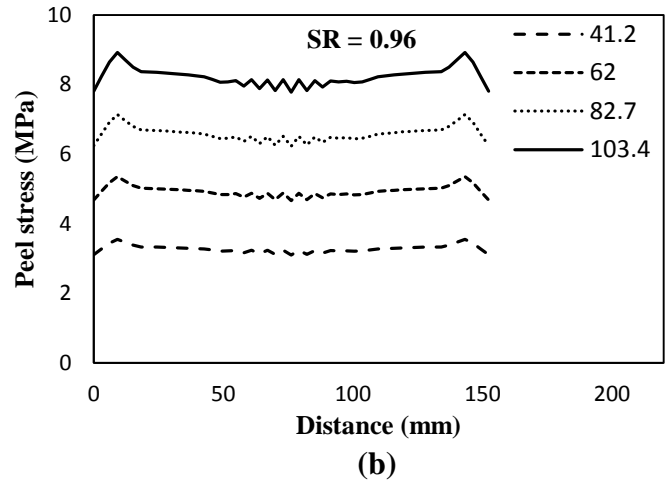
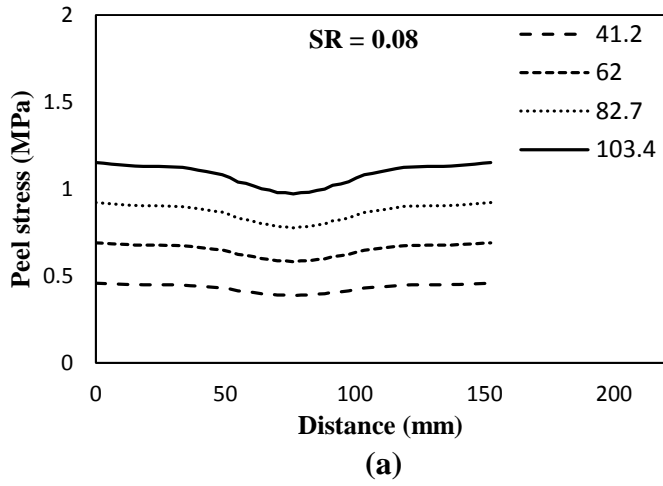
(c)



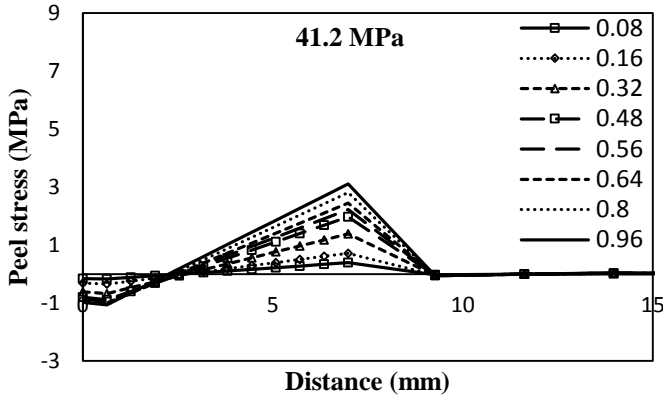
(d)

Figure 1.11: Variation of peel stress in X-X direction for 1" crack length at different loads (a) 41.2 MPa, (b) 62 MPa, (c) 82.7 MPa and (d) 103.4 MPa

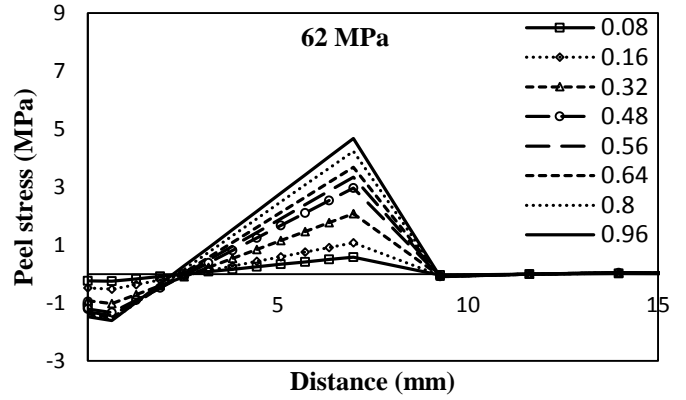




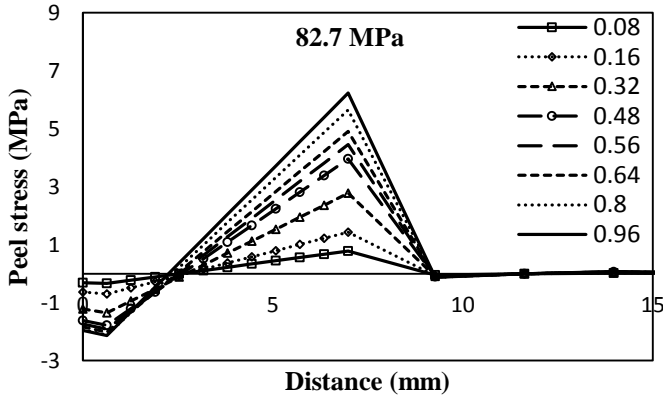
**Figure 1.12: Variation of peel stress in X-X direction for 1” crack length at different SR (a) 0.08 and (b) 0.96**



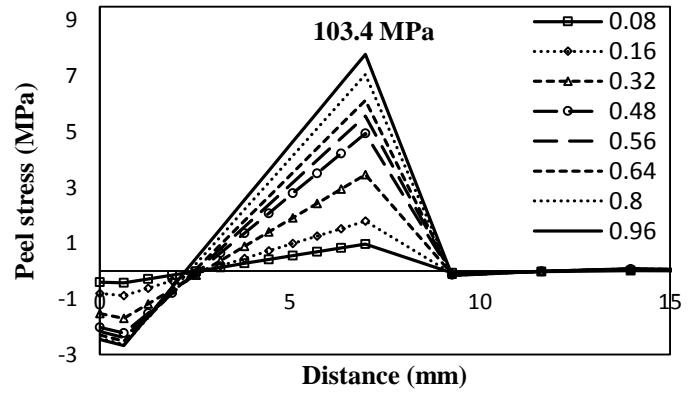
(a)



(b)



(c)



(d)

Figure 1.13: Variation of peel stress along Y-Y direction for 1" crack length at different loads (a) 41.2 MPa, (b) 62 MPa, (c) 82.7 MPa and (d) 103.4 MPa

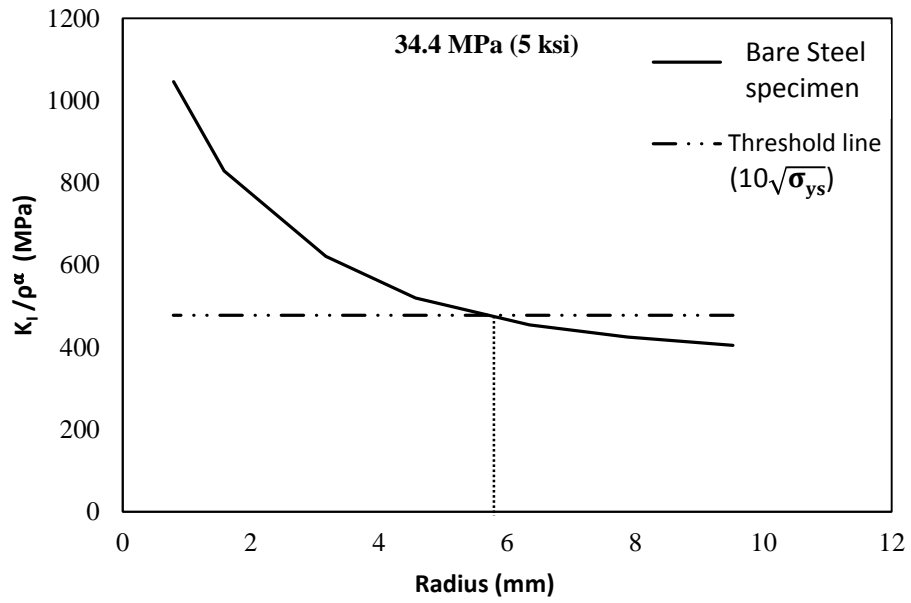


**Figure 1.14:  $K_I / \rho^\alpha$  versus crack stop hole radius of bare steel specimen having a crack of 2” for 34.4 MPa load**

<b>Sl. no.</b>	<b>Title</b>
1.1	Comparison between $K_I / \sqrt{\rho}$ Vs $K_I / \rho^\alpha$
1.2	Steel material property
1.3	CFRP and adhesive material properties
1.4	Dimensions of the specimen
1.5	Values of different parameters considered in the study
1.6	Comparison between $K_I / \sqrt{\rho}$ and $K_I / \rho^\alpha$ for different loads and radius of a bare steel specimen (2 inch crack)
1.7	RF values at 62 MPa load for different crack length, crack stop hole radius and SR
1.8	RF values at 82.7 MPa load for different crack length, crack stop hole radius and SR
1.9	RF values at 103.4 MPa load for different crack length, crack stop hole radius and SR
1.10	Variation of p0 to p8 with coefficients a, b, c, d and e

**Table 1.1: Comparison between  $K_I / \sqrt{\rho}$  Vs  $K_I / \rho^\alpha$**

Crack stress intensity factor ( $K_I$ )	Notch stress intensity factor ( $K_\rho$ )
$K_I / \sqrt{\rho}$	$K_\rho / \rho^\alpha$ (or) $K_I / \rho^\alpha$
$K_I / \sqrt{\rho} = \frac{\sigma_{y \max} * \sqrt{\pi}}{2}$	$K_\rho = \sigma_{yy}(X_c) * \sqrt{2\pi} \left( X_c + \frac{\rho}{2} \right)^\alpha$
CSIF considers only the stress at the edge of hole.	NSIF considers not only the stress at the edge of hole but also its distribution ahead of crack stop hole

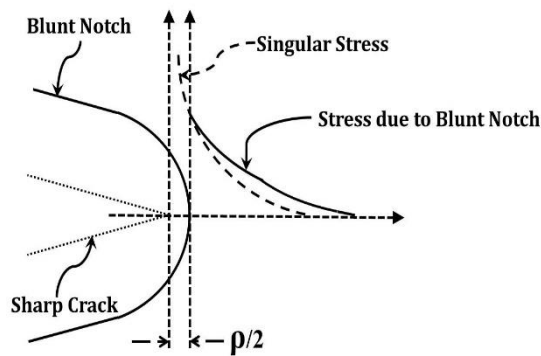


**Table 1.2: Steel material property  
(MISO,  $E_X = 200$  GPa,  $\nu_{xy} = 0.3$ )**

Strain	Stress
0	0
0.001508	301.6
0.016433	303.88
0.039968	376.88
0.090192	437.36
0.159939	461.92
0.25861	467.88

**Table 1.3: CFRP and adhesive material properties**

<b>Material</b>	<b>Adhesive</b>	<b>CFRP</b>
$E_x$ (GPa)	4.97	135
$E_y$ (GPa)	-	9
$E_z$ (GPa)	-	9
$G_{xy}$ (GPa)	-	5
$G_{zy}$ (GPa)	-	8
$G_{zx}$ (GPa)	-	5
$\nu_{xy}$	0.47	0.3
$\nu_{zy}$	-	0.02
$\nu_{zx}$	-	0.3

**Table 1.4: Dimensions of the specimen**

<b>Dimension</b>	<b>Value</b>
Width of the specimen (2b), mm	152.4
Height of the specimen (L), mm	294.2
Thickness of the steel plate (T), mm	3.175
length of CFRP and Adhesive, mm	127
Thickness of the CFRP, mm	0.375
Thickness of the Adhesive, mm	0.1

**Table 1.5: Values of different parameters considered in the study**

<b>Parameter</b>	<b>Values</b>	<b>Quantities</b>
Crack length (inch)	1, 1.5, 2, 2.5	4
Crack stop hole radii (inch)	3/8, 5/16, 1/4, 3/16, 1/8, 1/16, 1/32	7
CFRP layers	0, 1, 2, 4, 6, 7, 8, 10, 12	9
Load (MPa)	41.2, 62, 82.7, 103.4	4
	Total No. of analysis	1008

**Table 1.6: Comparison between  $K_I / \sqrt{\rho}$  and  $K_I / \rho^\alpha$  for different loads and radius of a bare steel specimen (2 inch crack)**

Radius mm (inch)	$K_I / \sqrt{\rho}$ (MPa)				$K_I / \rho^\alpha$ (MPa)			
	Applied Stress (MPa)							
	41.2	62	82.7	103.4	41.2	62	82.7	103.4
<b>9.53 (3/8)</b>	217	327	436	545	484	729	972	1215
<b>7.874 (5/16)</b>	224	338	450	563	508	765	1021	1276
<b>6.35 (2/8)</b>	236	355	473	592	545	821	1095	1369
<b>4.572 (3/16)</b>	258	389	518	648	623	938	1251	1565
<b>3.175 (1/8)</b>	290	436	582	727	743	1119	1492	1866
<b>1.58 (1/16)</b>	365	550	733	917	1081	1627	2171	2714
<b>0.79 (1/32)</b>	479	720	960	1201	1675	2520	3361	4203

**Table 1.7: RF values at 62 MPa load for different crack length, crack stop hole radius and SR**

Crack Length (mm)	Radius (mm)	62 MPa								
		SR								
		0	0.08	0.16	0.32	0.48	0.56	0.64	0.8	0.96
25.4	0.79375	1.00	0.76	0.60	0.45	0.36	0.33	0.30	0.26	0.23
	1.5875	1.00	0.69	0.54	0.40	0.32	0.30	0.27	0.24	0.21
	3.175	1.00	0.63	0.50	0.37	0.30	0.27	0.25	0.21	0.19
	4.572	1.00	0.60	0.47	0.35	0.28	0.25	0.23	0.20	0.18
	6.35	1.00	0.60	0.48	0.35	0.28	0.25	0.23	0.20	0.18
	7.874	1.00	0.62	0.49	0.36	0.29	0.26	0.24	0.21	0.18
	9.525	1.00	0.64	0.50	0.37	0.30	0.27	0.25	0.21	0.19
38.1	0.79375	1.00	0.75	0.58	0.42	0.34	0.31	0.29	0.25	0.22
	1.5875	1.00	0.73	0.57	0.41	0.33	0.30	0.28	0.24	0.21
	3.175	1.00	0.66	0.52	0.38	0.31	0.28	0.26	0.22	0.20
	4.572	1.00	0.59	0.46	0.33	0.27	0.25	0.23	0.20	0.18
	6.35	1.00	0.58	0.45	0.33	0.26	0.24	0.22	0.19	0.17
	7.874	1.00	0.59	0.47	0.34	0.27	0.24	0.23	0.19	0.17
	9.525	1.00	0.58	0.46	0.33	0.26	0.24	0.22	0.19	0.16
50.8	0.79375	1.00	0.73	0.56	0.41	0.33	0.30	0.27	0.24	0.21
	1.5875	1.00	0.75	0.58	0.42	0.34	0.31	0.28	0.24	0.22
	3.175	1.00	0.68	0.53	0.39	0.31	0.28	0.26	0.22	0.20
	4.572	1.00	0.62	0.48	0.35	0.28	0.26	0.24	0.21	0.18
	6.35	1.00	0.63	0.50	0.36	0.29	0.26	0.24	0.21	0.18
	7.874	1.00	0.61	0.48	0.35	0.28	0.25	0.23	0.20	0.18
	9.525	1.00	0.57	0.43	0.29	0.23	0.21	0.19	0.17	0.15
63.5	0.79375	1.00	0.71	0.55	0.40	0.32	0.29	0.27	0.23	0.20
	1.5875	1.00	0.76	0.59	0.43	0.34	0.31	0.29	0.25	0.22
	3.175	1.00	0.71	0.55	0.41	0.33	0.30	0.27	0.24	0.21
	4.572	1.00	0.68	0.53	0.39	0.31	0.28	0.26	0.22	0.20
	6.35	1.00	0.65	0.51	0.37	0.30	0.27	0.25	0.21	0.19
	7.874	1.00	0.64	0.50	0.36	0.29	0.26	0.24	0.21	0.18
	9.525	1.00	0.62	0.48	0.35	0.28	0.25	0.23	0.20	0.17



**Table 1.8: RF values at 82.7 MPa load for different crack length, crack stop hole radius and SR**

Crack Length (mm)	Radius (mm)	82.7 MPa								
		SR								
		0	0.08	0.16	0.32	0.48	0.56	0.64	0.8	0.96
25.4	0.79375	1.00	0.89	0.78	0.59	0.47	0.43	0.40	0.34	0.30
	1.5875	1.00	0.92	0.72	0.53	0.43	0.39	0.36	0.31	0.28
	3.175	1.00	0.84	0.67	0.49	0.40	0.36	0.33	0.29	0.25
	4.572	1.00	0.80	0.64	0.47	0.37	0.34	0.31	0.27	0.24
	6.35	1.00	0.78	0.61	0.45	0.36	0.33	0.30	0.26	0.23
	7.874	1.00	0.76	0.60	0.44	0.35	0.32	0.29	0.25	0.22
	9.525	1.00	0.75	0.59	0.43	0.35	0.31	0.29	0.25	0.22
38.1	0.79375	1.00	0.84	0.74	0.54	0.43	0.39	0.36	0.31	0.28
	1.5875	1.00	0.94	0.74	0.54	0.44	0.40	0.37	0.32	0.28
	3.175	1.00	0.88	0.69	0.51	0.41	0.37	0.34	0.30	0.26
	4.572	1.00	0.80	0.62	0.45	0.36	0.34	0.31	0.27	0.24
	6.35	1.00	0.79	0.61	0.45	0.36	0.33	0.30	0.26	0.23
	7.874	1.00	0.80	0.63	0.46	0.37	0.33	0.31	0.26	0.23
	9.525	1.00	0.79	0.62	0.45	0.35	0.32	0.29	0.25	0.22
50.8	0.79375	1.00	0.79	0.69	0.50	0.40	0.37	0.34	0.29	0.26
	1.5875	1.00	0.93	0.75	0.55	0.44	0.40	0.37	0.32	0.28
	3.175	1.00	0.91	0.72	0.53	0.42	0.38	0.35	0.30	0.27
	4.572	1.00	0.85	0.66	0.48	0.39	0.36	0.33	0.29	0.25
	6.35	1.00	0.87	0.69	0.50	0.40	0.36	0.33	0.29	0.25
	7.874	1.00	0.84	0.66	0.48	0.38	0.35	0.32	0.28	0.24
	9.525	1.00	0.80	0.60	0.41	0.32	0.29	0.27	0.23	0.21
63.5	0.79375	1.00	0.55	0.48	0.35	0.28	0.25	0.23	0.20	0.18
	1.5875	1.00	0.61	0.50	0.36	0.29	0.26	0.24	0.21	0.18
	3.175	1.00	0.69	0.54	0.40	0.32	0.29	0.27	0.23	0.20
	4.572	1.00	0.66	0.52	0.38	0.30	0.27	0.25	0.22	0.19
	6.35	1.00	0.64	0.50	0.37	0.29	0.27	0.24	0.21	0.19
	7.874	1.00	0.67	0.52	0.38	0.30	0.27	0.25	0.22	0.19
	9.525	1.00	0.66	0.51	0.37	0.29	0.27	0.24	0.21	0.18

**Table 1.9: RF values at 103.4 MPa load for different crack length, crack stop hole radius and SR**

Crack Length (mm)	Radius (mm)	103.4 MPa								
		SR								
		0	0.08	0.16	0.32	0.48	0.56	0.64	0.8	0.96
25.4	0.79375	1.00	0.89	0.85	0.70	0.56	0.52	0.48	0.41	0.36
	1.5875	1.00	0.95	0.90	0.66	0.53	0.48	0.45	0.39	0.34
	3.175	1.00	1.02	0.84	0.62	0.50	0.45	0.42	0.36	0.32
	4.572	1.00	1.01	0.80	0.59	0.47	0.43	0.39	0.34	0.30
	6.35	1.00	0.98	0.78	0.57	0.45	0.41	0.38	0.33	0.29
	7.874	1.00	0.96	0.76	0.56	0.44	0.40	0.37	0.32	0.28
	9.525	1.00	0.96	0.76	0.55	0.45	0.40	0.37	0.31	0.28
38.1	0.79375	1.00	0.80	0.76	0.62	0.50	0.45	0.42	0.36	0.32
	1.5875	1.00	0.93	0.89	0.66	0.53	0.48	0.44	0.38	0.34
	3.175	1.00	1.04	0.87	0.64	0.52	0.47	0.43	0.37	0.33
	4.572	1.00	1.02	0.79	0.57	0.46	0.43	0.40	0.35	0.31
	6.35	1.00	1.02	0.79	0.57	0.46	0.42	0.39	0.34	0.30
	7.874	1.00	1.04	0.82	0.60	0.47	0.43	0.40	0.34	0.30
	9.525	1.00	1.03	0.81	0.59	0.46	0.42	0.38	0.33	0.29
50.8	0.79375	1.00	0.72	0.69	0.55	0.44	0.40	0.37	0.32	0.28
	1.5875	1.00	0.91	0.89	0.66	0.53	0.48	0.44	0.38	0.34
	3.175	1.00	1.07	0.90	0.66	0.53	0.48	0.44	0.38	0.34
	4.572	1.00	1.07	0.84	0.61	0.49	0.45	0.42	0.36	0.32
	6.35	1.00	1.12	0.88	0.64	0.51	0.47	0.43	0.37	0.33
	7.874	1.00	1.11	0.87	0.63	0.50	0.46	0.42	0.36	0.32
	9.525	1.00	1.06	0.79	0.55	0.43	0.39	0.36	0.31	0.27
63.5	0.79375	1.00	0.34	0.33	0.26	0.21	0.19	0.18	0.15	0.13
	1.5875	1.00	0.44	0.42	0.32	0.25	0.23	0.21	0.18	0.16
	3.175	1.00	0.55	0.48	0.35	0.28	0.26	0.23	0.20	0.18
	4.572	1.00	0.66	0.53	0.39	0.31	0.28	0.26	0.22	0.20
	6.35	1.00	0.71	0.55	0.41	0.32	0.29	0.27	0.23	0.20
	7.874	1.00	0.68	0.53	0.38	0.30	0.28	0.25	0.22	0.19
	9.525	1.00	0.71	0.55	0.40	0.32	0.29	0.26	0.23	0.20

**Table 1.10: Variation of p0 to p8 with coefficients a, b, c, d and e**

<b>Coefficients</b>	<b>Coefficients</b>				
	<b>a</b>	<b>b</b>	<b>c</b>	<b>d</b>	<b>e</b>
<b>p0</b>	-110.89	295.52	-287.52	123.38	-21.838
<b>p1</b>	865.95	-2280.41	2173.62	-894.09	139.119
<b>p2</b>	143.349	-379.829	366.42	-154.47	25.45
<b>p3</b>	-1797.94	4698.83	-4425.16	1782.47	-265.94
<b>p4</b>	782.65	-2105.27	2063.69	-881.88	144.22
<b>p5</b>	-3004.58	7977.57	-7701.86	3237.37	-524.64
<b>p6</b>	11390.37	-29942.73	28459.53	-11647.63	1793.74
<b>p7</b>	-5885.82	15336.06	-14367.75	5729.39	-835.76
<b>p8</b>	898.28	-2241.40	1969.42	-706.97	84.74

# CHAPTER 2

## Numerical Studies on Halting Crack Growth using Crack-stop Hole and Asymmetrically Bonded CFRP Patch

### 2.1 Introduction

Due to fatigue load cracks appear in structural members resulting in an increase in stress near the crack tip. The effect of crack is measured in terms of stress intensity factor SIF ( $K$ ) and they are of three different types  $K_I$ ,  $K_{II}$  and  $K_{III}$ . All the three SIF's depend on the relation between the directions of load applied, crack front and crack propagation. In the present study, only  $K_I$  corresponding to mode-I is considered. If the cracked specimen is left unrepaired for a long time it leads to sudden failure. To prevent such occurrence, various retrofitting techniques are employed which can be broadly classified into two groups [1]: (a) Local retrofitting techniques which include crack stop holes, peening, Gas Tungsten Arc (GTA) welding that modify the local stress state and (b) Global retrofitting techniques that include strengthening with steel plate or composite laminates. The objective of any retrofitting fitting method is to reduce the SIF at the crack tip. Crack stop holes has been used as a repair technique for years in the field of aircrafts. The expression for SIF ( $K_I$ ) value (Eq. 1) for specimen as shown in Fig. 1a was first provided by Irwin [2]. Creagor and Paris [3] proposed an expression of  $K_I$  (Eq. 2) for a specimen with a crack and crack stop hole as shown in Fig. 1b.

$$K_I = \sigma_{applied} * \sqrt{\pi a} \quad (1)$$

$$K_I = \frac{\sigma_{y \max} * \sqrt{\pi \rho}}{2} \quad (2)$$

Later Boukharouba et al. [4] has given an expression of  $K_I$  (Eq. 3) for a crack stop hole which is a function of characteristic distance ( $X_c$ , the distance up to which the stress remains constant) and stress gradient ( $\alpha$ ).

$$K_I = \sigma_{yy}(X_c) * \sqrt{2\pi} \left( X_c + \frac{\rho}{2} \right)^\alpha \quad (3)$$

To arrive at the optimum crack stop hole radius Barsom [5], has proposed a threshold value of  $K_I / \rho^\alpha$  as given in Eq. 4. Figure 2 shows the usage of the equation proposed by Barsom [5]. It shows the variation of  $K_I / \rho^\alpha$  with crack stop hole radius and intersection of this curve with threshold value given by Barsom [5] leads to optimum crack stop hole radius to be drilled.

$$\frac{K_I}{\sqrt{\rho}} = 10\sqrt{\sigma_{ys}} \quad (4)$$

When the site conditions are such that the maximum size of the hole that can be drilled is less than the optimum crack stop hole radius, the crack may then reinitiate after a few loading cycles. Therefore, an undersized crack stop hole is only a temporary measure or a partial solution which needs to be complemented. One way to reinforce the undersized crack stop hole is by means of carbon fiber reinforced polymer (CFRP) patch which has a high strength to weight ratio. The present study involves studying the effectiveness of combined action of crack stop hole and asymmetrically bonded CFRP as repair technique. Asymmetrically bonded case is considered because in practical situations it may be difficult to apply CFRP on both sides of the cracked specimen due to in-accessibility to the other side. Typically, single sided patched specimens are more critical than double sided patched specimens due to the eccentricity induced in case of single sided patched specimen.

Lee and Lee [6] has carried out experimental and analytical study and proposed a successive analysis approach to predict the skewed crack front in case of single sided repaired panel which is important in predicting the exact fatigue life of a cracked specimen. The results indicate that single sided repair technique is effective only in case of thin cracked specimen than thick specimens.

A comparison between single sided and double sided repair technique was carried out by Belhouari et al. [7], Albedah et al. [8]. The difference between the two studies is the shape of the CFRP patch considered. The results are represented in the form of mass gain by the use of the double sided repair over the single sided repair. The results show that the single sided repair is effective only when crack length is less and the difference between double sided repair and single sided repair becomes constant as the patch thickness is increased. The results hold only if bending of plate is not considered due to asymmetric difference in stiffness in case of single sided repair. Experimental study conducted by Schubbe and Mall [9] on asymmetrically repaired center cracked aluminium plate with composite patch shows that fatigue life has increased by four times. It is also observed that there is significant bending due to asymmetric stiffness resulting in non-uniform crack growth across the thickness of repaired panel. Schubbe and Mall [10] has carried out finite element analysis of a cracked thick metallic structure asymmetrically bonded with composite patch using three layer technique and predicted the fatigue crack growth rate on unpatched face to be in good agreement with the experimental result.

Arendt and Sun [11] developed a finite elemental model to study the behaviour of out of plane deformation that occurs in single sided repaired panel. The outcome of the study show that there

is increase in strain energy release rate due to increase in adhesive thickness or decrease in adhesive shear modulus and this results in usage of adhesive with less thickness and higher shear modulus. It is also observed that, crack instability occurs due to asymmetric repair. Another study, carried out by Achour et al. [12] on repair of crack at notches by numerical analysis show that, there is decrease in SIF of about 80% due to the presence of patch and the properties like adhesive shear modulus and its thickness should be optimized for effective repair. Bachir et al. [13] has studied the effect of patch size, adhesive properties and crack length on SIF. From their study it is clear that as the crack length increases, its effect on SIF is nominal. The range after which there is no effect on SIF depends on the adhesive properties and patch dimensions.

A parameter called effective stress intensity factor ( $K_{mod}$ ) in case of single sided patch repair method has been developed by Duong and Wang [14].  $K_{mod}$  is dependent on  $K_{min}$ ,  $K_{max}$ ,  $K_{mean}$ ,  $K_{rms}$ ,  $K_b$  (SIF due to bending) and it is validated with test results. Wang et al. [15] has proposed an upper limit of root mean square of the SIF along the crack front and it showed good agreement with the finite element results. Their results indicate that usage of thicker reinforcement is better in reducing the out of plane bending. A comparison between different fatigue crack retardation methods has been done by Domazet [16] and the results show that use of CFRP and cold worked crack stop holes has been proved to be more effective in arresting the cracks. Song and Shieh [17] has carried out work on crack stop holes. Their results show that by drilling a hole of size 3mm the fatigue life has been increased to 443% and 174% in case of aluminium alloy and stainless steel respectively. From the literature it is clear that there is a need to study the combined action of crack stop hole and CFRP application as a repair technique.

## 2.2 Geometry and finite element model

The specimen geometry is taken from the experimental work of Barsom and Nicol [18] and modified from double edge notch specimen to central crack specimen to model the effect of crack stop hole. The dimensions of the specimen are given in Table 1 and its geometry is shown in the Fig. 3.

The magnitudes of loads applied are 41.2 MPa (6 ksi), 62 MPa (9 ksi), 82.7 MPa (12 ksi), 103.4 MPa (15 ksi) which were reported as loads that the bridge girders are generally subjected to as given in [19]. The connection between CFRP, steel plate and CFRP, adhesive, shown in Fig. 4 are modeled using bonded contact. In bonded contact, contacting surfaces are assumed to be glued together throughout the analysis. To create bonded contact, contact and target elements needs to be defined on the faces of elements, where they come into contact. In this study multi point

constraint (MPC) algorithm is used for bonded contact. CFRP laminate is modeled as an orthotropic material. The CFRP material properties are taken from [20] and in the present study, the eight different layers of CFRP (expressed in terms of stiffness ratio) are varied ranging from 0 to 10 layers. The thickness of the lamina reported in the reference is 0.375mm and CFRP patch length ( $l$ ) is taken as 127 mm based on the numerical study by Zhao [21]. The properties of composite lamina and adhesive are given in the Table 2.

Incremental meshing as given in [22] is employed around the hole (Fig. 5) to capture the sharp stress gradient because the value of stress at the edge of the hole is sensitive to element size. The number of elements used around the hole is 6 elements in thickness direction, 20 elements in radial direction and 48 elements in angular direction. Although the applied loads are less than the yield stress of steel, localized yielding occurs at crack tip. Therefore, to take into account the local yielding behavior, a nonlinear Finite Element Analysis (FEA) is carried out in this research work using ANSYS 12.0 software. The material model used for Steel is Multi Linear Isotropic hardening as shown in Fig. 6. For modeling all components (i.e. steel plate, adhesive, and CFRP plate) Solid 186 element is used. Solid 186 element has mid side nodes and it performs better in stress singularity regions and for nonlinear analysis.

## **2.3 Results and discussion**

This numerical study is aimed at studying the combined action of crack stop hole and asymmetrically bonded CFRP patch in arriving at appropriate crack stop hole radius when subjected to static tensile load. In addition, the variation of peel stress at CFRP edge with SR and load is also studied.

### **2.3.1 NSIF Calculation**

From literature it is observed that the existing equations for crack stress intensity factor given by Creagor and Paris [3] was unconservative due to the fact that it does not take into account the characteristic distance ( $X_c$ ) from the hole edge up to which the stress remains constant and the linear decrease in stress at a gradient ( $\alpha$ ) thereafter. To overcome the above problem, the stress intensity factor was calculated using NSIF (Eq. 5) proposed by Boukharouba et al. [4]), which includes the effect of  $X_c$  and  $\alpha$ . The output from FEA is used to determine  $X_c$  and  $\alpha$  needed to evaluate NSIF using Eq. 5.

$$K_I = \sigma_{yy}(X_c) * \sqrt{2\pi} \left( X_c + \frac{\rho}{2} \right)^\alpha \quad (5)$$

Where,  $\sigma_{yy}$ = Stress at characteristic distance  $X_c$ ,  $\rho$ = Radius of the notch and  $\alpha$ = Stress gradient. Figure 7 shows typical variation in stress ahead of a crack stop hole in log-log plot for one particular case (2 inch crack length, 82.7 MPa loading, 9.525 mm (3/8 inch) hole radius, without CFRP).

Having established the importance of NSIF, the combined action of CFRP patches and crack stop hole is studied numerically by carrying out nonlinear FEA. The parameter used for comparison of results obtained from nonlinear analysis is  $K_I / \rho^\alpha$ . The results were expressed as a variation of  $K_I / \rho^\alpha$  with stiffness ratio and crack stop hole radius.

In asymmetrically bonded CFRP specimen, eccentricity to load path is developed that leads to bending of the specimen. The bending results in compression (patched side) on one side of the specimen caused reduced SIF while the tension (unpatched) side of the specimen experiences increase in SIF. Therefore, N-SIF is calculated on two surfaces (patched and unpatched sides) of specimen to elucidate the difference in the SIF reduction due CFRP.

### 2.3.2 Effect of stiffness ratio (SR) and crack stop hole radius ( $\rho$ ) on $K_I / \rho^\alpha$

Stiffness ratio (SR) is defined as the ratio of axial stiffness of composite plate to axial stiffness of steel plate (Eq.6). It is assumed that the axial load is transferred in the ratio of their stiffness.

$$SR = \frac{t_{CFRP} E_{CFRP}}{t_{Steel} E_{Steel}} \quad (6)$$

Figure 8 shows the variation of  $K_I / \rho^\alpha$  with stiffness ratio calculated on patched side (includes specimen without patch) for a crack length of 25.4 mm (1 inch) and for applied loads of 41.2 MPa, 62 MPa, 82.7 MPa and 103.4 MPa. In general, it can be observed that there is a decrease in  $K_I / \rho^\alpha$  with increase in stiffness ratio of up to 0.4 (5 layers) after which there is a slight increase of  $K_I / \rho^\alpha$  with stiffness ratio. This is due to excessive bending towards CFRP patch causing opening of the crack. In addition, it is obvious from Figs. 8a (41.2 MPa), 8b (62 MPa) and 8c (82.7 MPa) that the effect of first two to three layers are significant as can be seen from the steepness of the curves whereas with increase in number of layers (stiffness ratio), the percentage reduction in  $K_I / \rho^\alpha$  decreases as shown by the flattening of the curve. In Fig. 8d (103.4 MPa) it can be observed that there is a kink in  $K_I / \rho^\alpha$  curves corresponding to crack stop hole radii from



3.175 to 7.874 mm for stiffness ratio less than 0.1. The kink in  $K_I/\rho^\alpha$  curves for smaller crack stop hole radii indicates that for higher applied stress of 103.4 MPa, lesser number of layers is not sufficient to cause a reduction in  $K_I/\rho^\alpha$ . Whereas when the stiffness ratio crosses beyond 0.1, the stiffness of CFRP is sufficient enough to cause a reduction in  $K_I/\rho^\alpha$ . Such a situation does not arise for a crack stop hole radius of 9.525 mm since a larger radius hole increases the size of the blunt (cracks with lessened sharpness) thereby preventing an increase in  $K_I/\rho^\alpha$ .

Figure 9 shows the variation of  $K_I/\rho^\alpha$  with stiffness ratio calculated on unpatched side (includes specimen w/o patch) for a crack length of 1" and for applied loads of 41.2 MPa, 62 MPa, 82.7 MPa and 103.4 MPa. It is obvious from Fig. 9 that there is no effect of SR on  $K_I/\rho^\alpha$ , since the crack closure effect due CFRP is very little on the unpatched side. Whereas it can be observed that there is a decrease in value of  $K_I/\rho^\alpha$  due to increase in crack stop hole radii. The behavior for other crack lengths (1.5", 2" and 2.5") is observed to be same as that of 1" crack length.

Through thickness variation of  $K_I/\rho^\alpha$  in steel plate for the case of 25.4 mm (1 inch) crack, 6.35 mm (0.25 inch) crack stop hole radii, 82.7 Mpa applied load and for different SR is shown in Fig. 10. The values of  $K_I/\rho^\alpha$  shown in Fig. 10 are calculated at a distance of 0\*T, 0.25\*T, 0.5\*T, 0.75\*T, 1\*T from unpatched side, where T is the thickness of steel plate. From Fig. 10 it is clear that as the number of CFRP layers are increasing the value of  $K_I/\rho^\alpha$  through thickness is decreasing and there is no effect of CFRP on unpatched side. After a SR of 0.32 it can be observed that the value of  $K_I/\rho^\alpha$  on patched side is not decreasing indicating saturation and that the additional CFRP layers are ineffective.

To account for through thickness variation of  $K_I/\rho^\alpha$  (Fig. 10), the parameter, root mean square value is calculated as given in Eq. 7.

$$K_{rms} = \sqrt{\frac{(K_{min})^2 + (K_{min} * K_{max}) + (K_{max})^2}{3}} \quad (7)$$

Equation 7 was proposed by Wang et al. [15], where  $K_{rms}$ ,  $K_{min}$  and  $K_{max}$  are respectively the root mean square, minimum and maximum SIF values of a specimen. The calculated values of  $K_{rms}$  for 25.4 mm (1 inch) crack length case is shown in Fig. 11. From the figure it can be observed that the behavior of root mean square value of  $K_I/\rho^\alpha$  with increase in SR is similar to  $K_I/\rho^\alpha$  of patched side (Fig. 8). It can also be observed that the root mean square value of  $K_I/\rho^\alpha$  is decreasing with increase of crack stop hole radii similar to Fig.8.

### 2.3.3 Reduction Factor (RF)

To account for the effect of CFRP patch in stress reduction, a reduction factor (RF) is introduced.

$$Reduction\ factor = \frac{(K_I / \rho^\alpha)_{with\ CFRP}}{(K_I / \rho^\alpha)_{w/o\ CFRP}} \quad (8)$$

The value of RF for patched side under different loads, crack length and crack stop hole radii is given in tables 3 to 6. It can be observed that with increase in SR there is a decrease in  $K_I / \rho^\alpha$  value. In addition, it can also be observed that with increase in load, the reduction in the value  $K_I / \rho^\alpha$  decreases since the number of CFRP layers used is not sufficient for reducing the stress intensity at the crack location. The percentage reduction in value of  $K_I / \rho^\alpha$  for SR of 0.8 is around 65% to 20% for loads varying from 41.2 MPa to 103.4 MPa. It should be noted that the RF values on unpatched side are not presented, since the difference observed in the value of  $K_I / \rho^\alpha$  on the unpatched side is not significant compared to that of bare steel specimen.

The RF factor is function of stiffness ratio (SR), applied load ( $\sigma_{applied}$ ), crack stop hole radius ( $\rho$ ) and crack length ( $2a$ ). This factor could be incorporated in Eq. 5 given by Boukharouba et al. (1995) as shown below:

$$K_I = [\sigma_{yy}(X_c) * \sqrt{2\pi} \left(X_c + \frac{\rho}{2}\right)^\alpha] * RF \quad (9)$$

For  $0 \leq SR \leq 0.80$

$$RF = a (SR^5) + b (SR^4) + c (SR^3) + d (SR^2) + e (SR) + 1 \quad (10)$$

Where, RF = Reduction Factor and SR = Stiffness Ratio

Eq. 10 is formulated such that the RF becomes unity when the SR becomes zero. This means that with no CFRP patches, Eq.9 merges with the original equation (Eq.5) provided by Boukharouba et al. (1995). The variables  $a, b, c, d$  and  $e$  are the coefficients of Eq. 10, dependent on  $\sigma_{applied}$ ,  $2a$  and  $\rho$  as given in Eq. 11.

$$\begin{aligned} & p0 + p1 * x + p2 * z + p3 * y + p4 * z * x + p5 * x * y + p6 * y * z + p7 * x * \\ & y * z + p8 * x^2 + p9 * y^2 + p10 * z^2 + p11 * (x^2) * y + p12 * (x^2) * z + p13 * \\ & (y^2) * x + p14 * (y^2) * z + p15 * (z^2) * x + p16 * (z^2) * \\ & y \end{aligned} \quad (11)$$

Note: In Eq.11 the variables  $x, y$  and  $z$  represent  $2a, \rho$  and  $\sigma_{applied}$  respectively. The coefficients of Eq. 11 vary with  $a, b, c, d$  and  $e$  as shown in Table 7. It should be noted that Eq.11 is empirical and the units of load, radius and crack length are in MPa, mm and mm respectively.

### 2.3.4 Effect of SR and load on peel stress

Peel stress ( $\sigma_{zz}$ ) at the CFRP edge causes de-bonding of CFRP from the specimen, due to large stiffness difference between adhesive and CFRP. In this research work, a study on peel stress for different loads and CFRP thicknesses (SR) has been carried out. The variation of peel stress has

been studied along the X-X and Y-Y lines as shown in Fig. 12. Figure 13 shows the variation of peel stress at CFRP edge along the line x-x for 4 different loads and 8 different SR's. From Fig. 13 it can be observed that as the number of CFRP layers increases, the magnitude of peel stress also increases until a SR of 0.56 beyond which the specimen starts bending (concaving towards CFRP side) resulting in a decrease in peel stress. Figure 14 shows the variation in peel stress for 4 different loads for SR of 0.08 (lowest) and 0.80 (highest). It is obvious from Fig. 14 that an increase in load causes an increase in peel stress. In addition, the peel stress variation along the line Y-Y is shown in Fig.15. From the plot it can be observed that there is a spike in peel stress at the CFRP edge due to sudden change in stiffness and with increase in SR, the magnitude of peel stress is increasing till SR of 0.56 and decreasing afterwards. It should be noted that the variation in peel stress shown in Figs 13-15 were based on a crack length of 1 inch and 0.25 inch crack stop hole radius.

## 2.4 Numerical example illustrating the usage of proposed equation

Two numerical examples are given illustrating the usage of the proposed equation and describing the effect of crack stop hole radii and SR.

### 2.4.1 Example 1

Consider a load of 34.4 MPa (5 ksi) acting on a specimen with center crack of length 2". The steel and CFRP properties and dimensions are the same as considered in this paper. The site conditions are such that the maximum radius of hole that can be drilled is 4mm. Determine the number of CFRP layers required to arrest the crack.

*Solution:* The solution to the problem is carried out in a step by step format as shown below: 1. Calculate  $K_I/\rho^a$  of a bare steel specimen and plot the variation of the same with respect to various crack stop hole radii (0.375" to 1/32") as shown in Fig. 16.

2. Plot the threshold line given by Barsom (1985) (Eq. 4) in the same plot of  $K_I/\rho^a$  versus crack stop hole radii to determine the threshold radius. The threshold radius in this case is 6mm which is greater than the 4mm hole that can be drilled at site necessitating the need to reinforce the crack with CFRP patch to prevent crack re-initiation.

3. Now, as a start assume that 1 layer of CFRP patch is required with a crack stop hole radii of 3 mm.

4. Input the parameters  $2a$  (50.8 mm),  $\rho$  (3 mm) and  $\sigma_{applied}$  (34.4 MPa) in Eq.11 and determine coefficients  $a$  through  $e$  by using corresponding  $p0$  through  $p16$  for each coefficient using Table 7.

5. Using the coefficients  $a$  through  $e$  obtained from Step 4 and  $SR$  from Eq. 6, calculate  $RF$  using Eq. 10. The  $RF$  value comes to around 0.391.

6. From Fig. 16, the value of  $K_I/\rho^a$  of a bare steel specimen with crack stop hole radius of 3 mm is approximately 600 MPa. The corresponding value of specimen reinforced with 1 CFRP layer will be 234.6 MPa ( $0.391 \times 600$ ).

7. The reduced  $K_I/\rho^a$  value (234.6 MPa) is now compared with  $10\sqrt{\sigma_{ys}}$  (477 MPa). This value (477 MPa) is greater than reduced  $K_I/\rho^a$  value (234.6 MPa) which indicates that 1 layer of CFRP with 3 mm radius will not result in crack re-initiation. Since the site conditions in the problem permit up to 4mm crack stop hole radius, the assumed 1 layer of CFRP reinforcement with 3 mm crack stop hole radius (undersized) is valid.

A nonlinear FEA carried out for the above conditions ( $2a = 50.8$  mm,  $\rho = 3$ mm,  $SR = 0, 0.08$ , load = 34.4mm) and calculated  $K_I/\rho^a$  for bare steel specimen and patched specimen with 1 layer are respectively 591 MPa and 269 MPa, which indicate that the  $RF$  value is 1, 0.456 respectively. It can be observed that the difference is -14.6% between proposed equation and FEA indicating the accuracy of the proposed equation.

#### 2.4.2 Example 2

Consider a load of 51.7 MPa (7.5 ksi) acting on a specimen with center crack of length ( $2a$ ) 44.45 mm (1.75"). The steel and CFRP properties and dimensions are the same as considered in this paper. The site conditions are such that the maximum radius of hole that can be drilled is 10mm. Determine the number of CFRP layers required to arrest the crack.

*Solution:* The solution to the problem is carried out in a step by step format as shown below: 1. Figure 17 is plotted based on steps 1 and 2 in Ex.1.

2. Unlike Ex.1, there is no intersection between the threshold line and the bare steel specimen curve obtained from FEA indicating that a CFRP patch is mandatory (crack stop hole alone is not enough) to reduce the SIF.

3. From the given conditions, as a start it is assumed that 1 layer of CFRP patch with a crack stop hole radii of 9.525 mm is required to arrest a crack.

4. Input the parameters  $2a$  (44.45 mm),  $\rho$  (9.525 mm) and  $\sigma_{applied}$  (51.7 MPa) in Eq.11 and determine coefficients  $a$  through  $e$  by using corresponding  $p0$  through  $p16$  for each coefficient using Table 7.

5. Using the coefficients  $a$  through  $e$  obtained from Step 4 and  $SR$  from Eq. 6, calculate  $RF$  using Eq. 10. The  $RF$  value comes to around 0.5091.

6. From Fig. 17, the value of  $K_I/\rho^a$  of a bare steel specimen with crack stop hole radius of 9.525 mm is approximately 577 MPa. The corresponding value of specimen reinforced with 1 CFRP layer will be 293.75 MPa ( $0.5091*577$ ).

7. The reduced  $K_I/\rho^a$  value (293.75 MPa) is now compared with  $10\sqrt{\sigma_{ys}}$  (477 MPa). This value (477 MPa) is greater than reduced  $K_I/\rho^a$  value (293.75 MPa) which indicates that 1 layer of CFRP with 9.525 mm radius will not result in crack re-initiation. Since the site conditions in the problem permit up to 10 mm crack stop hole radius, the assumed 1 layer of CFRP reinforcement with 9.525 mm crack stop hole radius is valid.

8. The steps from 3 to 7 are repeated for the case of 5 layers of CFRP. Five layers of CFRP is used in this example to demonstrate that higher factor of safety can be achieved for the problem under consideration. The corresponding RF value comes out to be 0.3858.

9.  $K_I/\rho^a$  value corresponding to specimen reinforced with 5 CFRP layers will be 222.6 MPa ( $0.3858*577$ ).

A nonlinear FEA carried out for the above conditions ( $2a = 44.45$  mm,  $\rho = 9.525$  mm,  $SR = 0, 0.08, 0.4$  and load = 51.7 MPa). The values calculated for  $K_I/\rho^a$  of bare steel specimen and patched specimen with 1, 5 layers are 577.66 MPa, 296.2 MPa and 231.09 MPa, respectively. The corresponding RF values are 1, 0.51 and 0.4 respectively. It can be observed that the difference is 0.71% and 3.5% between proposed equation and FEA for a SR of 0.08 and 0.4 respectively, indicating the accuracy of the proposed equation.

## 2.5 CONCLUSIONS

This numerical study focuses on fracture mechanics approach to evaluate the effectiveness of the combined action of crack stop hole and asymmetrically bonded CFRP patch. The studies indicate that there is a significant reduction in  $K_I/\rho^a$  on patched side by using CFRP patch, the value of which reaches a minimum and then exhibits asymptotic behavior with increase in SR. This means that the effectiveness of a CFRP patch ceases to reduce the SIF when the additional thickness due to loading eccentricity results in excessive bending of the specimen.

While the bending hinders the decrease in SIF due to additional CFRP layers, it aids in decreasing the peel stress after reaching a certain stiffness ratio (prior to which the peel stress was increasing due to SR) as a result of concaving (bending of specimen) on the patched side. In addition, although it was also observed that the effect of increasing the size of crack stop hole lead to a reduction in SIF on both patched and unpatched side, the effect due CFRP was insignificant on the unpatched side behaving more or less similar to bare steel specimen.

A parametric study was carried out for various crack stop hole radii, stiffness ratio and magnitude of loads. A total of 640 nonlinear FEA (Tables 3-6) was carried out and the results of this study were curve fit to arrive at a reduction factor at the patched side. This reduction factor in terms of  $\rho$ ,  $2a$ , SR and  $\sigma_{applied}$  to include the effect of CFRP patch was used to modify the equation proposed by Boukharouba et al. [4]. The applicability of the developed reduction factor demonstrated using numerical examples indicate that there might be situations when it becomes mandatory to use CFRP patch since drilling a hole to reduce the stress at the crack tip is not a viable option (non-intersection between Eq. 4 and FE results for crack stop hole radius).

## REFERENCES

- [1] Shield C, Hajjar J, Nozaka K. Repair of fatigued steel bridge girders with carbon fiber strips. Report no-MN/RC-2002-04, Minnesota Department of Transportation, 2004.
- [2] Irwin GR. Analysis of stresses and strains near the end of a crack transversing a plate. Transactions, ASME, Journal of applied Mechanics 1957; 25: 361-364.
- [3] Creager M, and Paris PC. Elastic field equations for blunt cracks with reference to stress corrosion cracking. International Journal of Fracture Mechanics 1967; 3(4): 247-252.
- [4] Boukharouba T, Tamine T, Niu L, Chehimi C, Pluvinage G. The use of notch stress intensity factor as a fatigue crack initiation parameter. Engineering Fracture Mechanics 1995; 52(3): 503-512.
- [5] Barsom JM. Fracture Mechanics – Fatigue and Fracture 1985. Metals Handbook – Desk 398 Edition, American Society for Metals, Metals Park, Ohio.
- [6] Lee WY, Lee JJ, Fatigue behavior of composite patch repaired aluminium plate. Journal of Composite Material 2005; 39(16): 1449–1463.
- [7] Belhouari M, Bachir BB, Megueni M, Kaddouari K. Comparison of double and single bonded repairs to symmetric composite structures: a numerical analysis. Composite Structures 2004; 65: 47–53.
- [8] Albedah A, Bachir BB, Mhamdia R, Benyahia F, Es-Saheb M. Comparison between double and single sided bonded composite repair with circular shape. Materials and Design 2011; 32: 996–1000.
- [9] Schubbe JJ, Mall S. Investigation of a Cracked Thick Aluminum Panel Repaired with a Bonded Composite Patch. Engineering Fracture Mechanics 1999; 63: 305–323.
- [10] Schubbe JJ, Mall S. Modeling of Cracked Thick Metallic Structure with Bonded Composite Patch Repair using Three-layer Technique. Composite Structures 1999; 45: 185–193.

- [11] Arendt C, Sun CT. Bending Effects of Unsymmetric Adhesively Bonded Composite Repairs on Cracked Aluminum Panels. NASA CP 3274 1994; 33–48.
- [12] Achour T, Bachir BB, Serier B. Numerical analysis of the performance of the bonded composite patch in reducing stress concentration and repairing crack at notch. *Computational Material Science* 2003; 28: 41–48.
- [13] Bachir BB, Belhouari M, Serier B. Computation of the stress intensity factors for patched cracks with bonded composite repairs in mode I and mixed mode. *Composite Structures* 2002; 56: 401–406.
- [14] Duong CN, Wang CH. On the characterization of fatigue crack growth in a plate with a single-sided repair. *Transactions of the ASME, Journal of Engineering Materials and Technology* 2004; 126 (2): 192–198.
- [15] Wang CH, Rose LRF, Callinan R. Analysis of out-of-plane bending in one-sided bonded repair. *International Journal of Solids and Structures* 1998; 35(14): 1653–1675.
- [16] Domazet Z. Comparison of fatigue crack retardation methods. *Engineering Failure Analysis* 1996; 3 (2): 137–147.
- [17] Song PS, Shieh Y L. Stop drilling procedure for fatigue life improvement. *International Journal of Fatigue* 2004; 26(12): 1333–1339.
- [18] Barsom JM, McNicol RC. Effect of stress concentration on fatigue-crack initiation in HY-130 Steel. *Fracture Toughness and Slow-Stable Cracking* 1974; 4STM STP 559, 402 American Society for Testing and Materials: 183-204.
- [19] Fisher JW, Barthelemy BM, Mertz DR, Edinger JA. Fatigue behaviour of full scale welded bridge attachments. NCHR 12-15(3), March 1980 (80-29), Fritz Laboratory Reports, 1980.
- [20] Ramji M, Srilakshmi R, Bhanu Prakash M. Towards optimization of patch shape on the performance of bonded composite repair using FEM. *Composites: Part B* 2012; 45(1): 710–720.
- [21] Zhao XL, Zhang L. State-of-the-art review on FRP strengthened steel structures. *Engineering Structures* 2007; 29 (8): 1808–1823.
- [22] Nakmura T, Parks DM. Antisymmetrical 3D stress field near the crack front of a thin elastic plate. *International Journal of Solids and Structures* 1989; 25 (12): 1411-1426.





- Figure 2.1:** (a) Specimen with crack, (b) Specimen with crack and crack stop hole
- Figure 2.2:** Plot representing usage of equation proposed by Barsom [5] to arrive at optimum crack stop hole radii
- Figure 2.3:** Schematic representation of the specimen
- Figure 2.4:** Typical FE mesh of specimen
- Figure 2.5:** Circular meshing around the crack stop hole
- Figure 2.6:** Stress strain curve of steel
- Figure 2.7:** Stress distribution ahead of crack stop hole
- Figure 2.8:**  $K_I / \rho^\alpha$  versus SR on patched side for 25.4 mm (1 inch) crack length at different loads (a) 41.2 MPa, (b) 62 MPa, (c) 82.7 MPa and (d) 103.4 MPa
- Figure 2.9:**  $K_I / \rho^\alpha$  versus SR on unpatched side for 25.4 mm (1 inch) crack length at different loads (a) 41.2 MPa, (b) 62 MPa, (c) 82.7 MPa and (d) 103.4 MPa
- Figure 2.10:** Through thickness variation of  $K_I / \rho^\alpha$  of the specimen with different SR having a crack of 25.4 mm (1 inch), 6.35 mm (0.25 inch) crack stop hole radii and for an applied load of 82.7 MPa load
- Figure 2.11:**  $(K_I / \rho^\alpha)_{rms}$  versus SR for 25.4 mm (1 inch) crack length at different loads (a) 41.2 MPa, (b) 62 MPa, (c) 82.7 MPa and (d) 103.4 MPa
- Figure 2.12:** Schematic representation of the lines considered for peel stress distribution
- Figure 2.13:** Variation of peel stress in X-X direction for 25.4 mm (1 inch) crack length at different loads (a) 41.2 MPa, (b) 62 MPa, (c) 82.7 MPa and (d) 103.4 MPa
- Figure 2.14:** Variation of peel stress in X-X direction for 25.4 mm (1 inch) crack length at different SR (a) 0.08 and (b) 0.8
- Figure 2.15:** Variation of peel stress along Y-Y direction for 25.4 mm (1 inch) crack length at different loads (a) 41.2 MPa, (b) 62 MPa, (c) 82.7 MPa and (d) 103.4 MPa
- Figure 2.16:**  $K_I / \rho^\alpha$  versus crack stop hole radius of bare steel specimen having a crack of 50.8 mm (2 inch) for 34.4 MPa load
- Figure 2.17:**  $K_I / \rho^\alpha$  versus crack stop hole radius of bare steel specimen having a crack of 44.45 mm (1.75 inch) for 51.7 MPa load

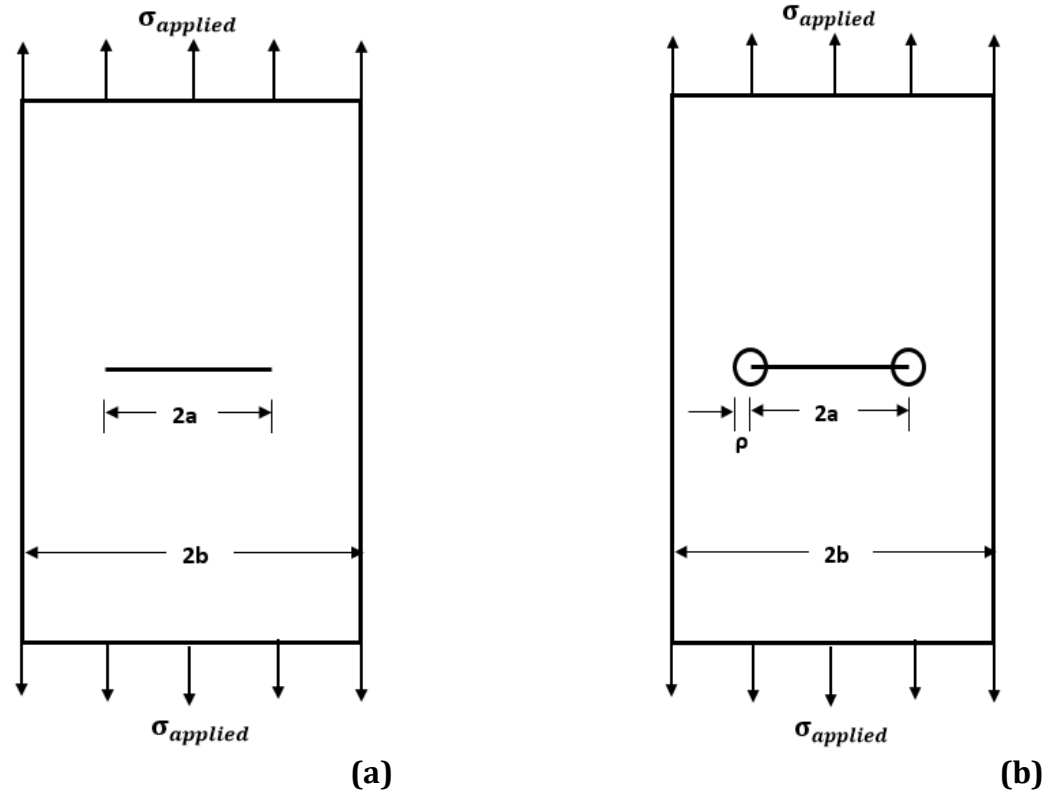


Figure 2.1: (a) Specimen with crack, (b) specimen with crack and crack stop hole

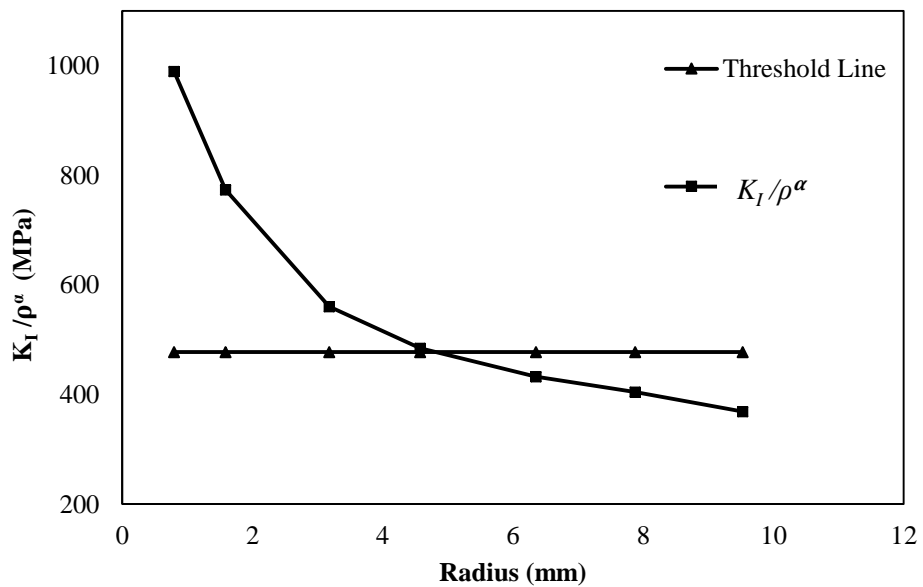


Figure 2.2: Calculation of optimum crack stop hole radii

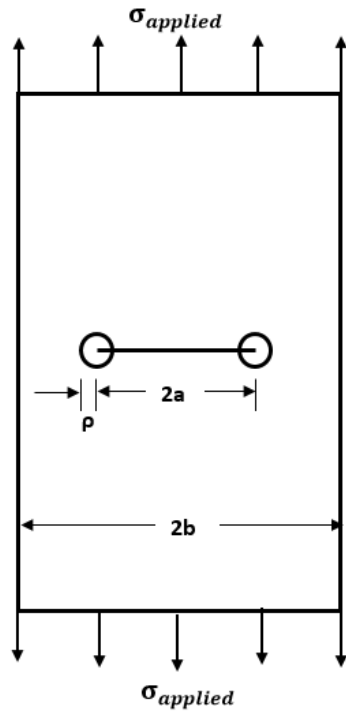
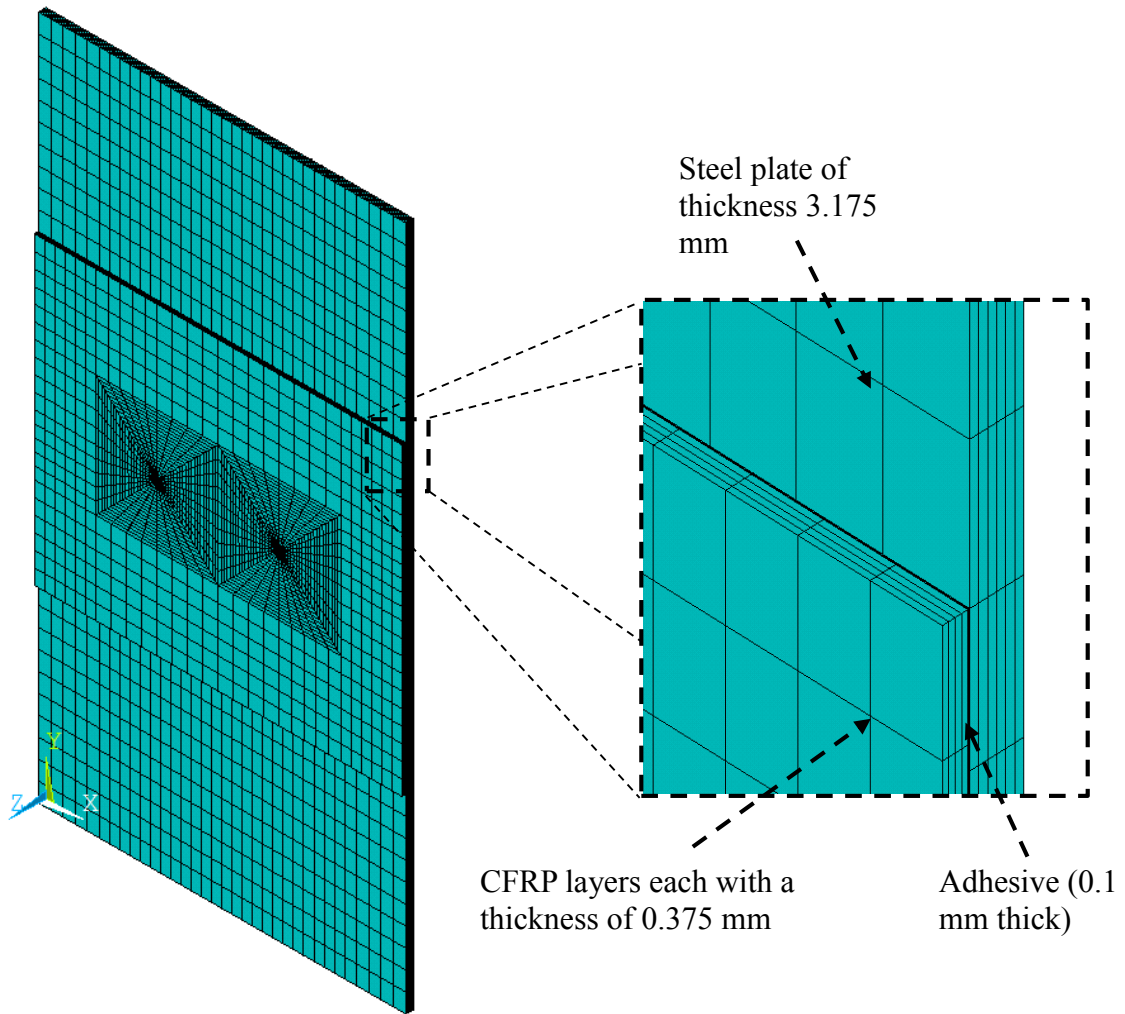
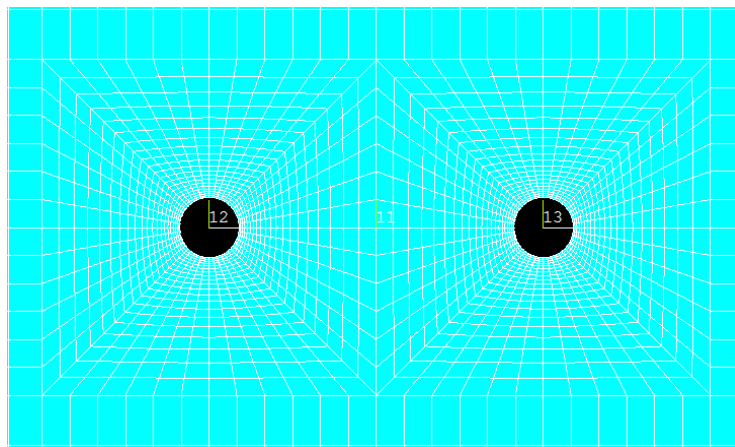


Figure 2.3: Specimen geometry



**Figure 2.4: Typical FE mesh of the specimen with asymmetrically bonded CFRP**



**Figure 2.5: Mesh around the crack stop hole**

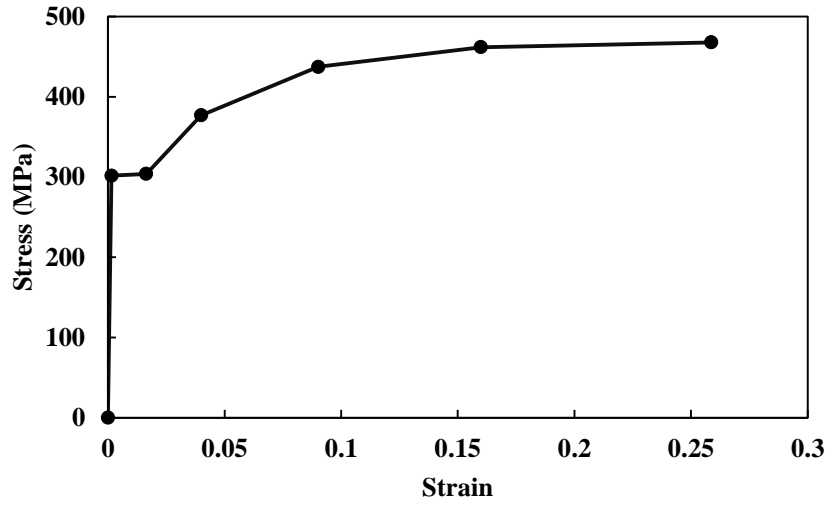


Figure 2.6: Stress strain curve for steel

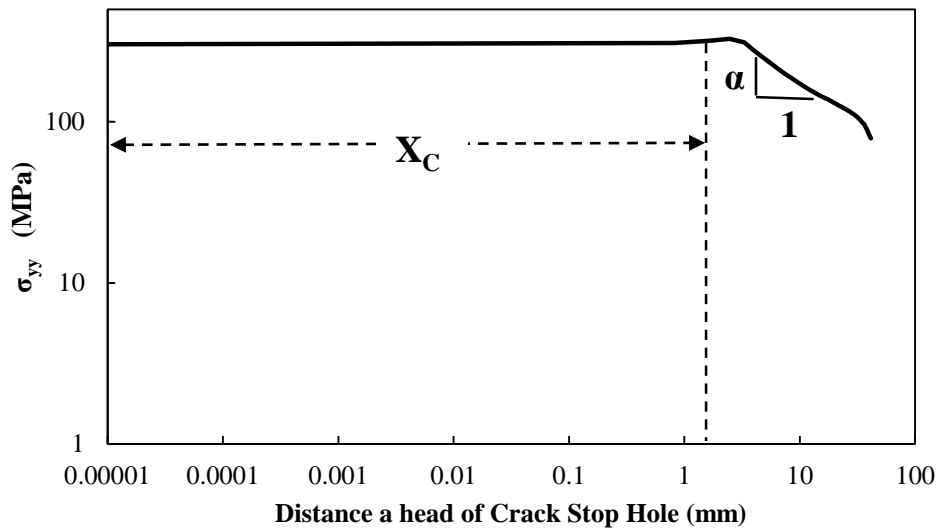
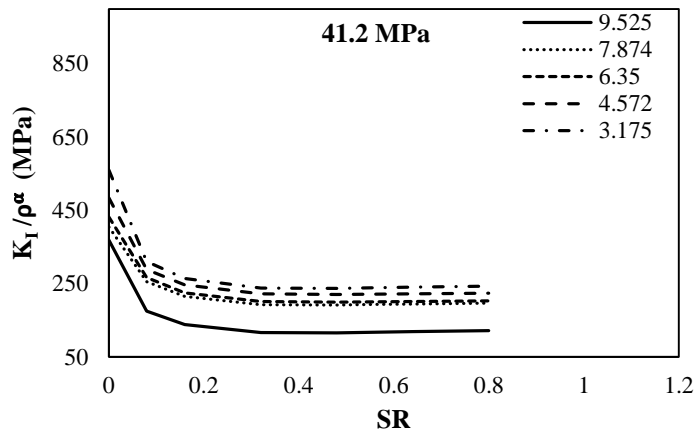
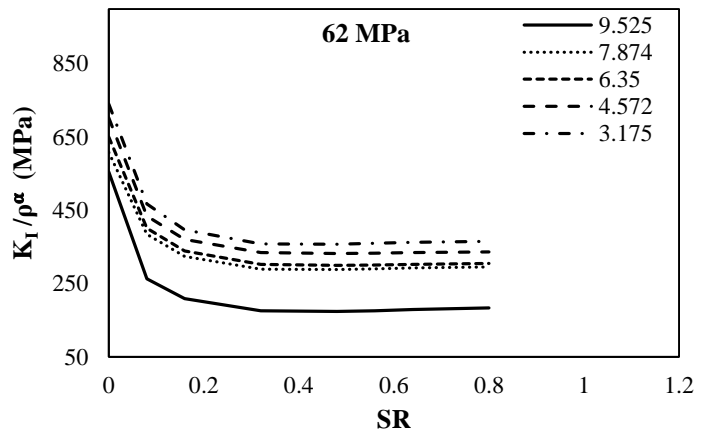


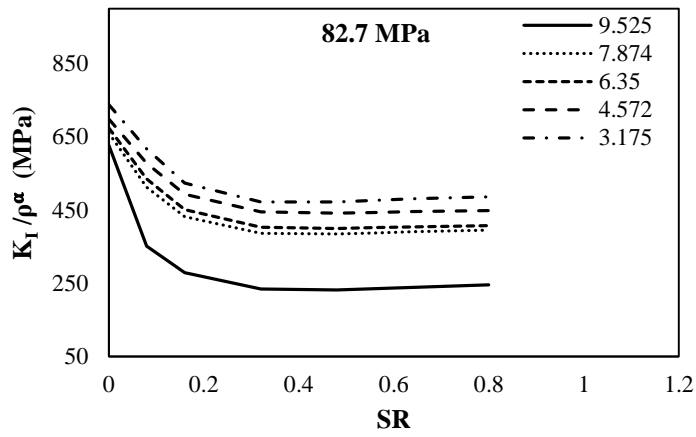
Figure 2.7: Stress distribution ahead of crack stop hole



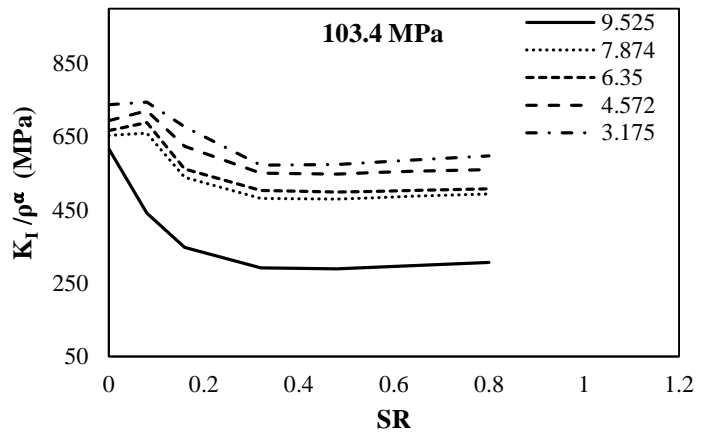
(a)



(b)

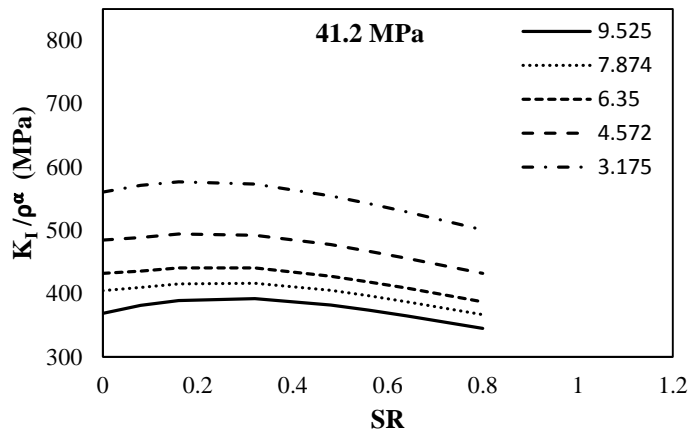


(c)

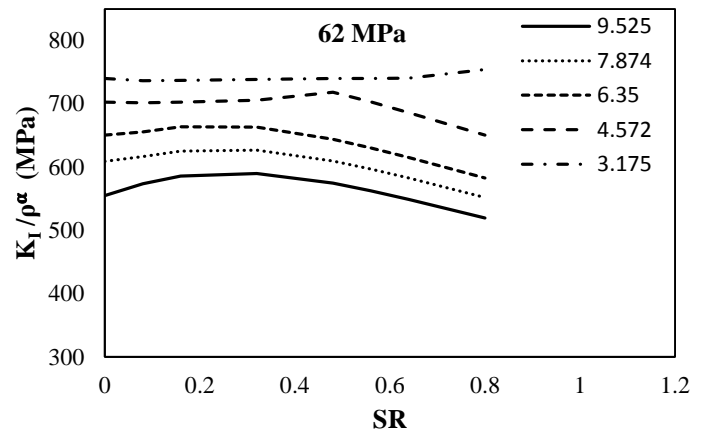


(d)

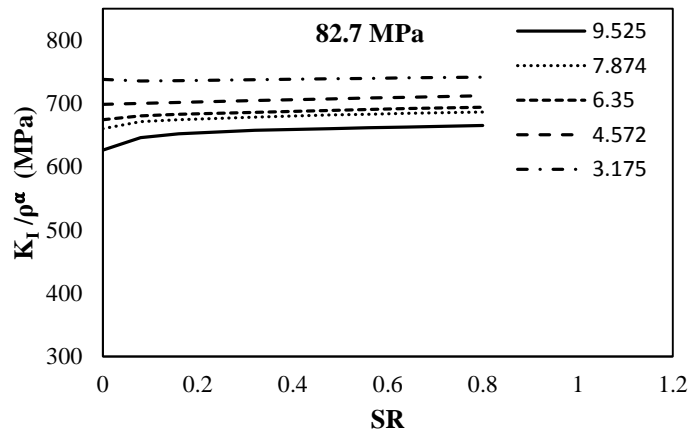
Figure 2.8:  $K_I/\rho^\alpha$  versus SR on patched side for 1" crack length at different loads (a) 41.2 MPa, (b) 62 MPa, (c) 82.7 MPa and (d) 103.4 MPa



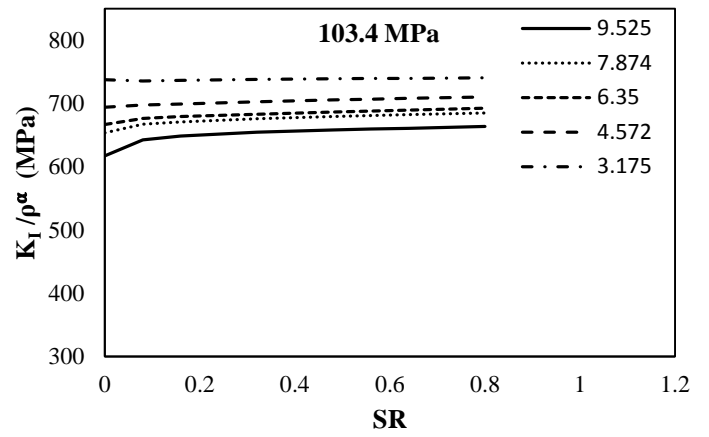
(a)



(b)



(c)



(d)

**Figure 2.9:  $K_I/\rho^\alpha$  versus SR on unpatched side for 1" crack length at different loads (a) 41.2 MPa, (b) 62 MPa, (c) 82.7 MPa and (d) 103.4 MPa**

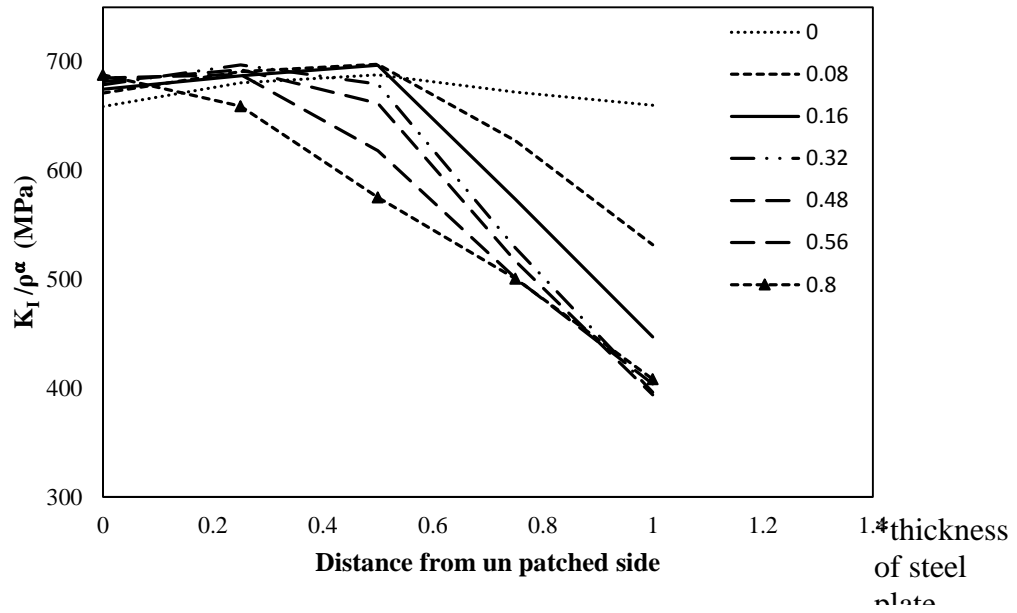
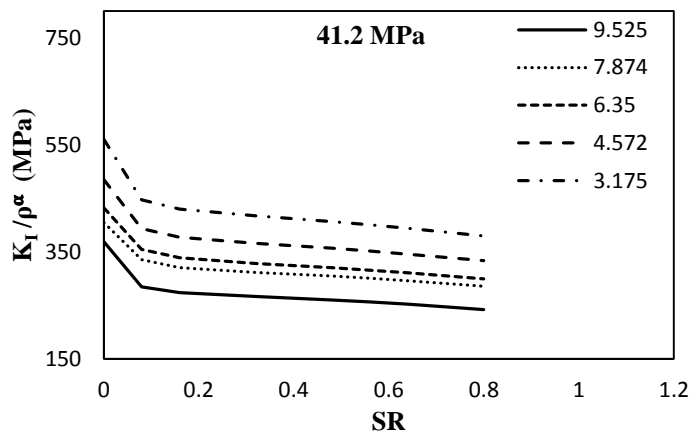
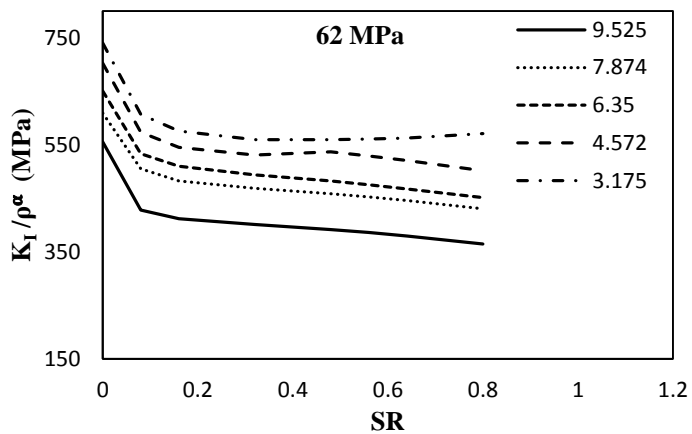


**Figure 2.10: Through thickness variation of  $K_I / \rho^\alpha$  of the specimen with different SR having a crack of 25.4 mm (1 inch), 6.35 mm (0.25 inch) crack stop hole radii and for an applied load of 82.7 MPa load**

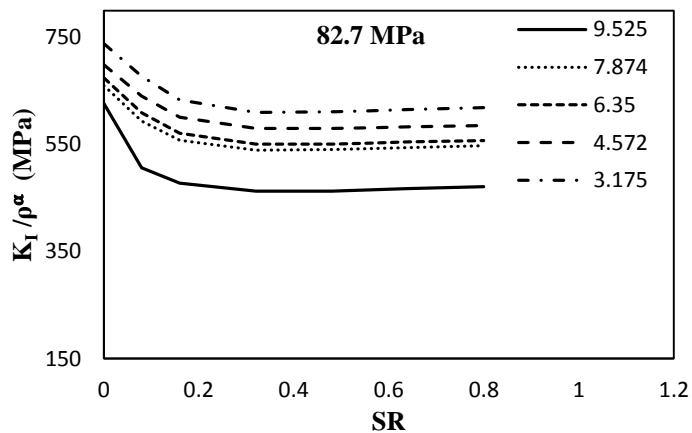




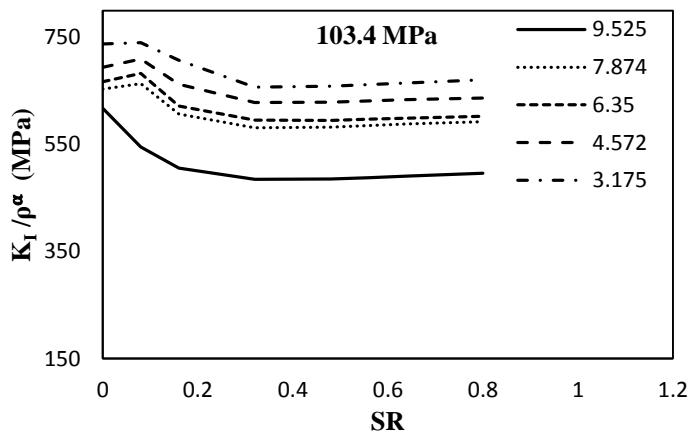
(a)



(b)



(c)



(d)

Figure 2.11:  $(K_I/\rho^\alpha)_{rms}$  versus SR for 1" crack length at different loads (a) 41.2 MPa, (b) 62 MPa, (c) 82.7 MPa and (d) 103.4 MPa

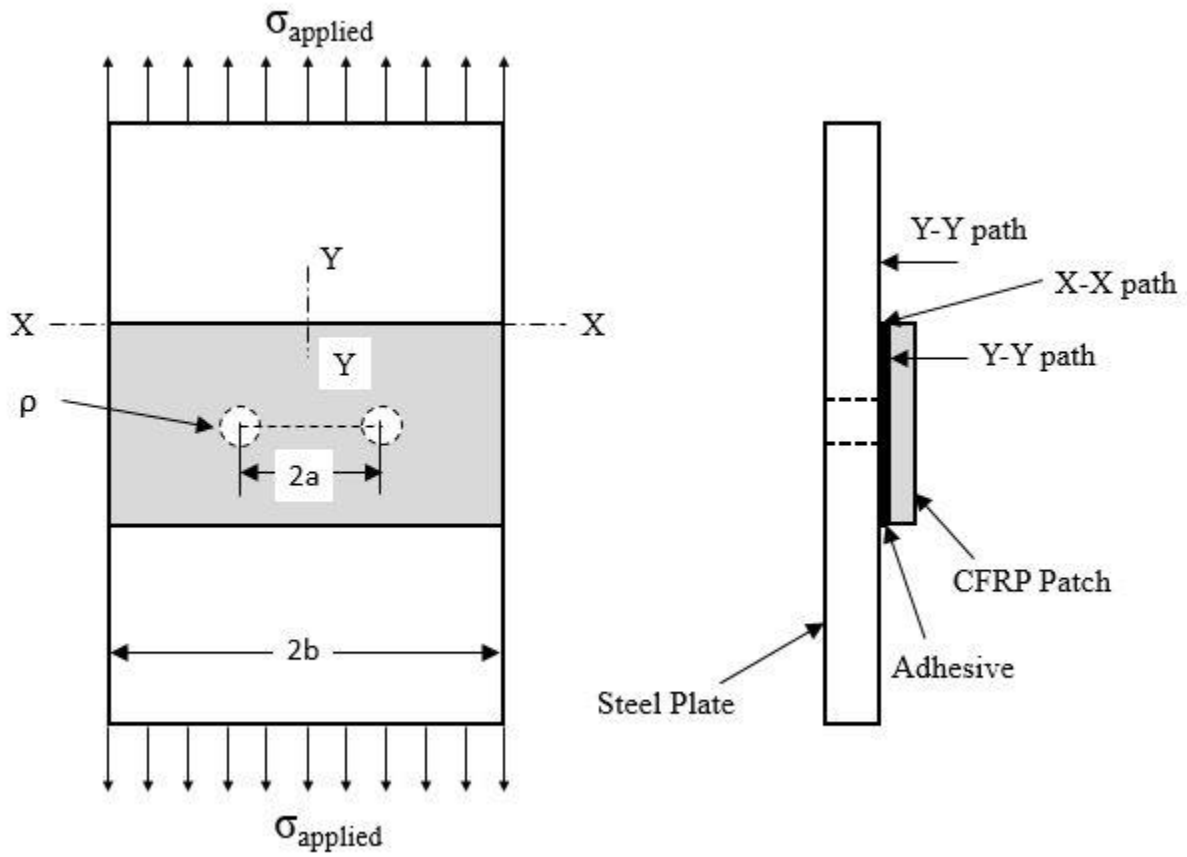
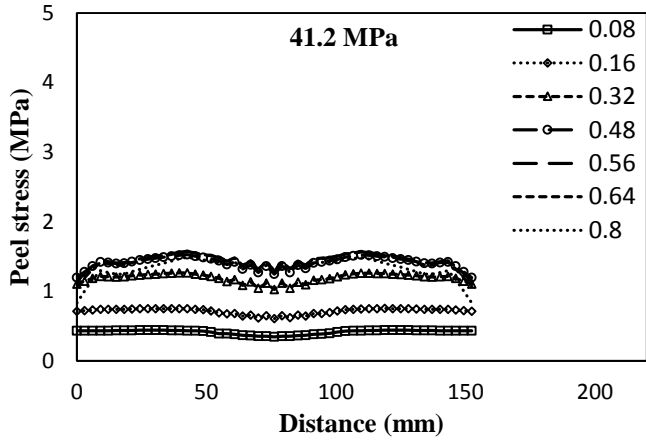
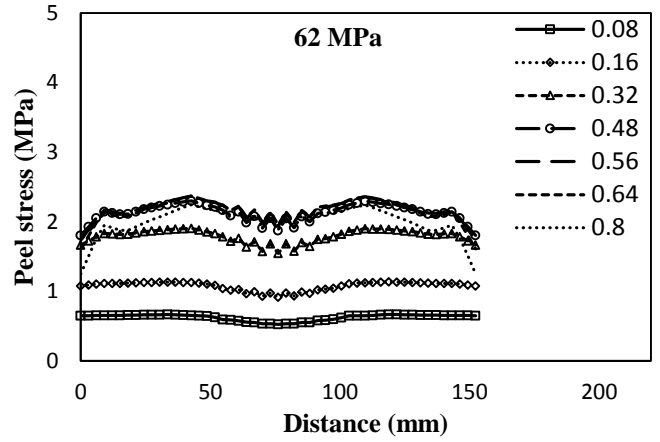


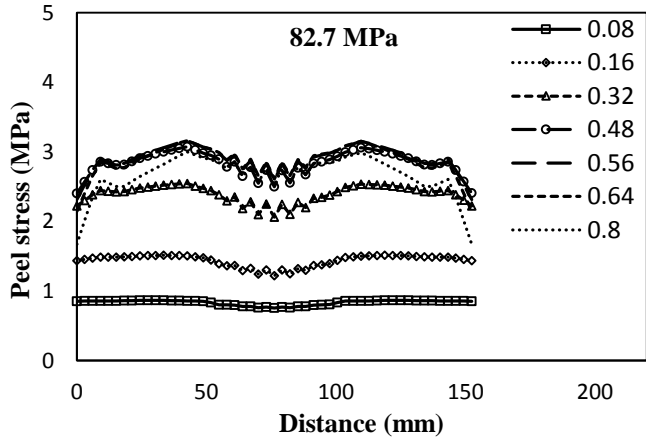
Figure 2.12: Schematic representation of the lines considered for peel stress distribution



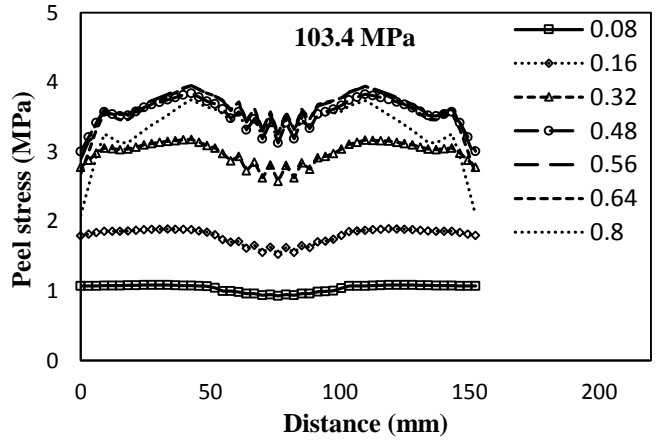
(a)



(b)

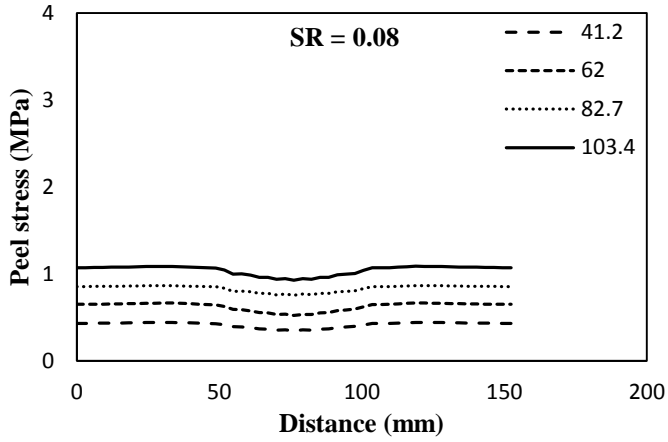


(c)

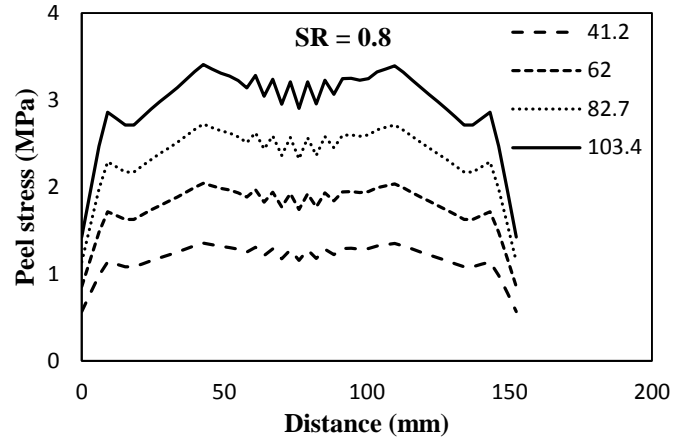


(d)

Figure 2.13: Variation of peel stress in X-X direction for 1" crack length at different loads (a) 41.2 MPa, (b) 62 MPa, (c) 82.7 MPa and (d) 103.4 MPa

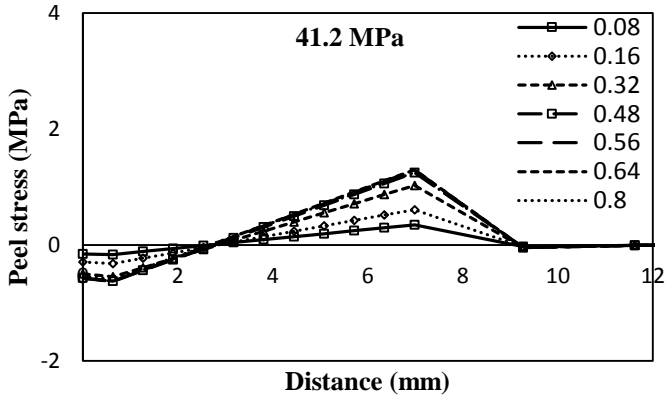


(a)

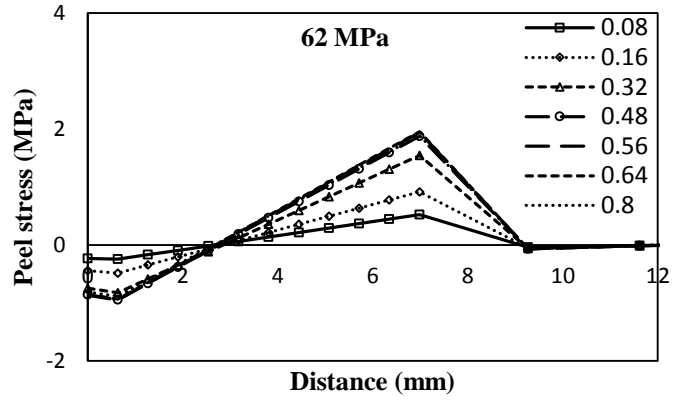


(b)

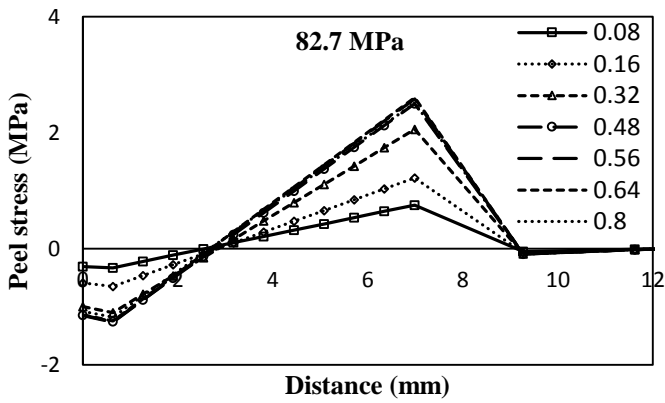
**Figure 2.14: Variation of peel stress in X-X direction for 1" crack length at different SR (a) 0.08 and (b) 0.80**



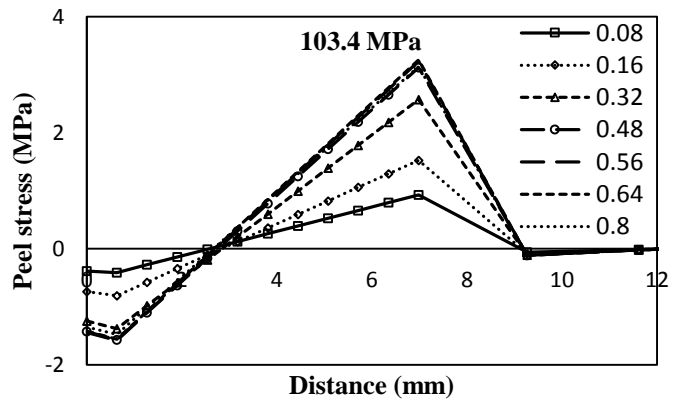
(a)



(b)



(c)



(d)

Figure 2.15: Variation of peel stress along Y-Y direction for 1” crack length at different loads (a) 41.2 MPa, (b) 62 MPa, (c) 82.7 MPa and (d) 103.4 MPa

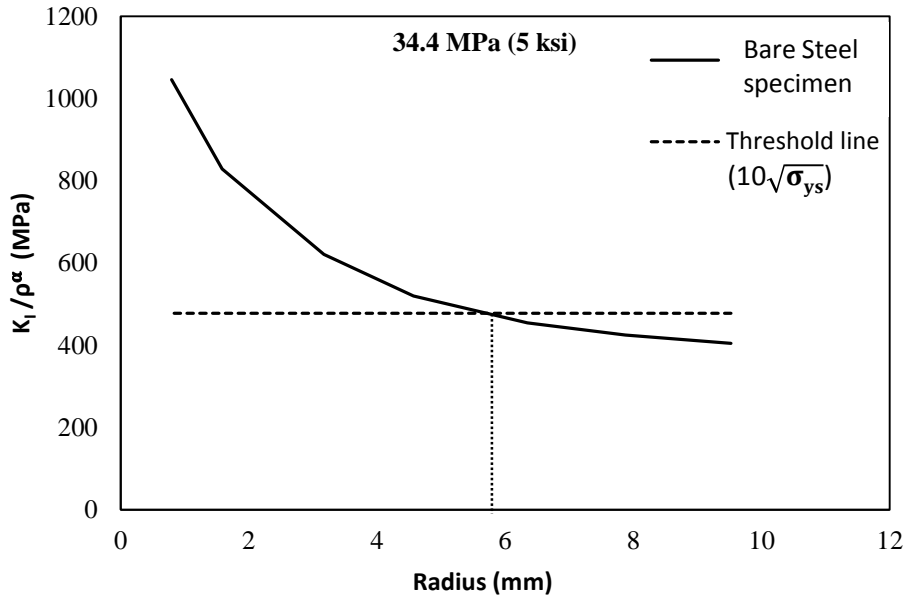


Figure 2.16:  $K_I/\rho^\alpha$  versus crack stop hole radius of bare steel specimen having a crack of 2” for 34.4 MPa load

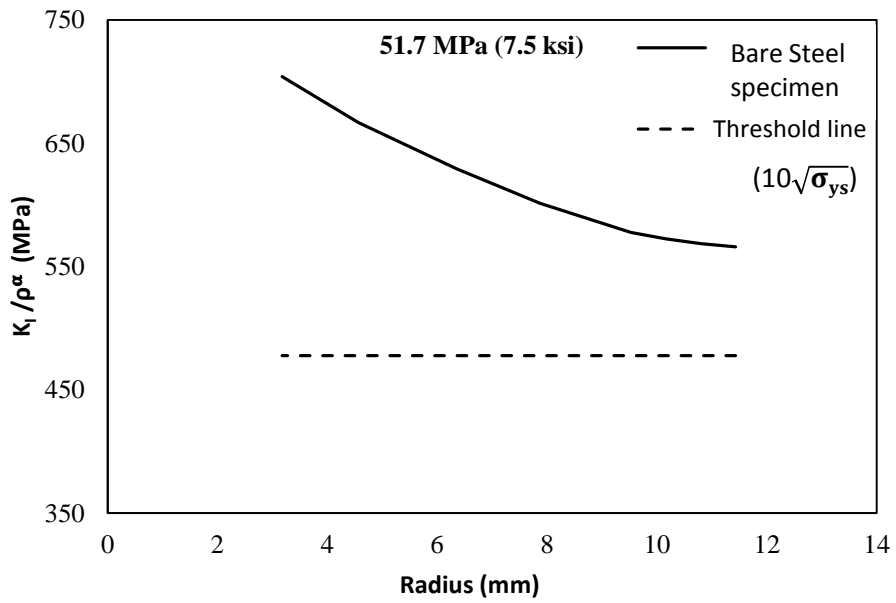


Figure 2.17:  $K_I/\rho^\alpha$  versus crack stop hole radius of bare steel specimen having a crack of 1.75” for 51.7 MPa load

<b>Sl. no.</b>	<b>Title</b>
2.1	Comparison between $K_I/\sqrt{\rho}$ Vs $K_I/\rho^\alpha$
2.2a	Steel material property used in this study
2.2b	CFRP and adhesive material properties used in this study
2.3	Dimensions of the specimen
2.4	Comparison between $K_I/\sqrt{\rho}$ and $K_I/\rho^\alpha$ for different loads and radius of a bare steel specimen (2” crack)
2.5a	RF Values at 41.2 MPa Load for different Crack Length, Crack Stop Hole Radius and SR
2.5b	RF Values at 62 MPa Load for different Crack Length, Crack Stop Hole Radius and SR
2.5c	RF Values at 82.7 MPa Load for different Crack Length, Crack Stop Hole Radius and SR
2.5d	RF Values at 103.4 MPa Load for different Crack Length, Crack Stop Hole Radius and SR
2.6	Variation of p0 to p8 with Coefficients a, b, c, d and e

**Table 2.1: Specimen details**

Width of the specimen ( $B$ ) mm	152.4 (6")
Height of the specimen ( $L$ ) mm	294.2 (11.5")
Length of the crack( $2a$ ) mm	25.4 (1"),38.1(1.5"), 50.8(2"), 63.5(2.5")
Thickness of the steel plate ( $T$ ) mm	3.175
Radius of the hole( $\rho$ ) mm (in.)	9.525 (3/8) 7.874 (5/16) 6.35 (2/8) 4.572 (3/16) 3.175 (1/8)

**Table 2.2: CFRP and Adhesive Material Properties**

<b>Material</b>	<b>Adhesive</b>	<b>CFRP</b>
$E_x$ (Gpa)	4.97	135
$E_y$ (Gpa)	-	9
$E_z$ (Gpa)	-	9
$G_{xy}$ (Gpa)	-	5
$G_{zy}$ (Gpa)	-	8
$G_{zx}$ (Gpa)	-	5
$\nu_{xy}$	0.47	0.3
$\nu_{zy}$	-	0.02
$\nu_{zx}$	-	0.3



**Table 2.3. RF Values at 41.2 MPa Load for different Crack Length, Crack Stop Hole Radius and SR**

Crack Length (mm)	Radius (mm)	41.2 MPa							
		SR							
		0	0.08	0.16	0.32	0.48	0.56	0.64	0.8
25.4	3.175	1.00	0.55	0.47	0.43	0.42	0.43	0.43	0.43
	4.572	1.00	0.60	0.51	0.46	0.46	0.46	0.46	0.46
	6.35	1.00	0.62	0.52	0.47	0.46	0.46	0.47	0.47
	7.874	1.00	0.63	0.53	0.48	0.47	0.48	0.48	0.49
	9.525	1.00	0.48	0.38	0.32	0.31	0.32	0.32	0.33
38.1	3.175	1.00	0.50	0.44	0.41	0.42	0.42	0.43	0.43
	4.572	1.00	0.49	0.43	0.44	0.48	0.49	0.51	0.52
	6.35	1.00	0.53	0.46	0.45	0.48	0.50	0.51	0.52
	7.874	1.00	0.56	0.47	0.43	0.44	0.44	0.44	0.44
	9.525	1.00	0.43	0.35	0.32	0.33	0.33	0.33	0.34
50.8	3.175	1.00	0.45	0.40	0.39	0.39	0.40	0.40	0.40
	4.572	1.00	0.44	0.38	0.39	0.42	0.43	0.43	0.44
	6.35	1.00	0.48	0.42	0.40	0.41	0.41	0.42	0.42
	7.874	1.00	0.49	0.42	0.40	0.41	0.42	0.42	0.42
	9.525	1.00	0.46	0.38	0.38	0.41	0.43	0.44	0.45
63.5	3.175	1.00	0.51	0.46	0.47	0.48	0.49	0.49	0.48
	4.572	1.00	0.43	0.39	0.39	0.40	0.41	0.41	0.41
	6.35	1.00	0.41	0.36	0.36	0.38	0.38	0.38	0.38
	7.874	1.00	0.42	0.37	0.37	0.38	0.38	0.38	0.38
	9.525	1.00	0.34	0.30	0.29	0.31	0.32	0.32	0.32

**Table 2.4. RF Values at 62 MPa Load for different Crack Length, Crack Stop Hole Radius and SR**

Crack Length (mm)	Radius (mm)	62 MPa							
		SR							
		0	0.08	0.16	0.32	0.48	0.56	0.64	0.8
25.4	3.175	1.00	0.63	0.54	0.48	0.48	0.49	0.49	0.49
	4.572	1.00	0.62	0.53	0.48	0.47	0.47	0.48	0.48
	6.35	1.00	0.62	0.52	0.47	0.46	0.46	0.47	0.47
	7.874	1.00	0.63	0.53	0.48	0.47	0.48	0.48	0.49
	9.525	1.00	0.48	0.38	0.32	0.31	0.32	0.32	0.33
38.1	3.175	1.00	0.68	0.59	0.56	0.57	0.57	0.58	0.58
	4.572	1.00	0.61	0.53	0.55	0.59	0.61	0.62	0.64
	6.35	1.00	0.60	0.52	0.51	0.55	0.56	0.58	0.59
	7.874	1.00	0.60	0.51	0.47	0.47	0.48	0.48	0.48
	9.525	1.00	0.45	0.37	0.34	0.34	0.35	0.35	0.35
50.8	3.175	1.00	0.67	0.59	0.58	0.59	0.60	0.60	0.60
	4.572	1.00	0.64	0.56	0.58	0.61	0.62	0.63	0.63
	6.35	1.00	0.63	0.55	0.53	0.54	0.55	0.55	0.55
	7.874	1.00	0.62	0.53	0.51	0.52	0.53	0.53	0.53
	9.525	1.00	0.57	0.47	0.46	0.50	0.52	0.53	0.55
63.5	3.175	1.00	0.74	0.68	0.70	0.73	0.73	0.74	0.73
	4.572	1.00	0.65	0.59	0.60	0.62	0.63	0.63	0.63
	6.35	1.00	0.63	0.56	0.56	0.58	0.59	0.59	0.59
	7.874	1.00	0.62	0.55	0.54	0.56	0.57	0.57	0.57
	9.525	1.00	0.49	0.42	0.42	0.45	0.46	0.46	0.47

**Table 2.5. RF Values at 82.7 MPa Load for different Crack Length, Crack Stop Hole Radius and SR**

Crack Length (mm)	Radius (mm)	82.7 MPa							
		SR							
		0	0.08	0.16	0.32	0.48	0.56	0.64	0.8
25.4	3.175	1.00	0.84	0.71	0.64	0.64	0.65	0.65	0.66
	4.572	1.00	0.83	0.71	0.64	0.63	0.64	0.64	0.64
	6.35	1.00	0.79	0.67	0.60	0.59	0.60	0.60	0.60
	7.874	1.00	0.78	0.65	0.59	0.58	0.59	0.59	0.60
	9.525	1.00	0.56	0.44	0.37	0.37	0.38	0.38	0.39
38.1	3.175	1.00	0.91	0.77	0.73	0.75	0.76	0.77	0.77
	4.572	1.00	0.83	0.74	0.77	0.83	0.85	0.86	0.87
	6.35	1.00	0.81	0.71	0.71	0.75	0.77	0.79	0.80
	7.874	1.00	0.82	0.69	0.64	0.64	0.64	0.65	0.65
	9.525	1.00	0.61	0.50	0.45	0.46	0.47	0.47	0.48
50.8	3.175	1.00	0.91	0.80	0.72	0.75	0.76	0.77	0.78
	4.572	1.00	0.88	0.75	0.78	0.83	0.84	0.85	0.85
	6.35	1.00	0.85	0.74	0.72	0.74	0.74	0.75	0.75
	7.874	1.00	0.84	0.73	0.70	0.72	0.72	0.73	0.73
	9.525	1.00	0.80	0.68	0.67	0.72	0.74	0.75	0.77
63.5	3.175	1.00	0.77	0.70	0.71	0.72	0.72	0.72	0.71
	4.572	1.00	0.66	0.59	0.60	0.59	0.60	0.61	0.61
	6.35	1.00	0.64	0.57	0.55	0.57	0.58	0.58	0.58
	7.874	1.00	0.68	0.57	0.57	0.59	0.60	0.60	0.60
	9.525	1.00	0.52	0.45	0.46	0.48	0.49	0.49	0.50

**Table 2.6. RF Values at 103.4 MPa Load for different Crack Length, Crack Stop Hole Radius and SR**

Crack Length (mm)	Radius (mm)	103.4 MPa							
		SR							
		0	0.08	0.16	0.32	0.48	0.56	0.64	0.8
25.4	3.175	1.00	1.01	0.92	0.78	0.78	0.79	0.80	0.81
	4.572	1.00	1.04	0.90	0.79	0.79	0.80	0.80	0.81
	6.35	1.00	1.03	0.84	0.75	0.75	0.75	0.76	0.76
	7.874	1.00	1.01	0.83	0.74	0.73	0.74	0.75	0.76
	9.525	1.00	0.72	0.56	0.47	0.47	0.48	0.48	0.50
38.1	3.175	1.00	1.03	1.02	0.97	0.98	0.99	0.99	0.99
	4.572	1.00	1.07	1.06	1.03	1.06	1.06	1.06	1.18
	6.35	1.00	1.06	1.00	0.98	1.04	1.06	1.07	1.07
	7.874	1.00	1.05	0.94	0.82	0.83	0.83	0.84	0.84
	9.525	1.00	0.81	0.66	0.59	0.60	0.61	0.62	0.63
50.8	3.175	1.00	0.97	0.97	0.98	0.99	1.00	1.01	1.02
	4.572	1.00	0.99	1.01	1.04	1.06	1.07	1.07	1.06
	6.35	1.00	1.01	1.00	1.00	1.01	1.01	1.01	1.00
	7.874	1.00	1.02	1.02	0.97	0.98	0.98	0.98	0.95
	9.525	1.00	1.01	0.99	0.97	1.00	1.09	1.08	1.07
63.5	3.175	1.00	0.57	0.57	0.57	0.58	0.58	0.58	0.58
	4.572	1.00	0.54	0.54	0.56	0.58	0.59	0.60	0.61
	6.35	1.00	0.57	0.58	0.60	0.63	0.64	0.65	0.66
	7.874	1.00	0.56	0.56	0.58	0.61	0.62	0.63	0.62
	9.525	1.00	0.60	0.56	0.57	0.56	0.56	0.56	0.55

**Table 2.7. Variation of p0 to p17 with Coefficients a, b, c, d and e**

<b>Coefficients</b>	<b>Coefficients</b>				
	<b>a</b>	<b>b</b>	<b>c</b>	<b>d</b>	<b>e</b>
<b>p0</b>	122.5048	-274.9671	228.3312	-84.3530	12.1584
<b>p1</b>	-16.4458	36.8579	-30.3436	11.1201	-1.6882
<b>p2</b>	-6.8661	15.0436	-12.1666	4.4407	-0.7032
<b>p3</b>	64.2822	-141.7998	114.2317	-40.8409	6.2260
<b>p4</b>	0.4088	-0.8977	0.7210	-0.2571	0.0387
<b>p5</b>	-0.6554	1.3921	-1.0893	0.3925	-0.0684
<b>p6</b>	-0.7378	1.6648	-1.3614	0.4828	-0.0674
<b>p7</b>	0.0038	-0.0089	0.0076	-0.0030	0.0005
<b>p8</b>	0.1413	-0.3220	0.2714	-0.1031	0.0167
<b>p9</b>	-3.4026	7.5153	-6.0635	2.1714	-0.3312
<b>p10</b>	0.0436	-0.0956	0.0770	-0.0276	0.0041
<b>p11</b>	-0.0056	0.0129	-0.0108	0.0039	-0.0005
<b>p12</b>	-0.0021	0.0048	-0.0040	0.0015	-0.0003
<b>p13</b>	0.0735	-0.1596	0.1263	-0.0444	0.0067
<b>p14</b>	-0.0127	0.0256	-0.0188	0.0063	-0.0010
<b>p15</b>	-0.0019	0.0041	-0.0032	0.0011	-0.0001
<b>p16</b>	0.0050	-0.0109	0.0086	-0.0029	0.0004

# CHAPTER 3

## Numerical Studies on Halting inclined Crack Growth using Crack-stop Hole and CFRP Patch

### 3.1 Introduction

Due to fatigue load cracks appear in structural members leading to a rise in stress close to the crack tip. If the cracked specimen is left unrepaired for a long time it leads to sudden failure. To prevent such occurrence, various retrofitting techniques are employed which can be broadly classified into two groups [1]: (a) Local retrofitting techniques which include crack stop holes, peening, Gas Tungsten Arc (GTA) welding that modify the local stress state and (b) Global retrofitting techniques that include strengthening with steel plate or composite laminates. The effect of crack is measured in terms of stress intensity factor SIF ( $K$ ) and those are of three different types  $K_I$ ,  $K_{II}$ ,  $K_{III}$ , depending on the relation between the directions of load applied, crack front and crack propagation as shown in fig. 1 [2]. The objective of any retrofitting fitting method is to reduce the SIF at the crack tip. In the present case, a study on effect of crack stop hole and CFRP patch on halting crack growth when the crack is inclined with respect to loading direction is carried out. When the crack is inclined with respect to loading direction as shown in Fig. 2 it undergoes mixed mode of cracking involving mode I and mode II [3]. But due to presence of crack stop hole mixed mode of cracking turns into mode I cracking and this can be understood by observing the stress contours (Fig. 3) of cracked specimen having an inclined crack ( $0^\circ$ ,  $15^\circ$ ,  $60^\circ$ ) for an applied load of 103.4 MPa. From the Fig. 3 it is obvious that maximum values of  $\sigma_{yy}$  (normal stress) and  $\sigma_{xy}$  (shear stress) are not occurring at same point and it can be observed that the maximum value of  $\sigma_{xy}$  is not changing with crack inclination.

Crack stop holes has been used as a repair technique for years in the field of aircrafts. The expression for SIF ( $K_I$ ) value (Eq. 1) for specimen as shown in Fig. 4a was first provided by Irwin [4]. Creagor and Paris [5] proposed an expression of  $K_I$  (Eq. 2) for specimen with crack and crack stop hole as shown in Fig. 4b.

$$K_I = \sigma_{applied} * \sqrt{\pi a} \quad (1)$$

$$K_I = \frac{\sigma_{y max} * \sqrt{\pi \rho}}{2} \quad (2)$$

The relationship between two terms,  $K_I / \sqrt{\rho}$  and maximum stress at the edge of the hole ( $\sigma_{y \max}$ ) (Eq. 2) given by Creagor and Paris [5] using LEFM concepts is obtained by substituting  $r=\rho/2$  and  $\Theta=0$  in Eq. 4. The expressions (Eqs.3, 4 & 5) represent the stress state at the edge of the notch obtained by shifting the origin to a distance half of the radius ( $\rho/2$ ) behind the crack front as shown in Fig 5.

$$\sigma_x = \frac{K_I}{\sqrt{2\pi r}} \cos \frac{\theta}{2} \left( 1 - \sin \frac{\theta}{2} \sin \frac{3\theta}{2} \right) - \frac{K_I}{\sqrt{2\pi r}} \frac{\rho}{2r} \cos \frac{3\theta}{2} \quad (3)$$

$$\sigma_y = \frac{K_I}{\sqrt{2\pi r}} \cos \frac{\theta}{2} \left( 1 - \sin \frac{\theta}{2} \sin \frac{3\theta}{2} \right) + \frac{K_I}{\sqrt{2\pi r}} \frac{\rho}{2r} \cos \frac{3\theta}{2} \quad (4)$$

$$\tau_{xy} = \frac{K_I}{\sqrt{2\pi r}} \cos \frac{\theta}{2} \left( \sin \frac{\theta}{2} \sin \frac{3\theta}{2} \right) - \frac{K_I}{\sqrt{2\pi r}} \frac{\rho}{2r} \sin \frac{3\theta}{2} \quad (5)$$

Equation 2 has been derived based on LEFM approach, but if yielding of material is allowed maximum stress a head of the crack stop hole remains constant for a distance of  $X_c$  which is known as characteristic distance. Substituting  $\theta = 0$  and  $r = X_c + \frac{\rho}{2}$  in Eq. 4 and rearranging the terms as shown below, Eq. 6 is obtained.

$$\sigma_y = \frac{K_I}{(2\pi(X_c + \frac{\rho}{2}))^{\frac{1}{2}}} \left[ 1 + \frac{\rho}{2(X_c + \frac{\rho}{2})} \right]$$

$$\sigma_y = \frac{K_I}{(2\pi(X_c + \frac{\rho}{2}))^{\frac{1}{2}}} \left[ \frac{2X_c + \rho + \rho}{2(X_c + \frac{\rho}{2})} \right]$$

$$\sigma_y = \frac{K_I}{(2\pi(X_c + \frac{\rho}{2}))^{\frac{1}{2}}} \left[ \frac{2(X_c + \rho)}{2(X_c + \frac{\rho}{2})} \right]$$

$$\sigma_y = \frac{K_I}{(2\pi)^{\frac{1}{2}}} \cdot \frac{(X_c + \rho)}{(X_c + \frac{\rho}{2})^{3/2}}$$

$$K_I = \sigma_y (2\pi)^{\frac{1}{2}} \frac{(X_c + \frac{\rho}{2})^{3/2}}{(X_c + \rho)} \quad (6)$$

Later Boukharouba et al. [6] has given expression of  $K_I$  (Eq. 7) for a crack with crack stop hole which is a function of characteristic distance ( $X_c$ ) and stress gradient ( $\alpha$ ) based on his experimental study.

$$K_\rho = \sigma_{yy}(X_c) * \sqrt{2\pi} \left(X_c + \frac{\rho}{2}\right)^\alpha \quad (7)$$

To arrive at the optimum crack stop hole radius Barsom [7], has proposed threshold value of  $K_I / \rho^\alpha$  as given in Eq. 8. Figure 6 shows the usage of the equation proposed by Barsom [7]. It shows the variation of  $K_I / \rho^\alpha$  with crack stop hole radius and intersection of this curve with threshold value given by Barsom [7] leads to optimum crack stop hole radius to be drilled.

$$\frac{K_I}{\sqrt{\rho}} = 10\sqrt{\sigma_{ys}} \quad (8)$$

When the site conditions are such that the maximum size of the hole that can be drilled is less than the optimum crack stop hole radius, the crack may then reinitiate after a few loading cycles. Therefore, an undersized crack stop hole is only a temporary measure or a partial solution which needs to be complemented. One way to reinforce the undersized crack stop hole is by means of carbon fiber reinforced polymer (CFRP) patch which has a high strength to weight ratio. The present study involves analysing the effectiveness of combined action of crack stop hole and bonded CFRP as repair technique.

A comparison between single sided and double sided repair technique was carried out by Belhouari et al. [8], Albedah et al. [9]. The difference between the two studies is the shape of the CFRP patch considered. The results are represented in the form of the mass gain by the use of the double sided repair over the single sided repair. The results show that the single sided repair is effective only when crack length is less and the difference between double sided repair and single sided repair becomes constant as the patch thickness is increased. The results hold only if bending of plate is not considered due to asymmetric difference in stiffness in case of single sided repair. A parameter called effective stress intensity factor ( $K_{mod}$ ) in case of single sided patch repair method has been developed by Duong and Wang [10].  $K_{mod}$  is dependent on  $K_{min}$ ,  $K_{max}$ ,  $K_{mean}$ ,  $K_{rms}$ ,  $K_b$  (SIF due to bending) and it is validated with test results. Wang et al. [11] has proposed an upper limit of root mean square of the SIF along the crack front and it showed good agreement with the finite element results. Their results indicate that usage of thicker reinforcement is better in reducing the out of plane bending. A comparison between different fatigue crack retardation



methods has been done by Domazet [12] and the results show that use of CFRP and cold worked crack stop holes has been proved to be more effective in arresting the cracks. Song and Shieh [13] has carried out work on crack stop holes. The results show that by drilling a hole of size 3mm the fatigue life has been increased to 443% and 174% in case of aluminium alloy and stainless steel respectively. From literature it is clear that there is a need to study the combined action of crack stop hole and CFRP application as a repair technique on inclined crack.

### **3.2 Geometry and FE modelling**

The specimen geometry is taken from the experimental work of Barsom and Nicol [14] and modified from double edge notch specimen to central crack specimen to model the effect of crack stop hole. The dimensions of the specimen are given in Table 1 and its geometry is shown in the Fig. 7.

The magnitudes of loads applied are 41.2 MPa (6 ksi), 62 MPa (9 ksi), 82.7 MPa (12 ksi), 103.4 MPa (15 ksi) which were reported as loads that the bridge girders are generally subjected to as given in [15]. The connection between CFRP, steel plate and CFRP, adhesive, shown in Fig. 8a are modeled using bonded contact. In bonded contact, contacting surfaces are assumed to be glued together throughout the analysis. To create bonded contact, contact and target elements needs to be defined on the faces of elements, where they come into contact. In this study multi point constraint (MPC) algorithm is used for bonded contact. CFRP laminate is modeled as an orthotropic material. The CFRP material properties are taken from [16] and in the present study number of CFRP layers varied are 6 which range from 0 to 8 numbers. The thickness of the lamina reported in the reference is 0.375mm and CFRP patch length ( $l$ ) is taken as 127 mm based on the numerical study by Zhao [17]. The properties of composite lamina and adhesive are given in the Table 2.

Incremental meshing as given in [18] is employed around the hole (Fig. 8b) to capture the sharp stress gradient because the value of stress at the edge of the hole is sensitive to element size. Number of elements used around the hole are 6 elements in thickness direction, 20 elements in radial direction and 48 elements in angular direction.

Although the applied loads are less than the yield stress of steel, localized yielding occurs at crack tip. Therefore, to take into account the local yielding behaviour, a nonlinear Finite Element Analysis (FEA) is carried out in this research work using ANSYS 12.0 software. The material

model used for Steel is Multi Linear Isotropic hardening as shown in Fig. 9. For modeling all components (i.e. steel plate, adhesive, and CFRP plate) Solid 186 element is used. Solid 186 element has mid side nodes and it performs better in stress singularity regions and for nonlinear analysis.

### 3.3 Results and discussion

This numerical study is aimed at studying the combined action of crack stop hole and the CFRP patch in arriving at the appropriate crack stop hole radius, number of CFRP layers when subjected to static tensile load. In addition to NSIF, the variation of peel stress at CFRP edge is also studied. First Section of results deal with the double sided repaired panel and next half deals with single sided repaired panels.

#### 3.3.1 NSIF Calculation

In LEFM frame work, the stress gradient is expressed as a function of  $1/\sqrt{r}$  singularity which indicates that when the radius approaches zero, it behaves like a sharp crack. However, the LEFM assumption is not valid if loading, crack geometry and the specimen thickness leads to yielding at notch tip. So, nonlinear FEA is carried out and NSIF is calculated on obtained results. The output from FEA is used to determine  $X_c$  and  $\alpha$  needed to evaluate  $K_I/\rho^\alpha$  using Eq. 9, which is a modified expression given by Boukharouba et al. [6].

$$\frac{K_I}{\rho^\alpha} = \sigma_{yy}(X_c) * \sqrt{2\pi} \left( \frac{X_c}{\rho} + \frac{1}{2} \right)^\alpha \quad (9)$$

where,  $\sigma_{yy}$ = Stress at characteristic distance  $X_c$ ,  $\rho$ = Radius of the notch and  $\alpha$ = Stress gradient. Figure 10 shows a typical variation in stress ahead of a crack stop hole in a log-log plot for one particular case [45 degrees, 2 inch crack length, 82.7 MPa loading, 9.525 mm (3/8 inch) hole radius, without CFRP]. And the results are expressed in terms of  $K_I/\rho^\alpha$ . Prior studies on CFRP–steel application indicate that CFRP patches are effective in arresting the cracks initiating from the notches. The results were expressed as a variation of  $K_I/\rho^\alpha$  with stiffness ratio and crack stop hole radius.

### 3.3.2 Effect of stiffness ratio (SR) and crack stop hole radii ( $\rho$ ) on $K_I / \rho^\alpha$ in case of symmetrically repaired panel

Stiffness ratio (SR) is defined as the ratio of axial stiffness of composite plate to axial stiffness of steel plate (Eq.10). It is assumed that the axial load is transferred in the ratio of their stiffness.

$$SR = \frac{t_{CFRP} E_{CFRP}}{t_{Steel} E_{Steel}} \quad (10)$$

Figure 11-13 shows the variation of  $K_I / \rho^\alpha$  with stiffness ratio (includes specimen w/o patch) for different crack inclination, crack length of 25.4 mm (1 inch) and for applied load of 41.2 MPa, 62 MPa, 82.7 MPa and 103.4 MPa. In general, it can be observed that there is a decrease in  $K_I / \rho^\alpha$  with an increase in stiffness ratio. The effect of the first two to three layers are significant as can be seen from the steepness of the curves whereas with increase in the number of layers (stiffness ratio), the percentage reduction in  $K_I / \rho^\alpha$  decreases as shown by the flattening of the curve.

### 3.3.3 Effect of SR and load on peel stress in case of symmetrically repaired panel

Peel stress ( $\sigma_{zz}$ ) at the CFRP edge causes debonding of CFRP from the specimen, due to the large stiffness difference between adhesive and CFRP. In this paper a study on peel stress for different loads and CFRP thicknesses (SR) has been carried out. The variation of peel stress has been studied along the X-X and Y-Y lines as shown in Fig. 14. Figure 15 shows the variation of peel stress on CFRP edge along the line x-x for 4 different loads and 5 different SR's of 45° inclined crack. From Fig. 15 it can be observed that as the number of CFRP layers increases, the magnitude of peel stress also increases. Similar observation can be made for Fig. 16 where the peel stress is plotted for 4 different loads with lower (SR = 0.08) and higher (SR = 0.64) SR. In addition, the peel stress variation along the line Y-Y is shown in Fig.17. From the plot it can be observed that there is a spike in peel stress at the CFRP edge due to sudden change in stiffness and with an increase in SR, the magnitude of peel stress also increases. It should be noted that the variation in peel stress shown in Figs 15-17 were based on a crack length of 25.4 mm (1 inch) and 9.525 mm (0.375 inch) crack stop hole radius.

### 3.3.4 Effect of Stiffness Ratio (SR) and Crack Stop Hole Radius ( $\rho$ ) on $K_I / \rho^\alpha$ in case of asymmetrically repaired panel

This numerical study is aimed at studying the combined action of crack stop hole and asymmetrically bonded CFRP patch in arriving at appropriate crack stop hole radius when

subjected to static tensile load. In addition, variation of peel stress at CFRP edge with SR and load is also studied.

In asymmetrically bonded CFRP specimen, eccentricity to load path is developed that leads to bending of the specimen. The bending results in compression (patched side) on one side of the specimen causing reduced SIF while the tension (unpatched) side of the specimen experiences increase in SIF. Therefore, N-SIF is calculated on two surfaces (patched and unpatched sides) of specimen to elucidate the difference in the SIF reduction due CFRP.

Figure 18 to 20 shows the variation of  $K_I/\rho^\alpha$  with stiffness ratio calculated on patched side (includes specimen without patch) for different crack inclination, crack length of 50.8 mm (2 inch) and for applied loads of 41.2 MPa, 62 MPa, 82.7 MPa and 103.4 MPa. In general, it can be observed that there is a decrease in  $K_I/\rho^\alpha$  with increase in stiffness ratio. In addition, it is obvious from Figs. 18 to 20 that there is a decrease in  $K_I/\rho^\alpha$  with increase in crack stop hole radii. From a to d in Figs. 18 to 20 we can observe that the gap between different curves is increasing as we go from 41.2 MPa to 103.4 MPa load. This is because at 41.2 MPa load lesser number of CFRP layers are enough to considerably decrease the value of  $K_I/\rho^\alpha$  than in the case of 103.4 MPa.

Figure 21 to 23 shows the variation of  $K_I/\rho^\alpha$  with stiffness ratio calculated on unpatched side (includes specimen w/o patch) for a crack length of 2 inch, different crack inclinations and for applied loads of 41.2 MPa, 62 MPa, 82.7 MPa and 103.4 MPa. It is obvious from Fig. 21 to 23 that there is very minimal effect of SR on  $K_I/\rho^\alpha$ , since the crack closure effect due CFRP is very little on the unpatched side. Whereas it can be observed that there is a decrease in value of  $K_I/\rho^\alpha$  due to increase in crack stop hole radii.

Through thickness variation of  $K_I/\rho^\alpha$  in steel plate for the case of 50.8 mm (2 inch) crack, 9.525 mm (0.375 inch) crack stop hole radii, 62 Mpa applied load and for different SR, crack inclinations is shown in Fig. 24. The values of  $K_I/\rho^\alpha$  shown in Fig. 24 are calculated at a distance of  $0*T$ ,  $0.25*T$ ,  $0.5*T$ ,  $0.75*T$ ,  $1*T$  from unpatched side, where T is the thickness of steel plate. From Fig. 24 it is clear that as the number of CFRP layers are increasing the value of  $K_I/\rho^\alpha$  through thickness is decreasing and there is no effect of CFRP on unpatched side. As it can be seen from the Fig. 24 that the value of  $K_I/\rho^\alpha$  is varying across the thickness. To account for through thickness variation of  $K_I/\rho^\alpha$  value, root mean square value of  $K_I/\rho^\alpha$  is calculated as given in Eq. 11.

$$K_{rms} = \sqrt{\frac{(K_{min})^2 + (K_{min} * K_{max}) + (K_{max})^2}{3}} \quad (11)$$

Equation 7 is proposed by Wang et al. [15], where  $K_{rms}$ ,  $K_{min}$  and  $K_{max}$  are respectively the root mean square, minimum and maximum SIF values of a specimen. The calculated values of  $K_{rms}$  for 50.8 mm (2 inch) crack length case for different crack inclination is shown in Fig. 25-27. From the figs. it can be observed that the behavior of rms value of  $K_I / \rho^a$  is similar to that of  $K_I / \rho^a$  of patched side (Fig. 18-20). It can also be observed that the rms value of  $K_I / \rho^a$  is decreasing with increase of crack stop hole radii and SR.

### 3.3.5 Effect of SR and load on peel stress in case of asymmetrically repaired panel

Peel stress ( $\sigma_{zz}$ ) at the CFRP edge causes debonding of CFRP from the specimen, due to large stiffness difference between adhesive and CFRP. In this paper a study on peel stress for different loads and CFRP thicknesses (SR) has been carried out. The variation of peel stress has been studied along the X-X and Y-Y lines as shown in Fig. 28. Figure 29 shows the variation of peel stress at CFRP edge along the line x-x for 4 different loads and 5 different SR's for  $45^\circ$  inclined crack. From Fig. 29 it can be observed that as the number of CFRP layers increases, the magnitude of peel stress also increases until SR of 0.48 beyond which the specimen starts bending (concaving towards CFRP side) resulting in a decreasing of peel stress. Figure 30 shows the variation in peel stress for 4 different loads, for SR of 0.08 (lower) and 0.64 (higher). It is obvious from the fig. 30 that an increase in load causes an increase in peel stress. In addition, the peel stress variation along the line Y-Y is shown in Fig.31. From the plot it can be observed that there is a spike in peel stress at the CFRP edge due to sudden change in stiffness and with increase in SR, the magnitude of peel stress is increasing till SR of 0.56 and decreasing afterwards. It should be noted that the variation in peel stress shown in Figs 29-31 were based on a crack length of 2 inch and 0.375 inch crack stop hole radius.

### 3.3.6 Comparison of $K_I / \rho^a$ and peel stress for different crack inclinations

Variation of NSIF and Peel stress with crack inclination is studied to understand the effect of crack inclination on application of CFRP. Fig. 32 shows the variation of  $K_I / \rho^a$  with SR for different crack inclination at different loads and for 2 inch (50.8 mm) crack with 0.375 inch (9.525 mm) crack stop hole radii. From the fig. it can be observed that there is no much variation w.r.t crack inclination this is because the condition of plate with crack has turned in to plate with hole criteria. The variation that is observed in Fig. 32 is quite opposite to the study conducted by Ramji

et al. [16], where it is observed that there is drastic change in value of with crack inclination. This is simply due to the presence of crack stop hole ahead of crack.

Figure 33 shows the variation of peel stress for different crack inclinations, SR of 0.4. From the fig. it can be observed that with increase in crack inclination the peel stress value is increasing in the initial half width portion of specimen and gradually decreasing in the next half portion, this is because of the axial strains increasing in the initial half portion as the crack is moving away from CFRP edge. And vice versa in next half portion of specimen width.

### 3.3.7 Reduction Factor (RF)

To account for the effect of CFRP patch in stress reduction, a reduction factor (RF) is introduced.

$$\text{Reduction factor} = \frac{(K_I / \rho^\alpha) \text{with CFRP}}{(K_I / \rho^\alpha) \text{w/o CFRP}} \quad (12)$$

RF for symmetrically repaired panel case under different conditions is given in table 3a through 3d. In case of asymmetrical repaired panel RF is calculated on patched side and its values are given in table 4a through 4d. It can be observed that with increase in SR there is a decrease in  $K_I / \rho^\alpha$  value. In addition, it can also be observed that with increase in load, the reduction in the value  $K_I / \rho^\alpha$  decreases since the number of CFRP layers used is not sufficient for crack closure. In case of symmetrically repaired panel the percentage reduction in value of  $K_I / \rho^\alpha$  for SR of 0.64 is around 80% to 70% for loads varying from 41.2 MPa to 103.4 Mpa and that in the case of asymmetrically repaired is around 58% to 35% respectively. It should be noted that the RF values on unpatched side in case of asymmetrically repaired panel are not presented, since the difference observed in the value of  $K_I / \rho^\alpha$  on the unpatched side is not significant compared to that of bare steel specimen.

This factor is function of stiffness ratio (SR), applied load ( $\sigma_{applied}$ ), crack stop hole radius ( $\rho$ ) and crack inclination ( $\theta$ ). This factor could be incorporated in Eq. 9 given by Boukharouba et al. (1995) as shown below:

$$\frac{K_I}{\rho^\alpha} = \sigma_{yy}(X_c) * \sqrt{2\pi} \left( \frac{X_c}{\rho} + \frac{1}{2} \right)^\alpha * RF \quad (13)$$

For  $0 \leq SR \leq 0.96$

$$RF = a (SR^5) + b (SR^4) + c (SR^3) + d (SR^2) + e (SR) + 1 \quad (14)$$

Where, RF = Reduction Factor and SR = Stiffness Ratio

Eq. 14 is formulated such that the RF becomes unity when the SR becomes zero. This means that with no CFRP patches, Eq.13 merges with the original equation (Eq.9) provided by Boukharouba

et al. (1995). The variables  $a, b, c, d$  and  $e$  are the coefficients of Eq. 14, dependent on  $\sigma_{applied}$ ,  $\theta$  and  $\rho$  as given in Eq. 15.

$$\begin{aligned}
 & p0 + p1 * x + p2 * z + p3 * y + p4 * z * x + p5 * x * y + p6 * y * z + p7 * x * \\
 & y * z + p8 * x^2 + p9 * y^2 + p10 * z^2 + p11 * (x^2) * y + p12 * (x^2) * z + p13 * \\
 & (y^2) * x + p14 * (y^2) * z + p15 * (z^2) * x + p16 * (z^2) * \\
 & y
 \end{aligned} \tag{15}$$

Note: In Eq.15 the variables  $x, y$  and  $z$  represent  $\theta, \rho$  and  $\sigma_{applied}$  respectively. The coefficients of Eq. 15 vary with symmetrically and asymmetrically repaired case and also with  $a, b, c, d$  and  $e$  as shown in Table 5 and Table 6. It should be noted that Eq.15 is empirical and the units of load and radius are in MPa and mm respectively. Two numerical examples are given illustrating the usage of the proposed equation and describing the effect of crack stop hole radii and SR for the case of symmetrically and asymmetrically repaired panel.

### 3.4 Numerical example illustrating the usage of proposed equation

Two numerical examples are given illustrating the usage of the proposed equation and describing the effect of crack stop hole radii and SR.

#### 3.4.1 Example 1

Consider a load of 62 MPa (9 ksi) acting on a specimen with center crack of length 2" and its inclination is  $30^0$ . The steel and CFRP properties and dimensions are the same as considered in this paper. The site conditions are such that the maximum radius of hole that can be drilled is 10 mm. Determine the number of CFRP layers required to arrest the crack when the site conditions allow to go with symmetric repair of the panel.

*Solution:* The solution to the problem is carried out in a step by step format as shown below: 1. Calculate  $K_I/\rho^a$  of a bare steel specimen and plot the variation of the same with respect to various crack stop hole radii (0.375" to 0.125") as shown in Fig. 34.

2. Plot the threshold line given by Barsom (1985) (Eq. 8) in the same plot of  $K_I/\rho^a$  versus crack stop hole radii to determine the threshold radius. From fig. 34 it can be observed that, crack stop hole alone is not enough to arrest the crack as it is getting flattened approximately after a hole radii of 9.525 mm (3/8 inch). Necessitating the need to reinforce the crack with CFRP patch to prevent crack re-initiation

3. For given conditions, as a start assume that 3 layer of CFRP patch is required with a crack stop hole radii of 7.874 mm (0.31 inch).

4. Input the parameters  $\theta$  (30),  $\rho$  (7.874) and  $\sigma_{applied}$  (62 MPa) in Eq.15 and determine coefficients  $a$  through  $e$  by using corresponding  $p0$  through  $p16$  for each coefficient using Table 5 (symmetrically repaired panel).
5. Using the coefficients  $a$  through  $e$  obtained from Step 4 and  $SR$  (0.24) from Eq. 10, calculate  $RF$  using Eq. 14. The  $RF$  value comes to around 0.409.
6. From Fig. 34, the value of  $K_I/\rho^\alpha$  of a bare steel specimen with crack stop hole radius of 7.874 mm is approximately 612 MPa. The corresponding value of specimen reinforced with 3 CFRP layer will be 250 MPa (0.409\*612).
7. The reduced  $K_I/\rho^\alpha$  value (250 MPa) is now compared with  $10\sqrt{\sigma_{ys}}$  (477 MPa). This value (477 MPa) is greater than reduced  $K_I/\rho^\alpha$  value (250 MPa) which indicates that 3 layer of CFRP with 7.874 mm radius will not result in crack re-initiation. Since the site conditions in the problem permit up to 10 mm crack stop hole radius, the assumed 3 layer of CFRP reinforcement with 7.874 mm crack stop hole radius (undersized) is valid.

A nonlinear FEA carried out for the above conditions ( $\theta= 30^0$ ,  $\rho= 7.874$  mm,  $SR = 0, 0.24$ , load = 62 MPa) and calculated  $K_I/\rho^\alpha$  for bare steel specimen and patched specimen with 3 layer are respectively 612 MPa and 240 MPa, which indicate that the  $RF$  value is 1, 0.3926 respectively. It can be observed that the difference is -4% between proposed equation and FEA indicating the accuracy of the proposed equation.

### 3.4.2 Example 2

Consider a load of 41.2 MPa (6 ksi) acting on a specimen with center crack of length 2" and its inclination is  $30^0$ . The steel and CFRP properties and dimensions are the same as considered in this paper. The site conditions are such that the maximum radius of hole that can be drilled is 8 mm. Determine the number of CFRP layers required to arrest the crack when the site conditions allow to apply patch only on one side.

*Solution:* The solution to the problem is carried out in a step by step format as shown below: 1. Calculate  $K_I/\rho^\alpha$  of a bare steel specimen and plot the variation of the same with respect to various crack stop hole radii (0.375" to 0.125") as shown in Fig. 35.

2. Plot the threshold line given by Barsom (1985) (Eq. 8) in the same plot of  $K_I/\rho^\alpha$  versus crack stop hole radii to determine the threshold radius. The threshold radius in this case is 8.5 mm which is greater than the 8 mm hole that can be drilled at site, necessitating the need to reinforce the crack with CFRP patch to prevent crack re-initiation.



3. Now, as a start assume that 2 layer of CFRP patch is required with a crack stop hole radii of 6.35 mm (0.25 inch).
4. Input the parameters  $\theta$  (30),  $\rho$  (6.35) and  $\sigma_{applied}$  (62 MPa) in Eq.15 and determine coefficients  $a$  through  $e$  by using corresponding  $p0$  through  $p16$  for each coefficient using Table 6 (asymmetrically repaired panel).
5. Using the coefficients  $a$  through  $e$  obtained from Step 4 and  $SR$  (0.16) from Eq. 10, calculate  $RF$  using Eq. 14. The  $RF$  value comes to around 0.4551.
6. From Fig. 35, the value of  $K_I/\rho^\alpha$  of a bare steel specimen with crack stop hole radius of 7.874 mm is approximately 520 MPa. The corresponding value of specimen reinforced with 3 CFRP layer will be 236 MPa (0.4551\*520).
7. The reduced  $K_I/\rho^\alpha$  value (236 MPa) is now compared with  $10\sqrt{\sigma_{ys}}$  (477 MPa). This value (477 MPa) is greater than reduced  $K_I/\rho^\alpha$  value (236 MPa) which indicates that 2 layer of CFRP with 6.35 mm radius will not result in crack re-initiation. Since the site conditions in the problem permit up to 10 mm crack stop hole radius, the assumed 2 layer of CFRP reinforcement with 6.35 mm crack stop hole radius (undersized) is valid.

A nonlinear FEA carried out for the above conditions ( $\theta= 30^0$ ,  $\rho= 6.35$  mm,  $SR = 0, 0.16$ , load = 62 MPa) and calculated  $K_I/\rho^\alpha$  for bare steel specimen and patched specimen with 2 layer are respectively 516 MPa and 245 MPa, which indicate that the  $RF$  value is 1, 0.474 respectively. It can be observed that the difference is 4% between proposed equation and FEA indicating the accuracy of the proposed equation.

### 3.5 Conclusions

A numerical analysis has been carried out to study the combined action of crack stop hole and CFRP patch in arresting the inclined cracks. The obtained results allow us to deduce the following conclusions:

- Application of CFRP on cracked specimen resulted in considerable decrease in the value of  $K_I/\rho^\alpha$ .
- The  $K_I/\rho^\alpha$  reaches minimum value and then exhibits asymptotic behaviour with increase in  $SR$  on the patched side.
- Symmetrically bonded specimen showed better results than asymmetrically bonded specimen.

- It can be observed that in case of asymmetrically bonded specimen, there is no effect on the unpatched side.
- $K_I/\rho^a$  value decreases with increase in crack stop hole radius.
- There is no influence of inclination of crack, because the condition of plate with crack is changed to plate with hole.

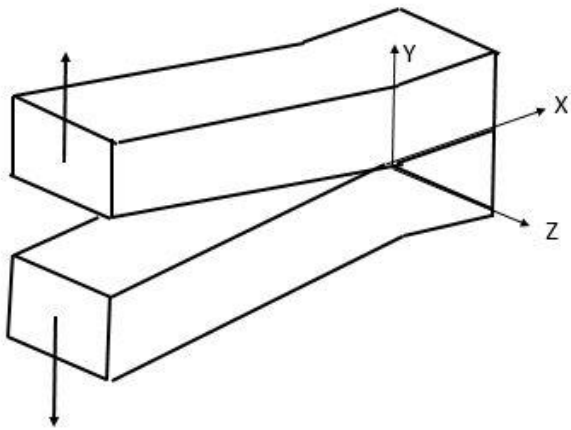
## REFERENCES

- [1] Shield C, Hajjar J, Nozaka K. Repair of fatigued steel bridge girders with carbon fiber strips. Report no-MN/RC-2002-04, Minnesota Department of Transportation, 2004.
- [2] Paris CP and Sih GC. Stress analysis of cracks. Fracture Toughness Testing and its Applications, ASTM STP 381, American Society for Testing and Materials, Philadelphia, 1965.
- [3] Anderson TL. Fracture Mechanics Fundamentals and Applications. Third edition, Taylor and Francis group, LLC, 2005.
- [4] Irwin GR. Analysis of stresses and strains near the end of a crack transversing a plate. Transactions, ASME, Journal of applied Mechanics 1957; 25: 361-364.
- [5] Creager M, and Paris PC. Elastic field equations for blunt cracks with reference to stress corrosion cracking. International Journal of Fracture Mechanics 1967; 3(4): 247-252.
- [6] Boukharouba T, Tamine T, Niu L, Chehimi C, Pluvinage G. The use of notch stress intensity factor as a fatigue crack initiation parameter. Engineering Fracture Mechanics 1995; 52(3): 503-512.
- [7] Barsom JM. Fracture Mechanics – Fatigue and Fracture 1985. Metals Handbook – Desk 398 Edition, American Society for Metals, Metals Park, Ohio.
- [8] Belhouari M, Bachir BB, Megueni M, Kaddouari K. Comparison of double and single bonded repairs to symmetric composite structures: a numerical analysis. Composite Structures 2004; 65: 47–53.
- [9] Albedah A, Bachir BB, Mhamdia R, Benyahia F, Es-Saheb M. Comparison between double and single sided bonded composite repair with circular shape. Materials and Design 2011; 32: 996–1000.
- [10] Duong CN, Wang CH. On the characterization of fatigue crack growth in a plate with a single-sided repair. Transactions of the ASME, Journal of Engineering Materials and Technology 2004; 126 (2): 192–198.
- [11] Wang CH, Rose LRF, Callinan R. Analysis of out-of-plane bending in one-sided bonded repair. International Journal of Solids and Structures 1998; 35(14): 1653–1675.

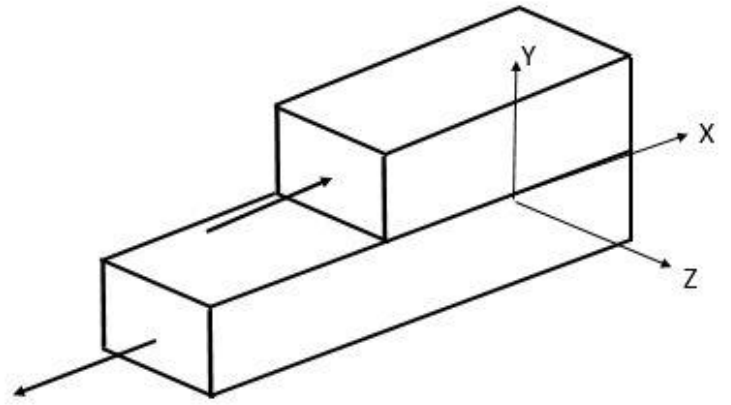
- [12] Domazet Z. Comparison of fatigue crack retardation methods. *Engineering Failure Analysis* 1996; 3 (2): 137–147.
- [13] Song PS, Shieh Y L. Stop drilling procedure for fatigue life improvement. *International Journal of Fatigue* 2004; 26(12): 1333–1339.
- [14] Barsom JM, McNicol RC. Effect of stress concentration on fatigue-crack initiation in HY-130 Steel. *Fracture Toughness and Slow-Stable Cracking* 1974; 4STM STP 559, 402 American Society for Testing and Materials: 183-204.
- [15] Fisher JW, Barthelemy BM, Mertz DR, Edinger JA. Fatigue behaviour of full scale welded bridge attachments. NCHR 12-15(3), March 1980 (80-29), Fritz Laboratory Reports, 1980.
- [16] Ramji M, Srilakshmi R, Bhanu Prakash M. Towards optimization of patch shape on the performance of bonded composite repair using FEM. *Composites: Part B* 2012; 45(1): 710–720.
- [17] Zhao XL, Zhang L. State-of-the-art review on FRP strengthened steel structures. *Engineering Structures* 2007; 29 (8): 1808–1823.
- [18] Nakamura T, Parks DM. Antisymmetrical 3D stress field near the crack front of a thin elastic plate. *International Journal of Solids and Structures* 1989; 25 (12): 1411-1426.

- Figure 3.1:** Three basic modes of crack surface displacements (a) Mode-I, (b) Mode-II, (c) Mode-III
- Figure 3.2:** Type of crack propagation modes possible when crack is inclined
- Figure 3.3:** Stress contours showing  $\sigma_{yy}$  and  $\sigma_{xy}$  respectively for (a)  $0^\circ$ , (b)  $15^\circ$ , (c)  $60^\circ$
- Figure 3.4:** (a) Specimen with crack, (b) specimen with crack and crack stop hole
- Figure 3.5:** Stress field a head of blunt notch
- Figure 3.6:** Calculation of optimum crack stop hole radii
- Figure 3.7:** Schematic representation of the specimen
- Figure 3.8a:** Typical FE mesh of specimen
- Figure 3.8b:** Circular meshing around the crack stop hole
- Figure 3.9:** Stress strain curve for steel
- Figure 3.10:** Stress distribution ahead of crack stop hole
- Figure 3.11:**  $K_I / \rho^\alpha$  versus SR for  $15^\circ$  inclined crack, 2 inch Crack Length at different loads (a) 41.2 MPa, (b) 62 MPa, (c) 82.7 MPa and (d) 103.4 MPa
- Figure 3.12:**  $K_I / \rho^\alpha$  versus SR for  $45^\circ$  inclined crack, 2 inch inch Crack Length at different loads (a) 41.2 MPa, (b) 62 MPa, (c) 82.7 MPa and (d) 103.4 MPa
- Figure 3.13:**  $K_I / \rho^\alpha$  versus SR for  $60^\circ$  inclined crack, 2 inch Crack Length at different loads (a) 41.2 MPa, (b) 62 MPa, (c) 82.7 MPa and (d) 103.4 MPa
- Figure 3.14:** Schematic representation of the lines considered for peel stress distribution
- Figure 3.15:** Variation of peel stress in X-X direction for  $45^\circ$  inclined crack, 2 inch crack length at different loads (a) 41.2 MPa, (b) 62 MPa, (c) 82.7 MPa and (d) 103.4 MPa
- Figure 3.16:** Variation of peel stress in X-X direction for  $45^\circ$  inclined crack, 2 inch crack length at different SR (a) 0.08, (b) 0.64
- Figure 3.17:** Variation of peel stress in Y-Y direction for  $45^\circ$  inclined crack, 2 inch crack length at different loads (a) 41.2 MPa, (b) 62 MPa, (c) 82.7 MPa and (d) 103.4 MPa
- Figure 3.18:**  $K_I / \rho^\alpha$  versus SR on patched side for  $15^\circ$  inclined crack, 2 inch Crack Length at different loads (a) 41.2 MPa, (b) 62 MPa, (c) 82.7 MPa and (d) 103.4 MPa
- Figure 3.19:**  $K_I / \rho^\alpha$  versus SR on patched side for  $45^\circ$  inclined crack, 2 inch Crack Length at different loads (a) 41.2 MPa, (b) 62 MPa, (c) 82.7 MPa and (d) 103.4 MPa
- Figure 3.20:**  $K_I / \rho^\alpha$  versus SR on patched side for  $60^\circ$  inclined crack, 2 inch Crack Length at different loads (a) 41.2 MPa, (b) 62 MPa, (c) 82.7 MPa and (d) 103.4 MPa
- Figure 3.21:**  $K_I / \rho^\alpha$  versus SR on unpatched side for  $15^\circ$  inclined crack, 2 inch Crack Length at different loads (a) 41.2 MPa, (b) 62 MPa, (c) 82.7 MPa and (d) 103.4 MPa

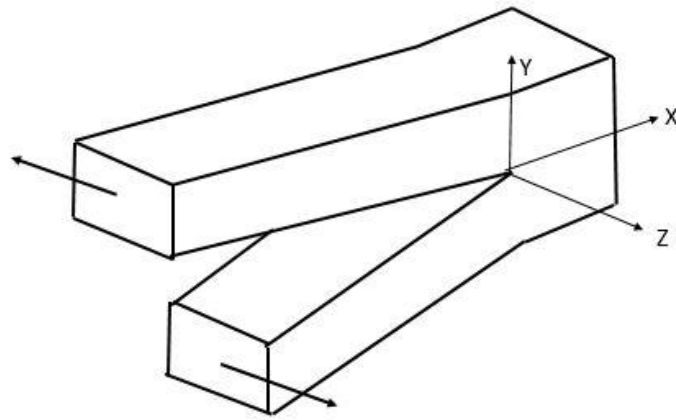
- Figure 3.22:**  $K_I / \rho^\alpha$  versus SR on unpatched side for 45<sup>0</sup> inclined crack, 2 inch Crack Length at different loads (a) 41.2 MPa, (b) 62 MPa, (c) 82.7 MPa and (d) 103.4 MPa
- Figure 3.23:**  $K_I / \rho^\alpha$  versus SR on unpatched side for 60<sup>0</sup> inclined crack, 2 inch Crack Length at different loads (a) 41.2 MPa, (b) 62 MPa, (c) 82.7 MPa and (d) 103.4 MPa
- Figure 3.24:** Through thickness variation of  $K_I / \rho^\alpha$  of the specimen for different SR having a crack of 50.8mm (2 inch), 9.525 mm (0.375 inch) crack stop hole radii and for an applied load of 62 MPa load having different crack inclination (a) 15<sup>0</sup>, (b) 45<sup>0</sup>, (c) 60<sup>0</sup>
- Figure 3.25:**  $(K_I / \rho^\alpha)_{rms}$  versus SR for 15<sup>0</sup> inclined crack having 2 inch crack length at different loads (a) 41.2MPa, (b) 62 MPa, (c) 82.7 MPa and (d) 103.4 MPa
- Figure 3.26:**  $(K_I / \rho^\alpha)_{rms}$  versus SR for 45<sup>0</sup> inclined crack having 2 inch crack length at different loads (a) 41.2MPa, (b) 62 MPa, (c) 82.7 MPa and (d) 103.4 MPa
- Figure 3.27:**  $(K_I / \rho^\alpha)_{rms}$  versus SR for 60<sup>0</sup> inclined crack having 2 inch crack length at different loads (a) 41.2 MPa, (b) 62 MPa, (c) 82.7 MPa and (d) 103.4 MPa
- Figure 3.28:** Schematic representation of the lines considered for peel stress distribution
- Figure 3.29:** Variation of peel stress in X-X direction for 45<sup>0</sup> inclined crack, 2 crack length at different loads (a) 41.2 MPa, (b) 62 MPa, (c) 82.7 MPa and (d) 103.4 MPa
- Figure 3.30:** Variation of peel stress in X-X direction for 45<sup>0</sup> inclined crack, 2 crack length at different SR (a) 0.08 and (b) 0.64
- Figure 3.31:** Variation of peel stress along Y-Y direction for 45<sup>0</sup> inclined crack, 2 crack length at different loads (a) 41.2 MPa, (b) 62 MPa, (c) 82.7 MPa and (d) 103.4 MPa
- Figure 3.32:** comparison of peel stress for different inclination of crack having 2 inch crack length, 0.375 inch crack stop hole radii of double sided repaired panel for different applied loads (a) 41.2 MPa, (b) 62 MPa, (c) 82.7 MPa and (d) 103.4 MPa
- Figure 3.33:** comparison of  $K_I / \rho^\alpha$  for different inclination of crack having 2 inch crack length, 0.375 inch crack stop hole radii of double sided repaired panel for different applied loads (a) 41.2 MPa, (b) 62 MPa, (c) 82.7 MPa and (d) 103.4 MPa
- Figure 3.34:**  $K_I / \rho^\alpha$  versus crack stop hole radius of bare steel specimen having a crack of 2 inch length and 30<sup>0</sup> inclination for 62 MPa load
- Figure 3.35:**  $K_I / \rho^\alpha$  versus crack stop hole radius of bare steel specimen having a crack of 2 inch length and 30<sup>0</sup> inclination for 41.2 MPa load



(a)



(b)



(c)

**Figure 3.1: Three basic modes of crack surface displacements (a) Mode-I, (b) Mode-II, (c) Mode-III**

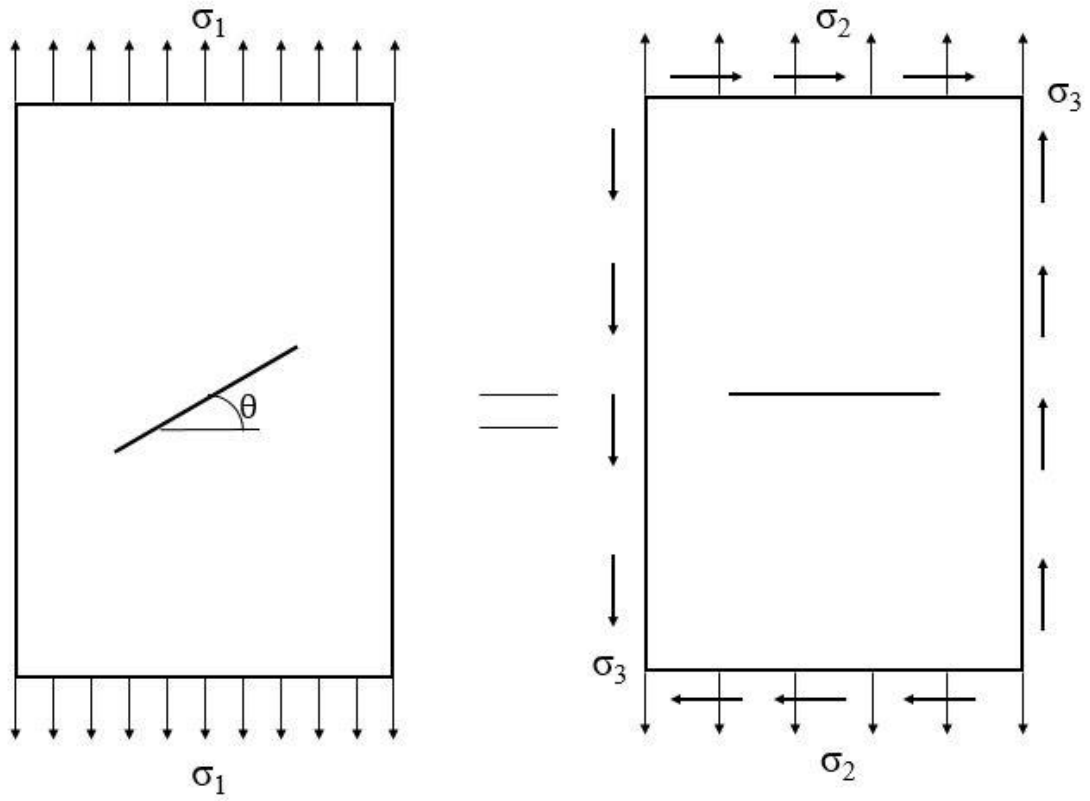
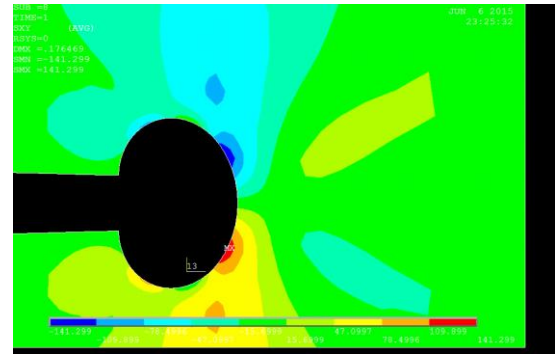
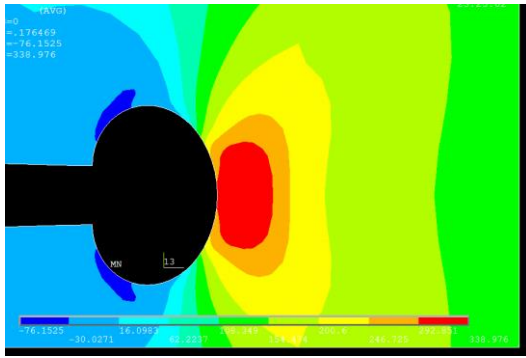
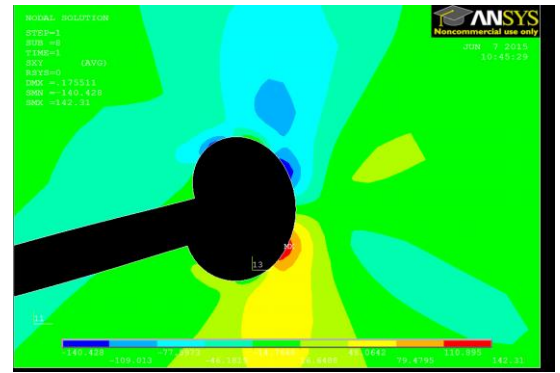
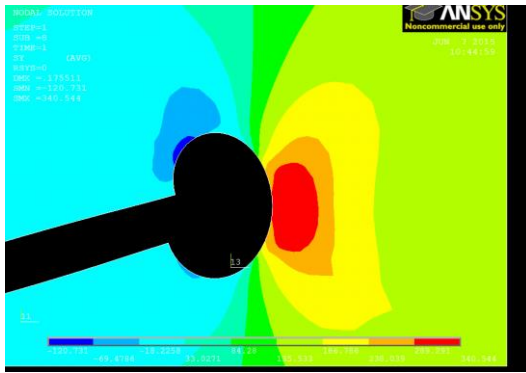


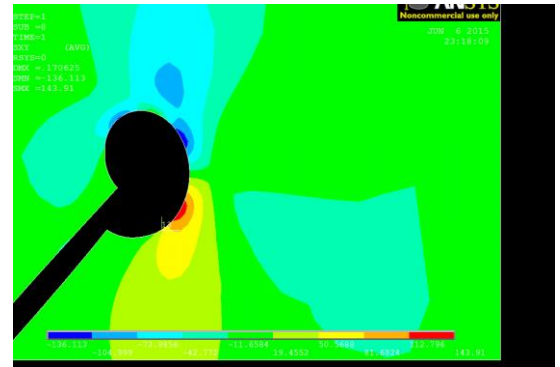
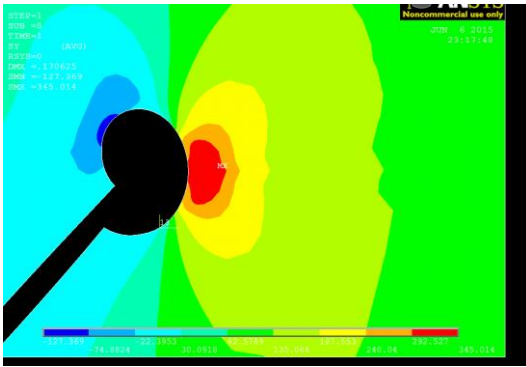
**Figure 3.2: Type of crack propagation modes possible when crack is inclined**



(a)



(b)



(c)

Figure 3.3: Stress contours showing  $\sigma_{yy}$  and  $\sigma_{xy}$  respectively for (a)  $0^\circ$ , (b)  $15^\circ$ , (c)  $60^\circ$



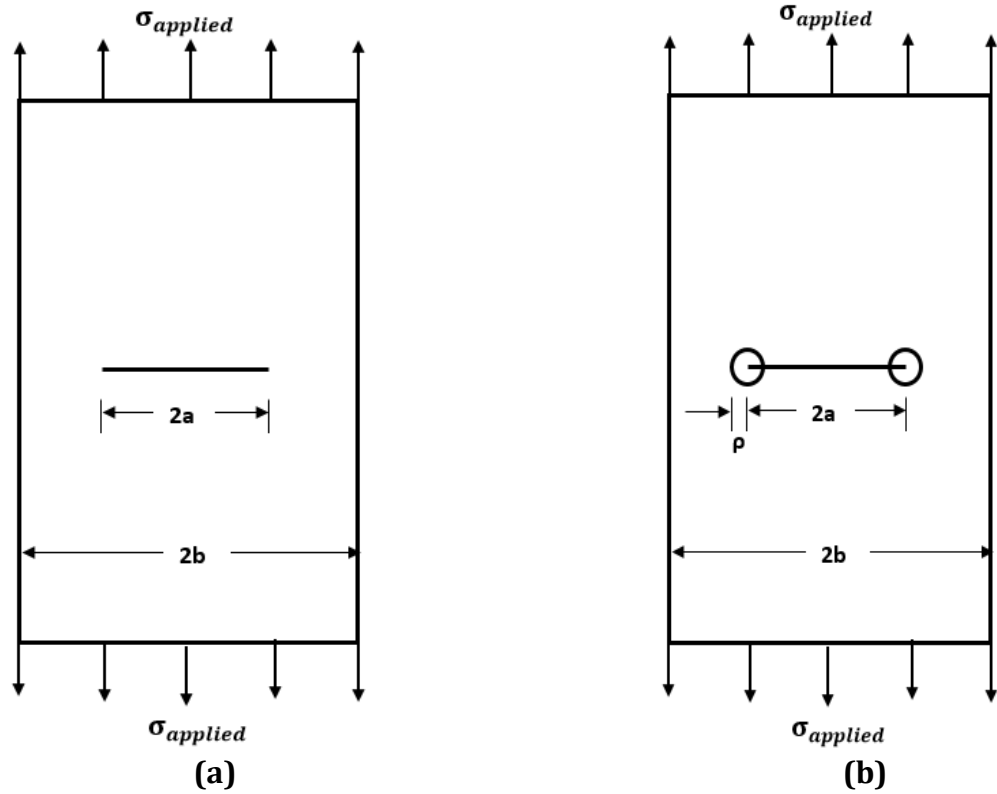


Figure 3.4: (a) Specimen with crack, (b) specimen with crack and crack stop hole

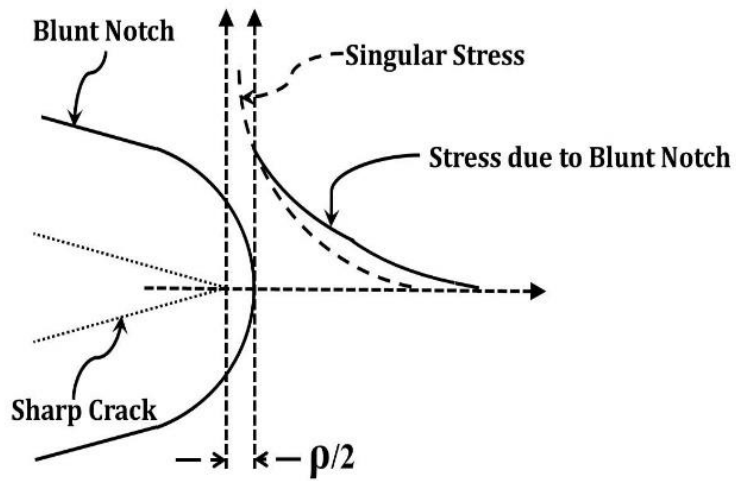


Figure 3.5: Stress field a head of blunt notch

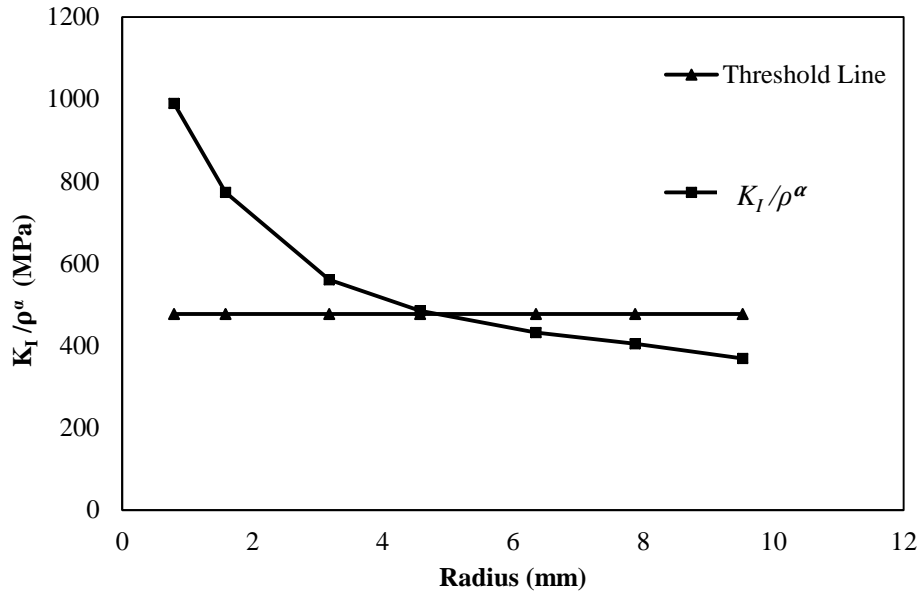


Figure 3.6: Calculation of optimum crack stop hole radii

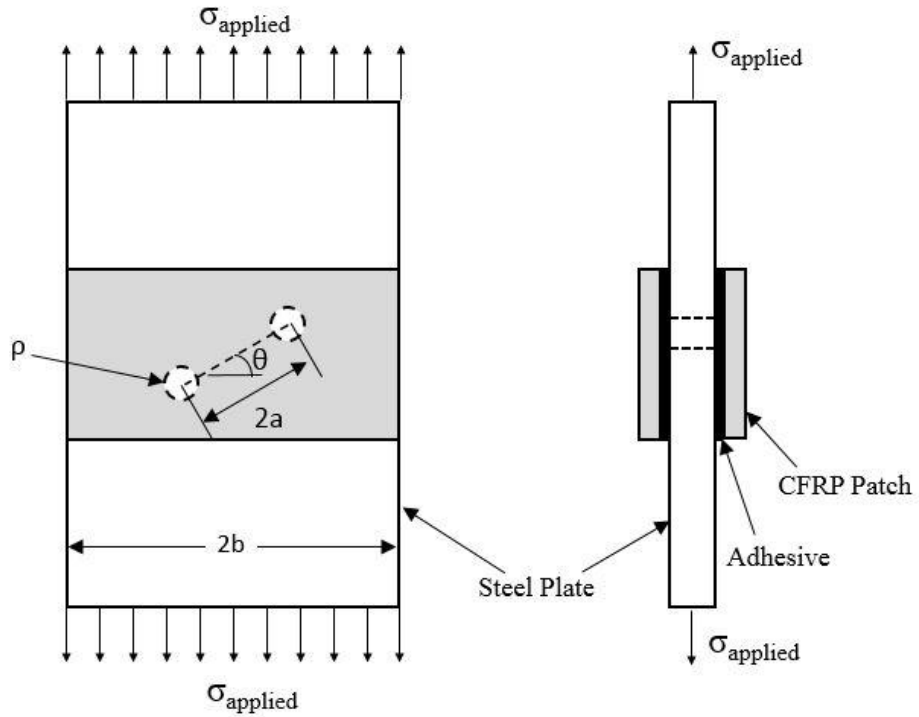
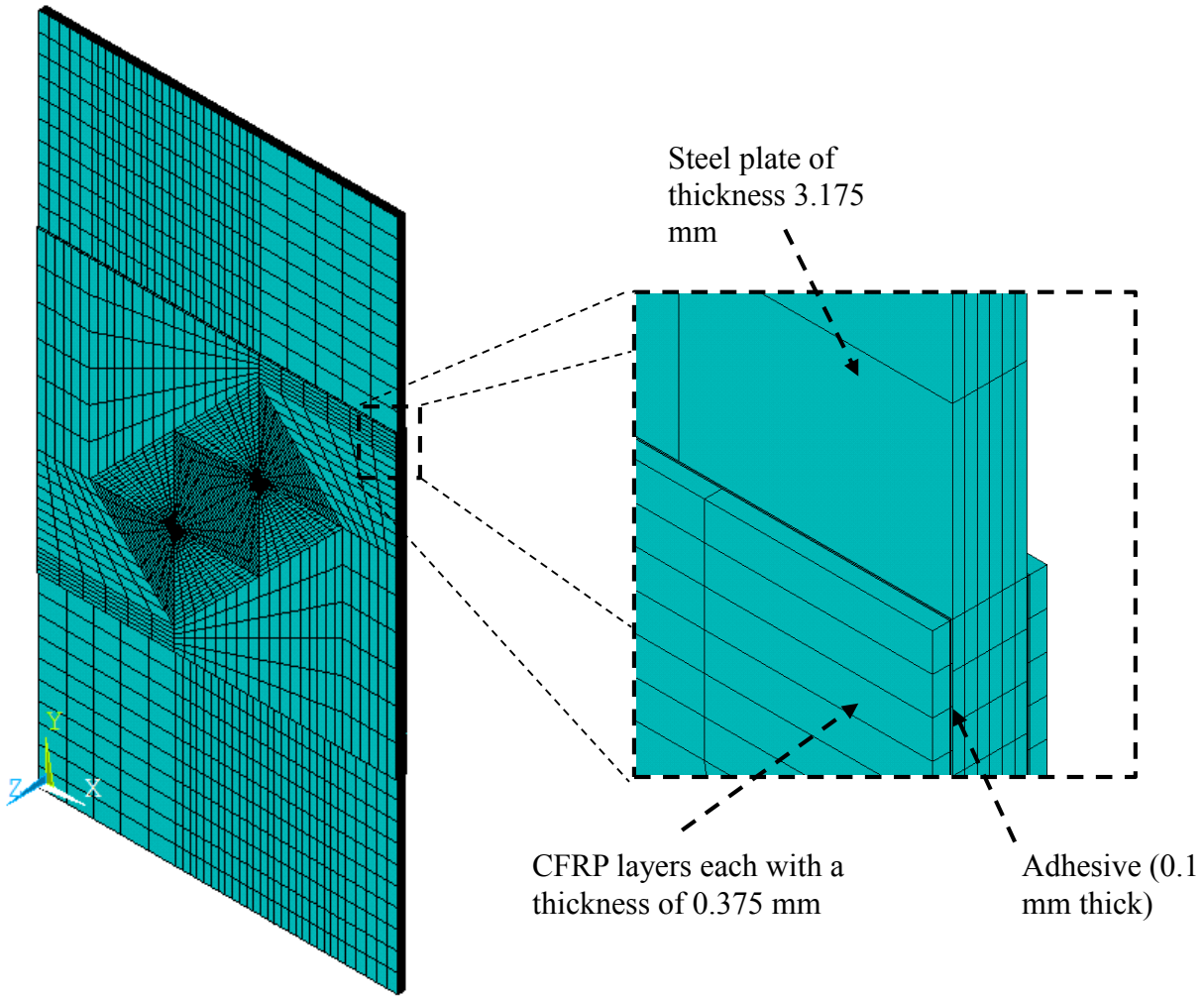
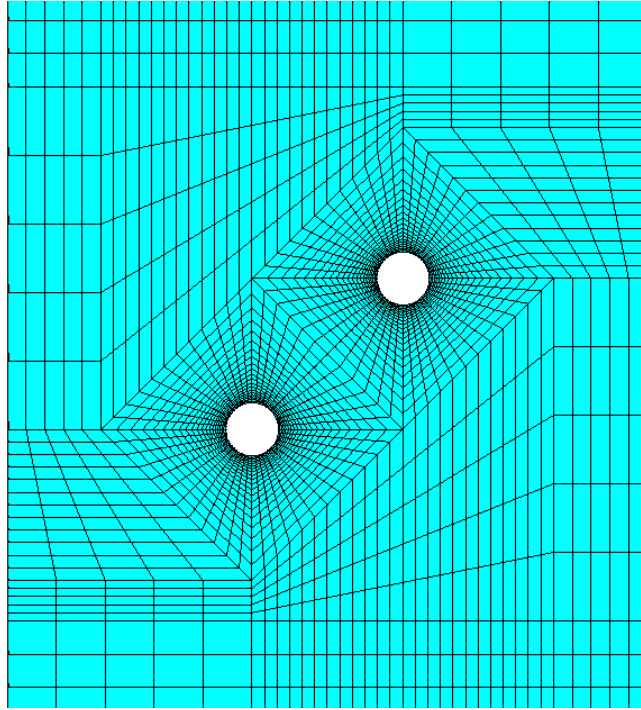


Figure 3.7: Schematic representation of the specimen



**Figure 3.8a: Typical FE mesh of specimen**



**Figure 3.8b: Circular meshing around the crack stop hole**

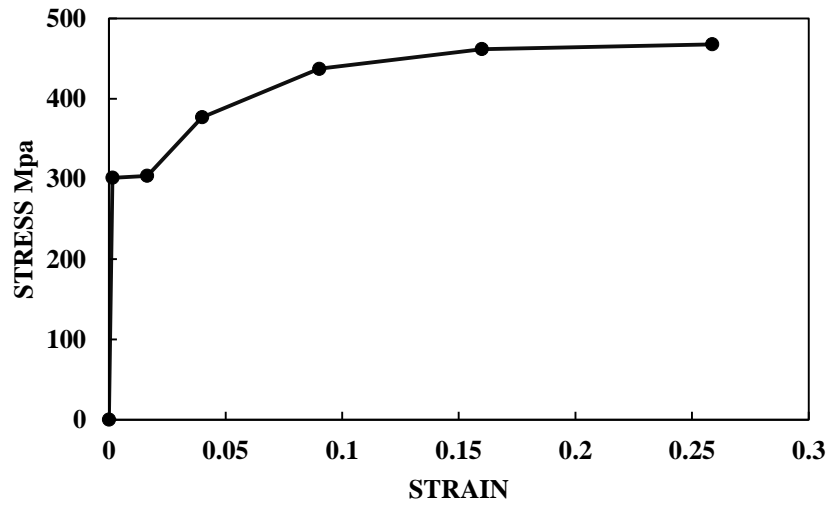


**Figure 3.9: Stress strain curve for steel**

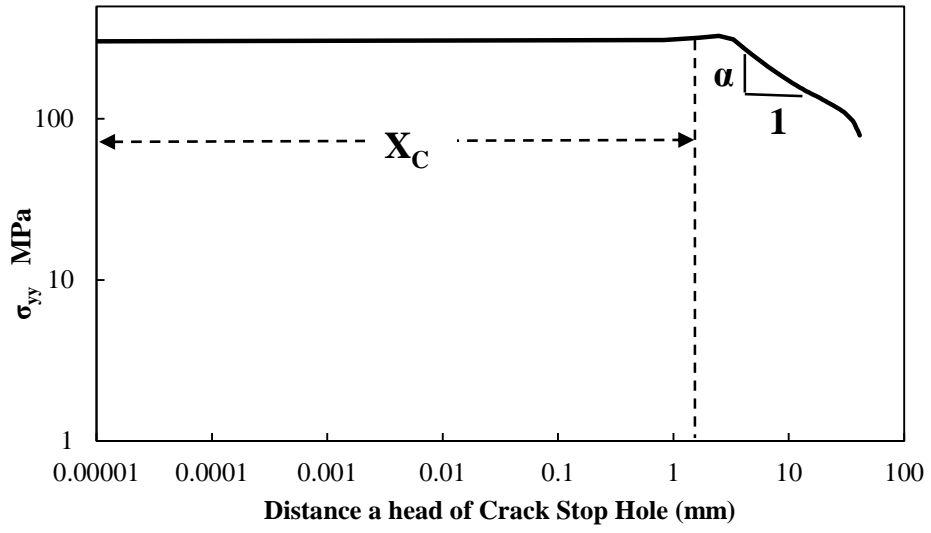
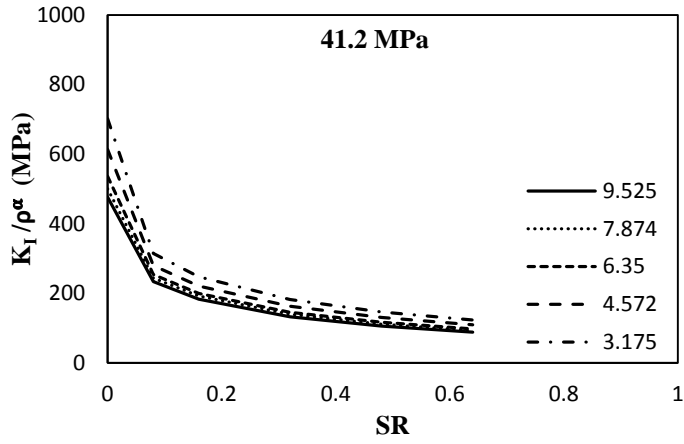
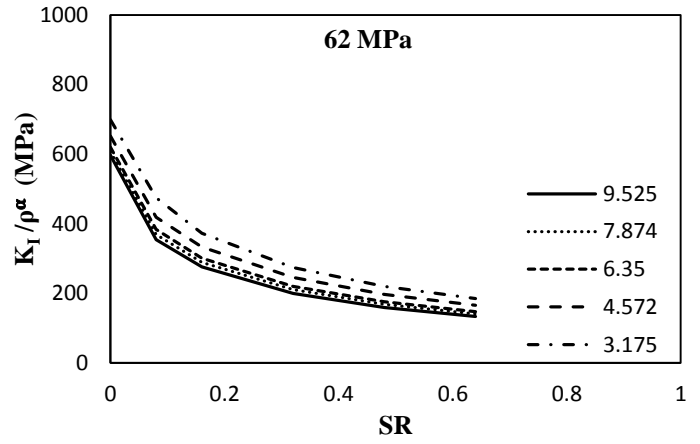


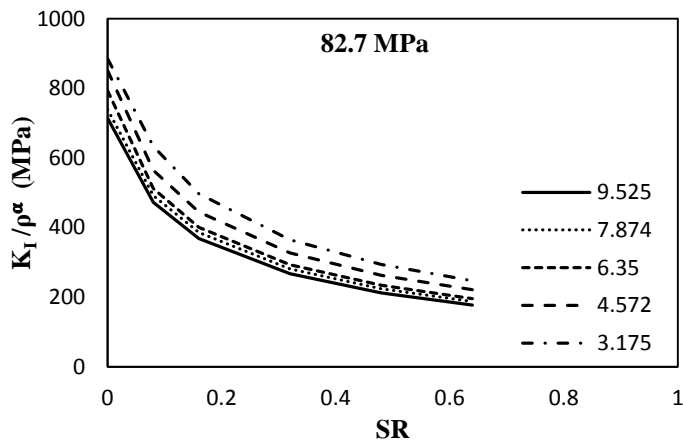
**Figure 3.10: Stress distribution ahead of crack stop hole**



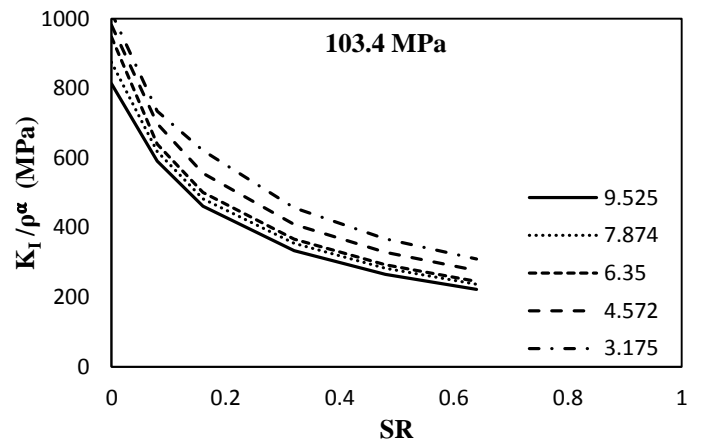
(a)



(b)

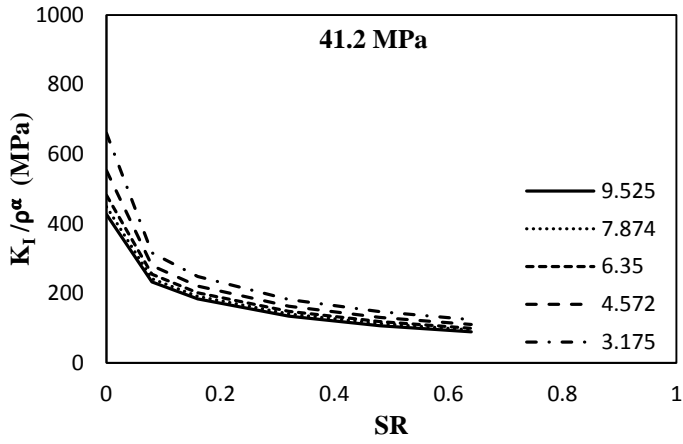


(c)

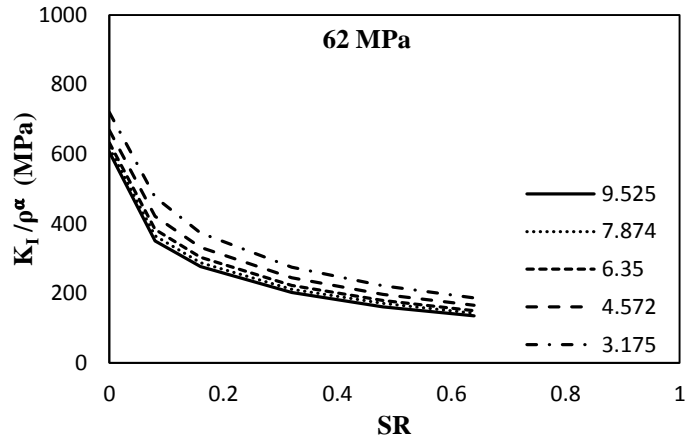


(d)

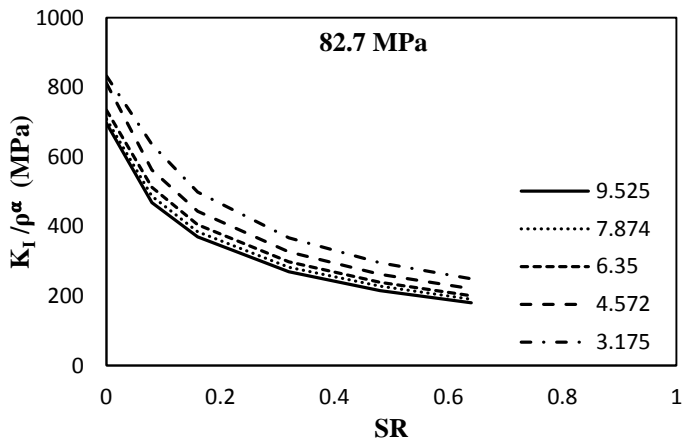
Figure 3.11:  $K_I/\rho^\alpha$  versus SR for  $15^\circ$  inclined crack, 2 inch Crack Length at different loads (a) 41.2 MPa, (b) 62 MPa, (c) 82.7 MPa and (d) 103.4 MPa



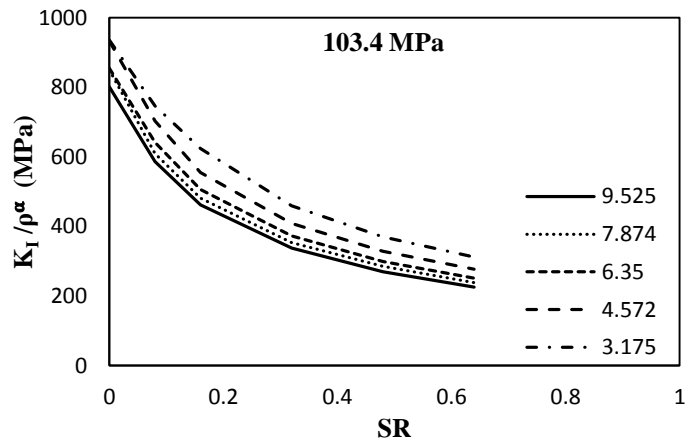
(a)



(b)

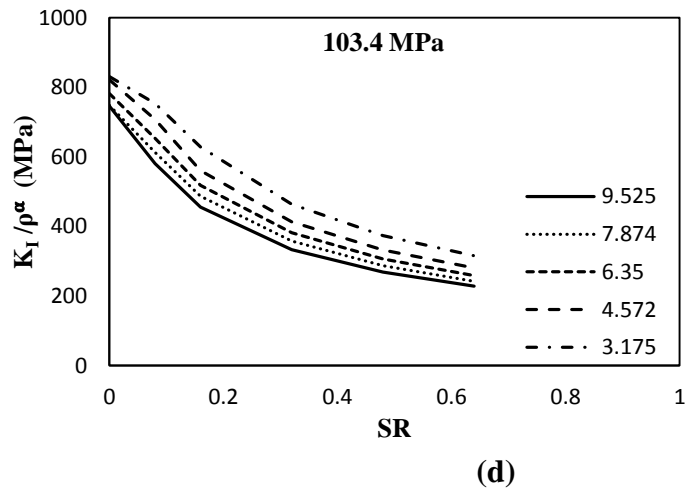
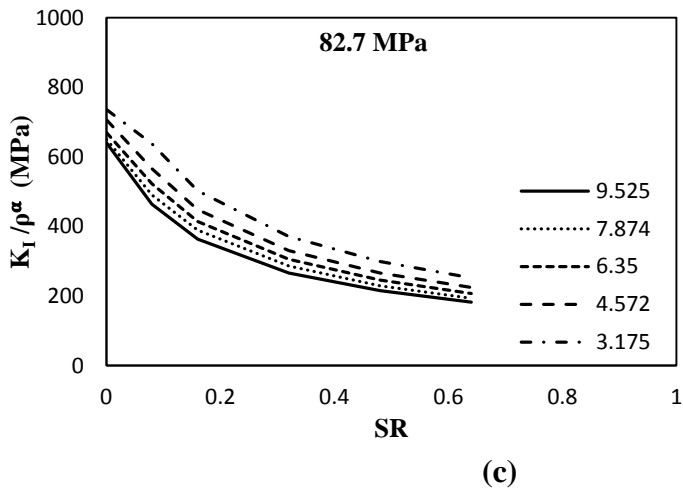
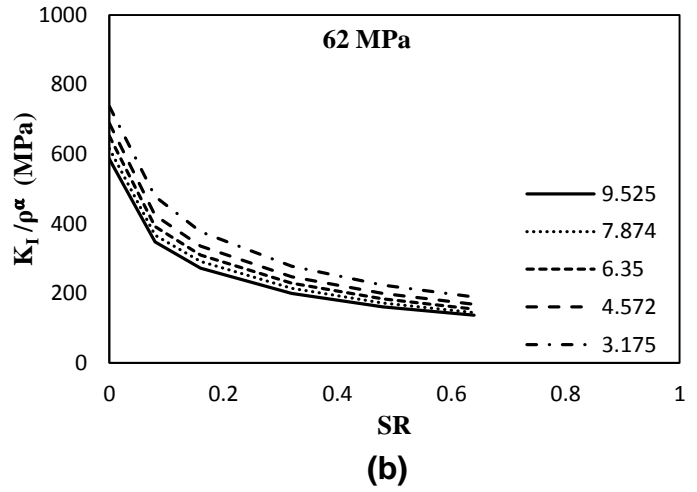
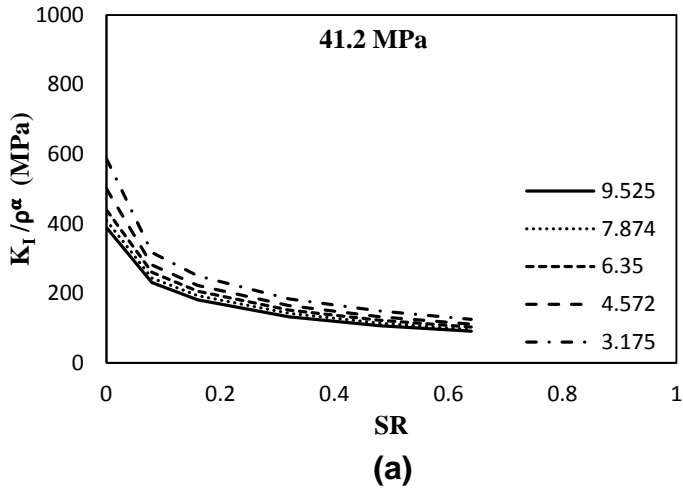


(c)



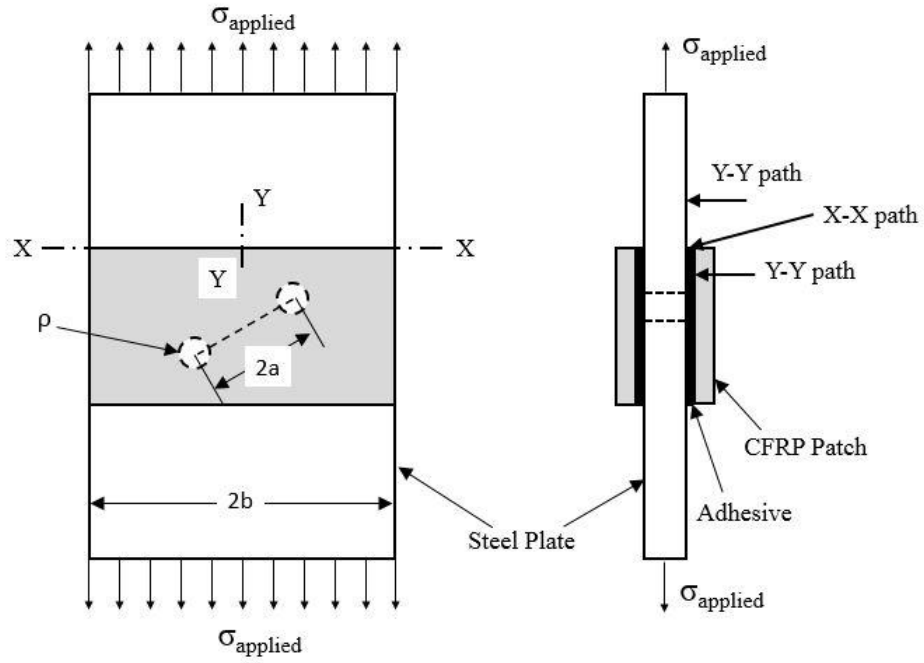
(d)

Figure 3.12:  $K_I / \rho^\alpha$  versus SR for  $45^\circ$  inclined crack, 2 inch Crack Length at different loads (a) 41.2 MPa, (b) 62 MPa, (c) 82.7 MPa and (d) 103.4 MPa

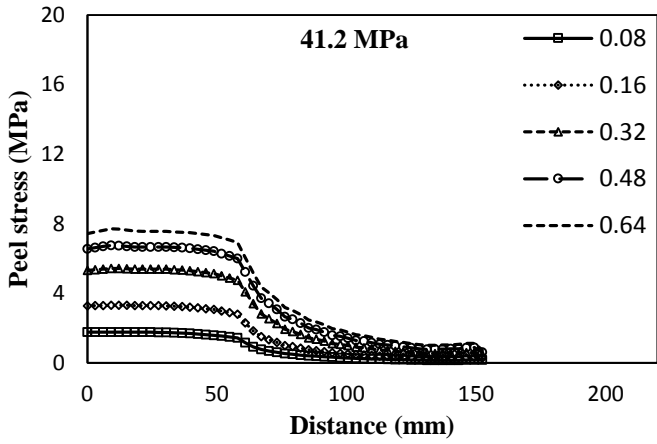


**Figure 3.13:  $K_I/\rho^\alpha$  versus SR for  $60^\circ$  inclined crack, 2 inch inch Crack Length at different loads (a) 41.2 MPa, (b) 62 MPa, (c) 82.7 MPa and (d) 103.4 MPa**

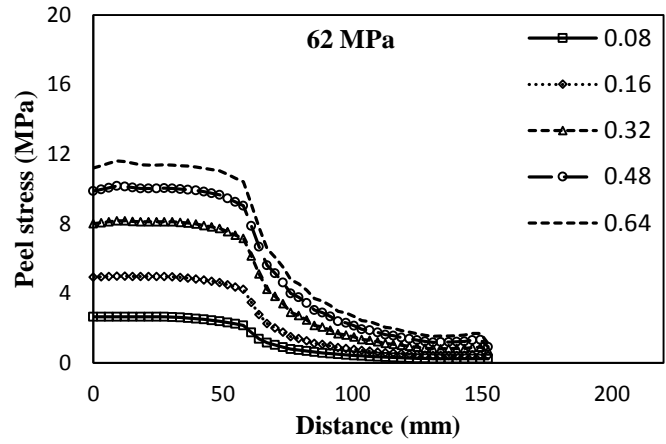




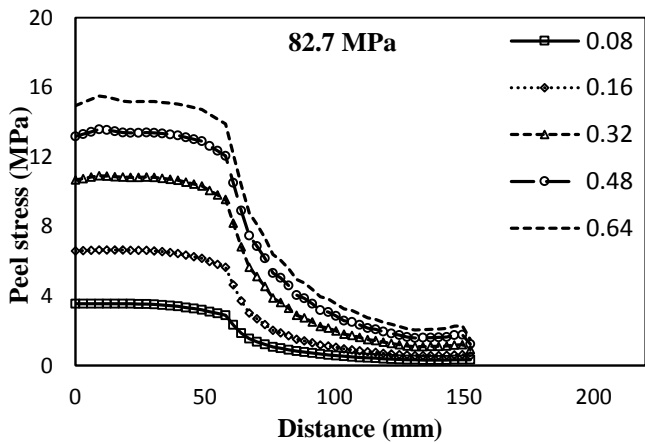
**Figure 3.14: Schematic representation of the lines considered for peel stress distribution**



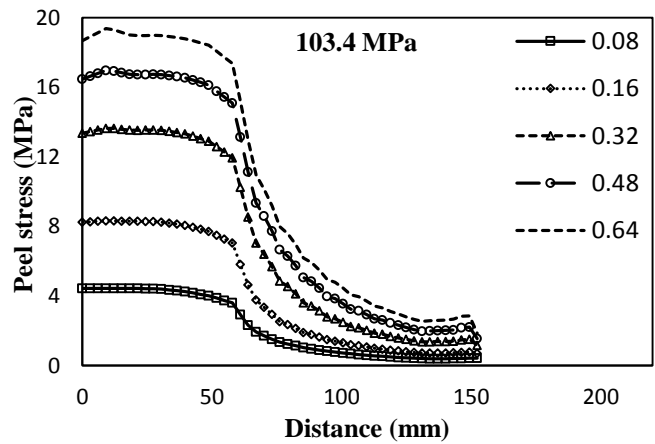
(a)



(b)

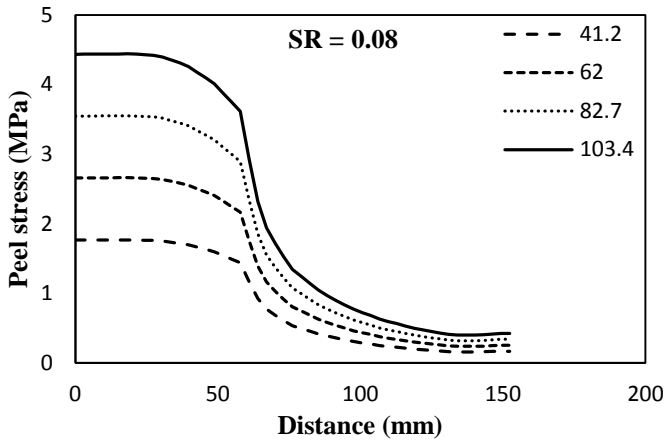


(c)

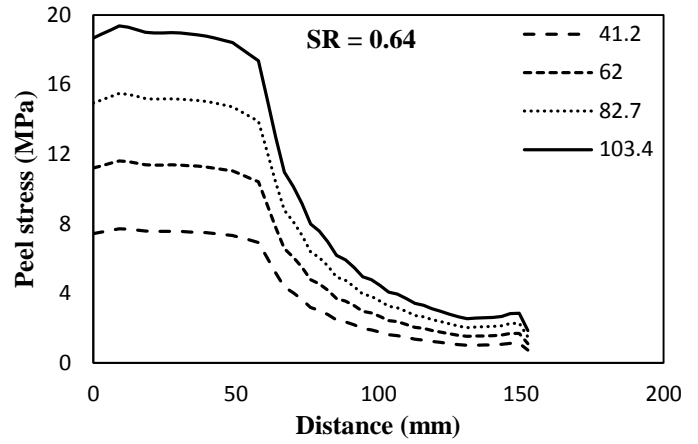


(d)

Figure 3.15: Variation of peel stress in X-X direction for 45° inclined crack, 2 inch crack length at different loads (a) 41.2 MPa, (b) 62 MPa, (c) 82.7 MPa and (d) 103.4 MPa

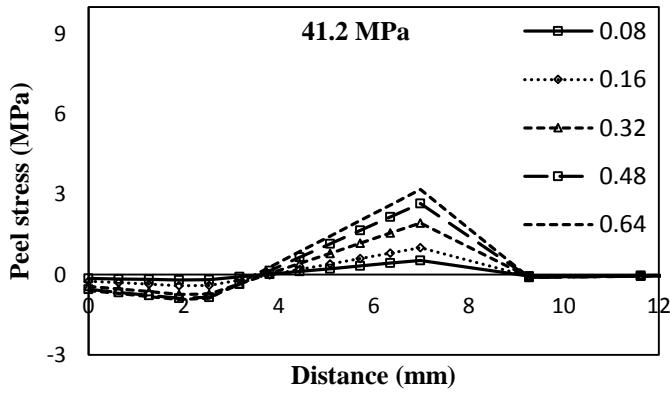


(a)

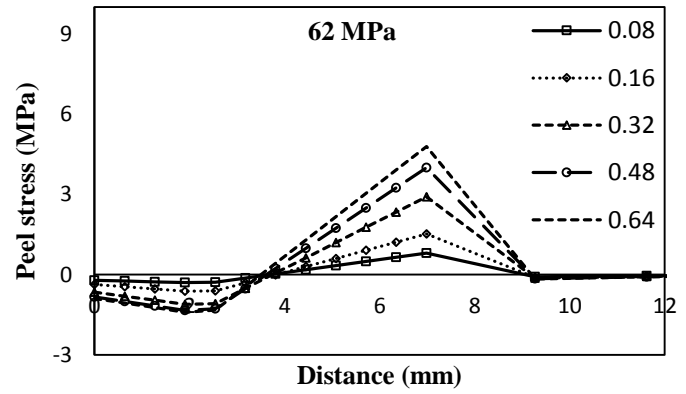


(b)

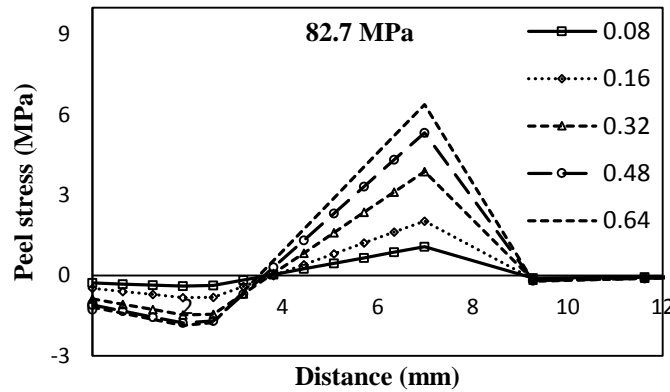
Figure 3.16: Variation of peel stress in X-X direction for 45° inclined crack, 2 inch crack length at different SR (a) 0.08 and (b) 0.64



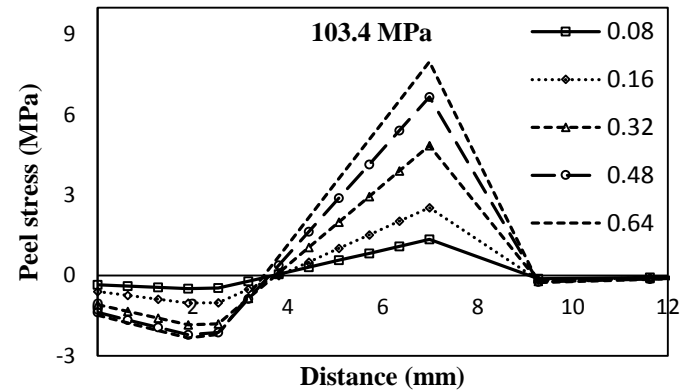
(a)



(b)

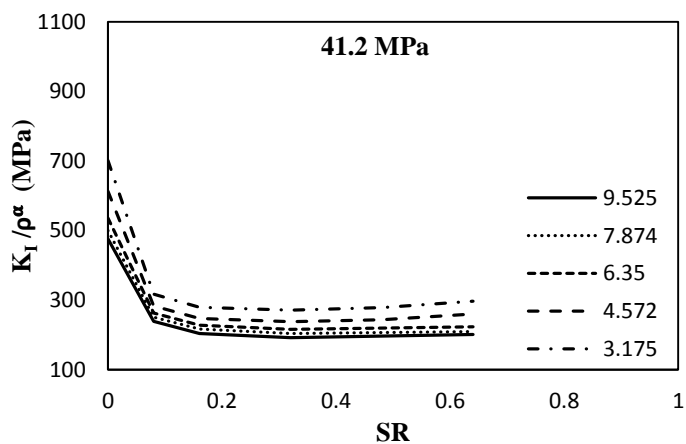


(c)

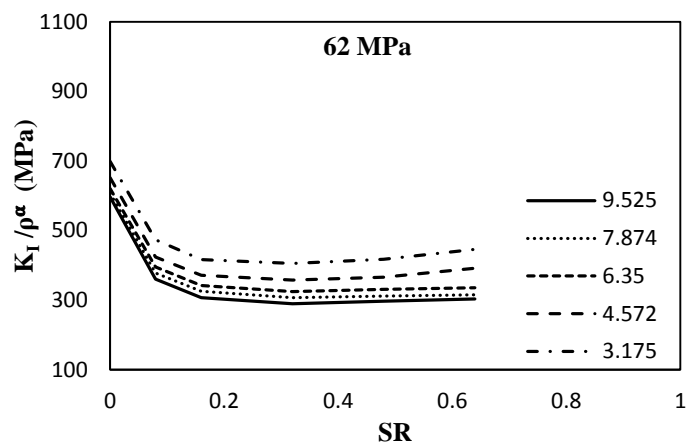


(d)

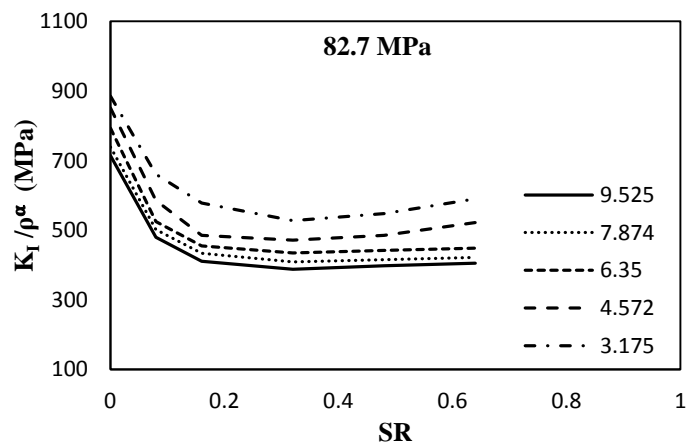
Figure 3.17: Variation of peel stress along Y-Y direction for 45° inclined crack, 2 inch crack length at different loads (a) 41.2 MPa, (b) 62 MPa, (c) 82.7 MPa and (d) 103.4 MPa



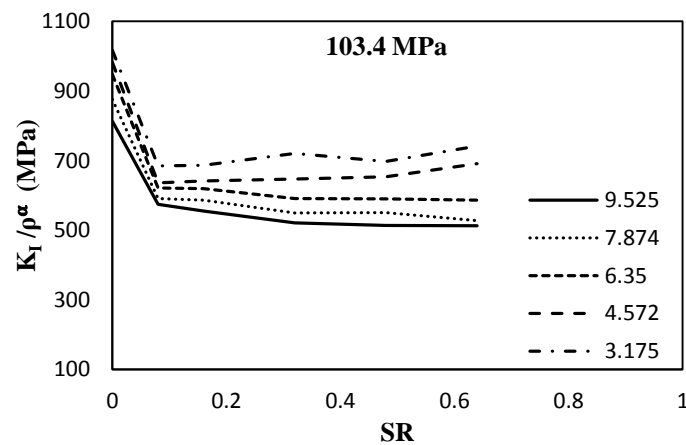
(a)



(b)



(c)



(d)

Figure 3.18:  $K_I / \rho^\alpha$  versus SR on patched side for  $15^\circ$  inclined crack, 2 inch Crack Length at different loads (a) 41.2 MPa, (b) 62 MPa, (c) 82.7 MPa and (d) 103.4 MPa

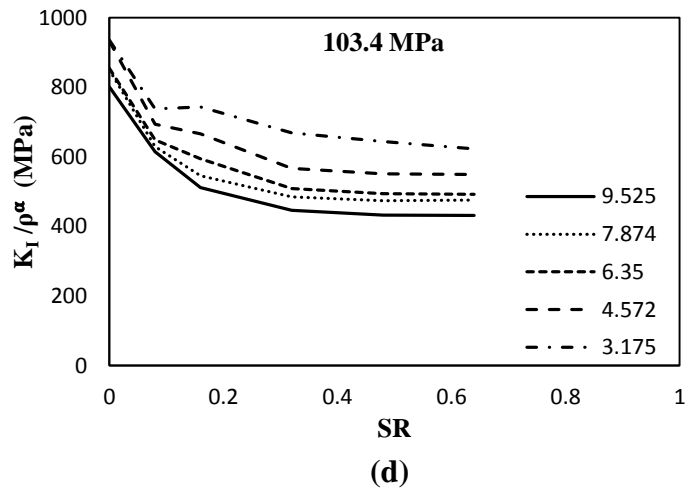
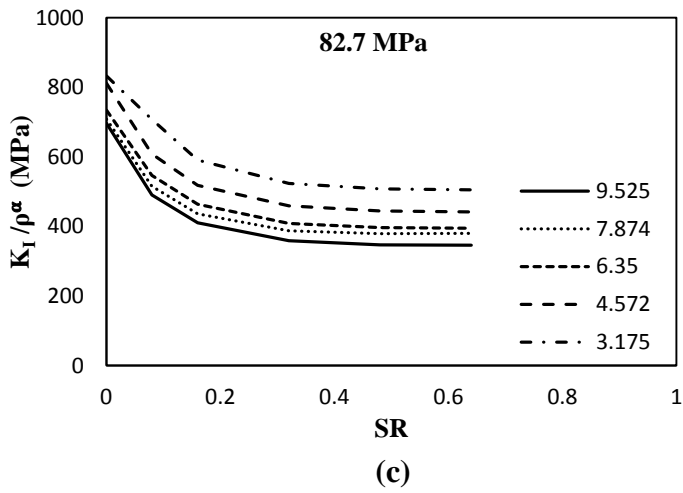
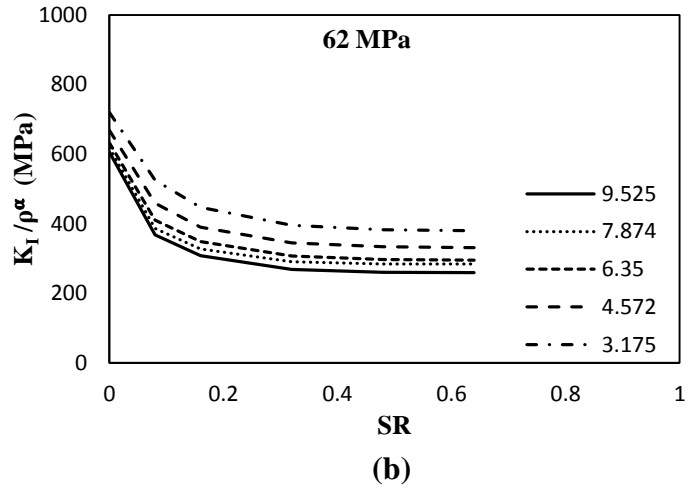
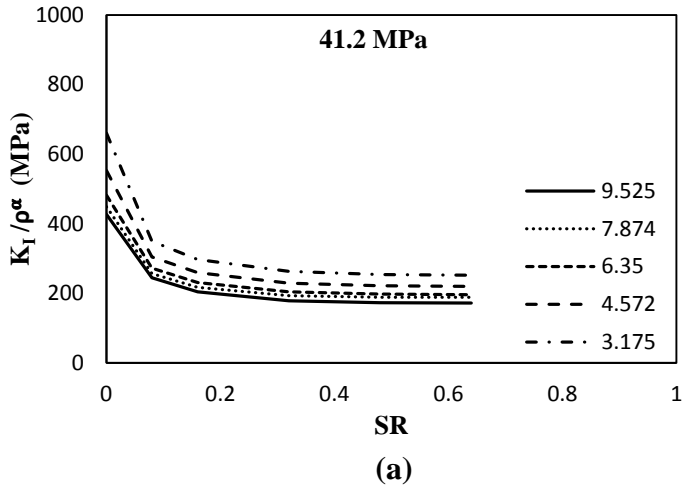
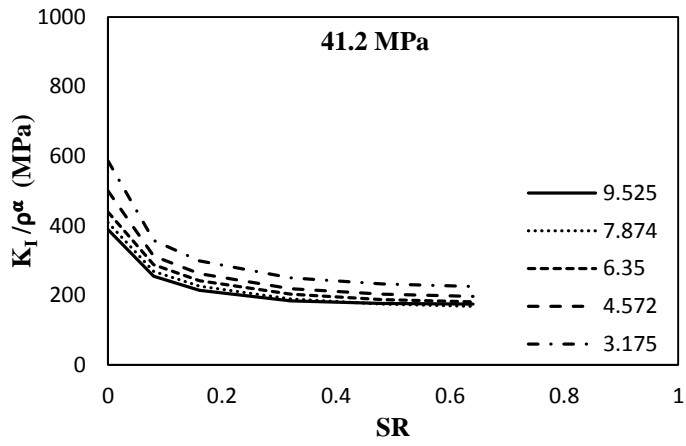
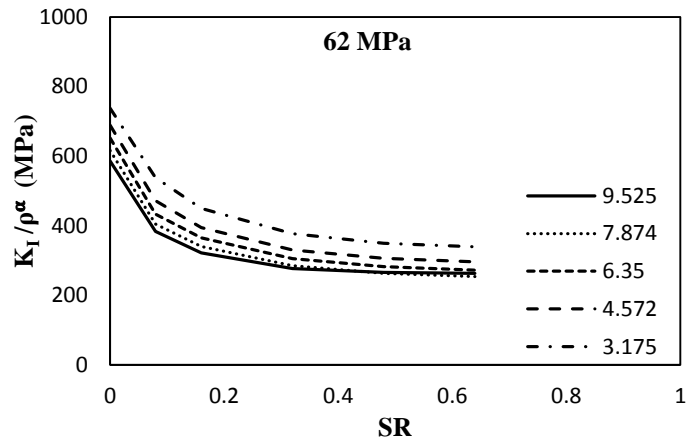


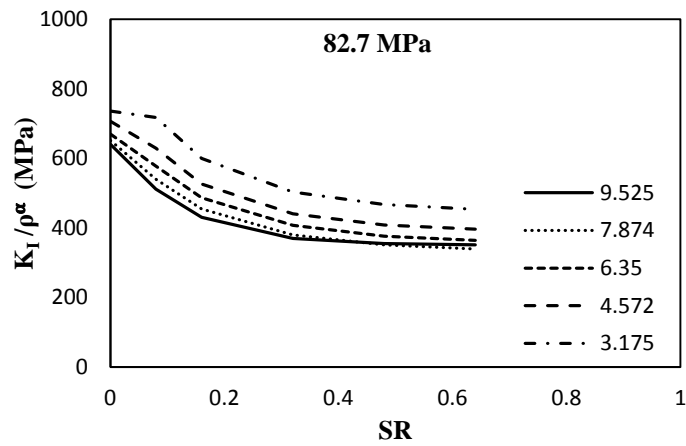
**Figure 3.19:  $K_I / \rho^\alpha$  versus SR on patched side for  $45^\circ$  inclined crack, 2 inch Crack Length at different loads (a) 41.2 MPa, (b) 62 MPa, (c) 82.7 MPa and (d) 103.4 MPa**



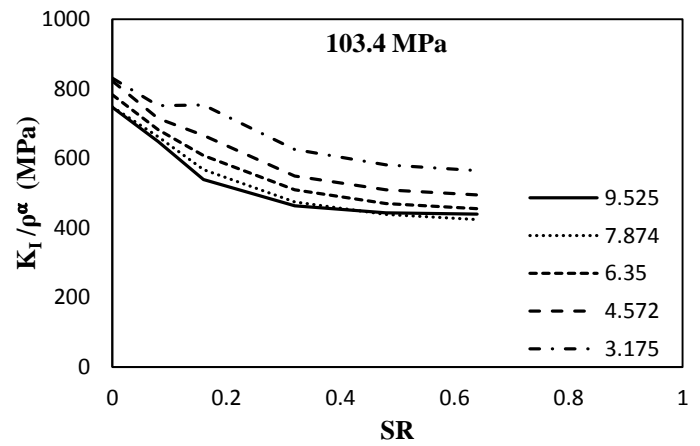
(a)



(b)

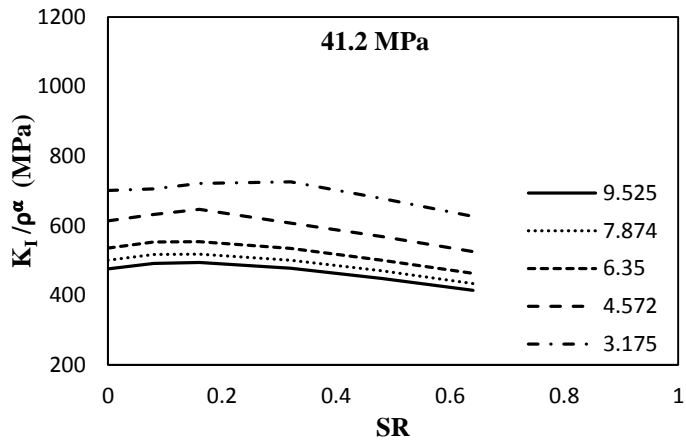


(c)

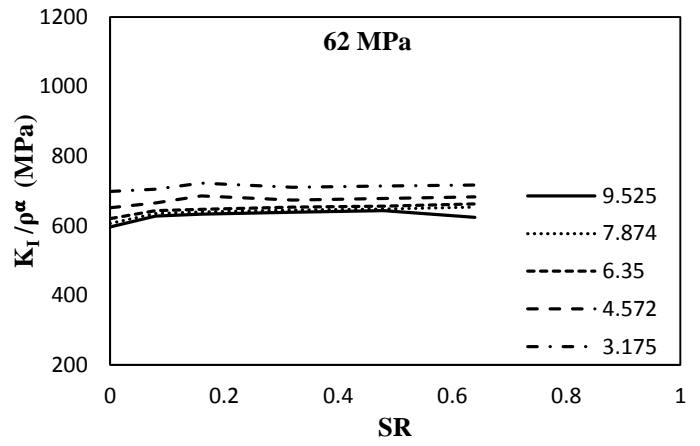


(d)

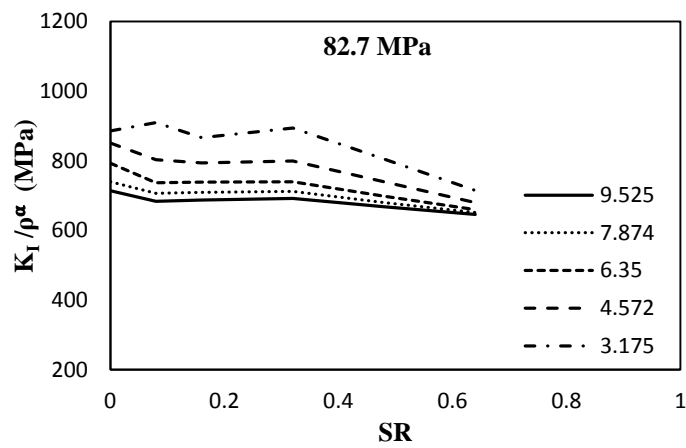
Figure 3.20:  $K_I/\rho^\alpha$  versus SR on patched side for  $60^\circ$  inclined crack, 2 inch Crack Length at different loads (a) 41.2 MPa, (b) 62 MPa, (c) 82.7 MPa and (d) 103.4 MPa



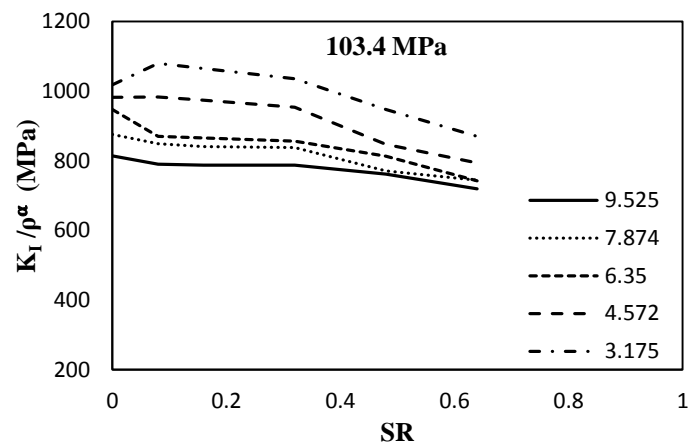
(a)



(b)



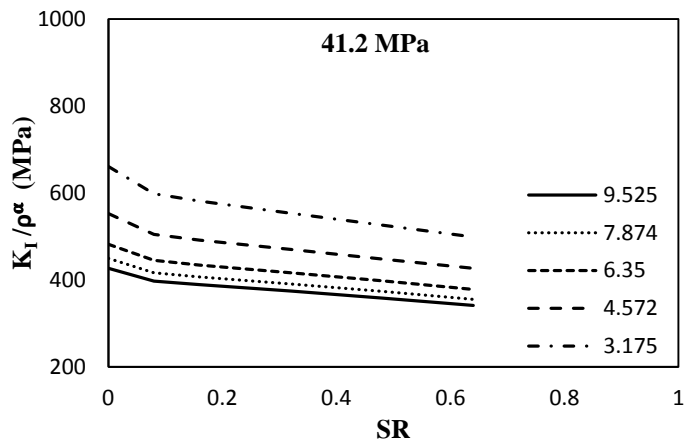
(c)



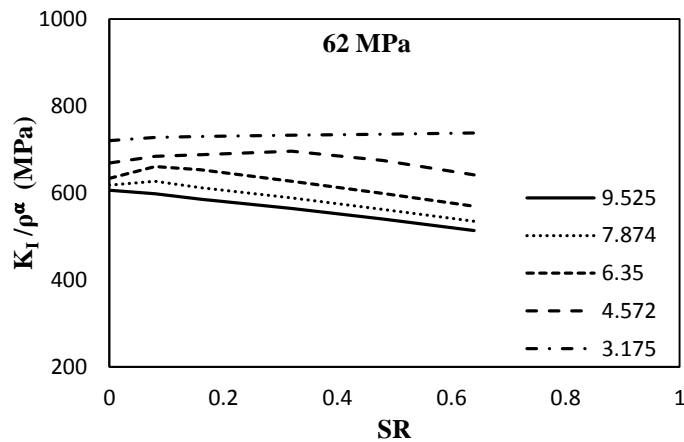
(d)

Figure 3.21:  $K_I / \rho^\alpha$  versus SR on unpatched side for  $15^\circ$  inclined crack, 2 inch Crack Length at different loads (a) 41.2 MPa, (b) 62 MPa, (c) 82.7 MPa and (d) 103.4 MPa

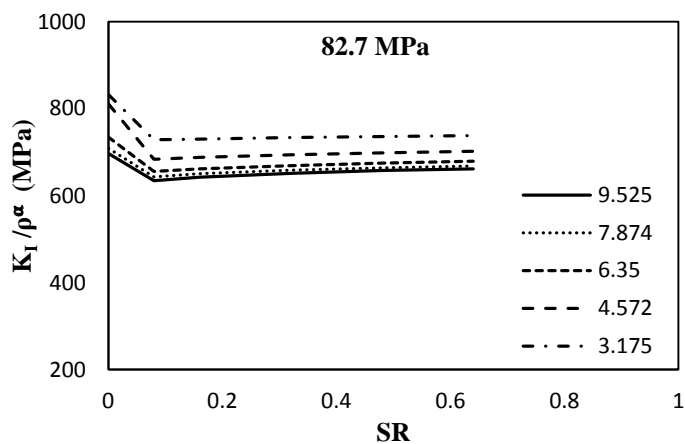




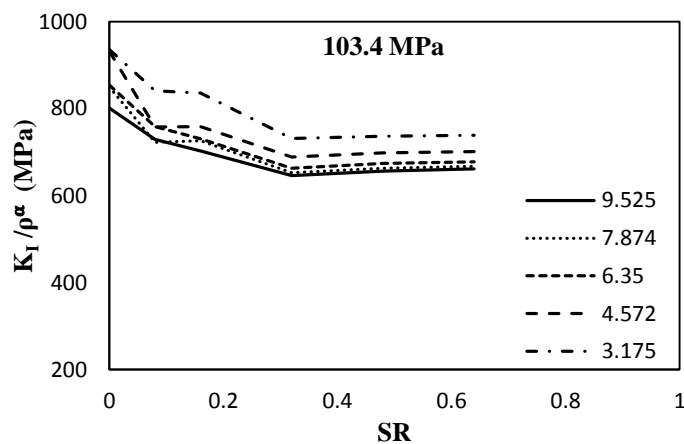
(a)



(b)

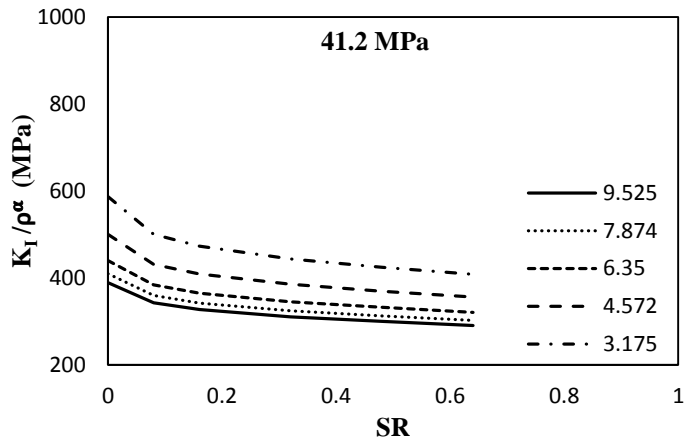


(c)

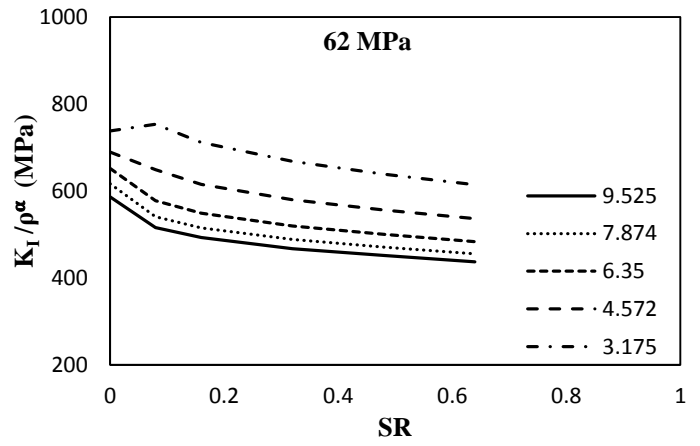


(d)

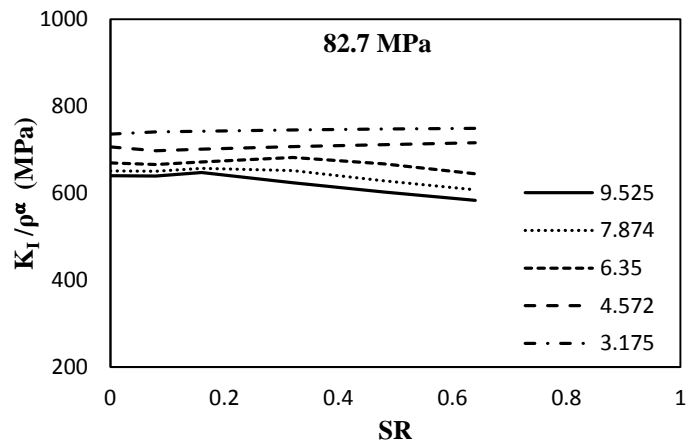
**Figure 3.22:  $K_I / \rho^\alpha$  versus SR on unpatched side for  $45^\circ$  inclined crack, 2 inch Crack Length at different loads (a) 41.2 MPa, (b) 62 MPa, (c) 82.7 MPa and (d) 103.4 MPa**



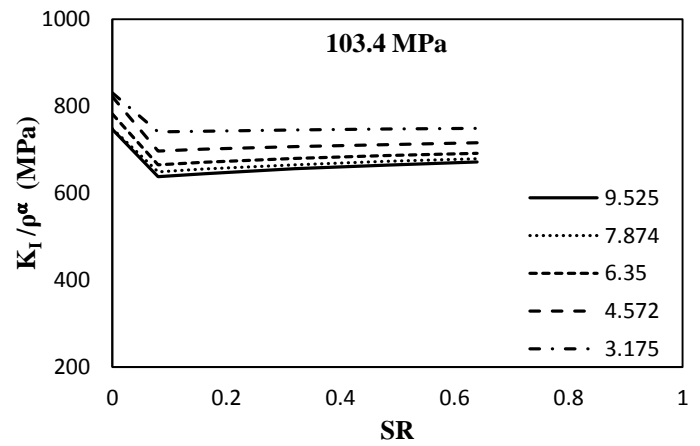
(a)



(b)

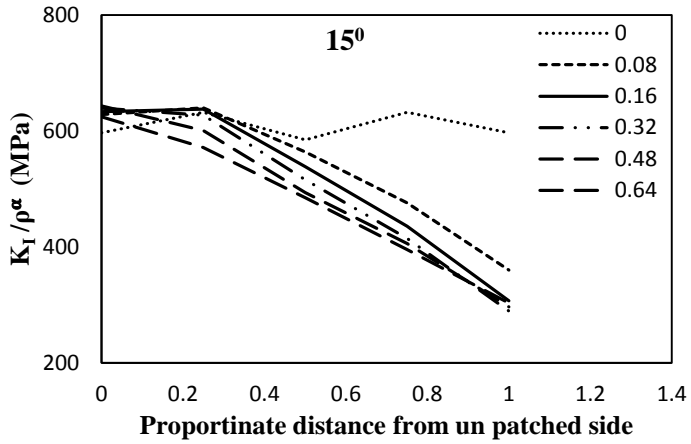


(c)

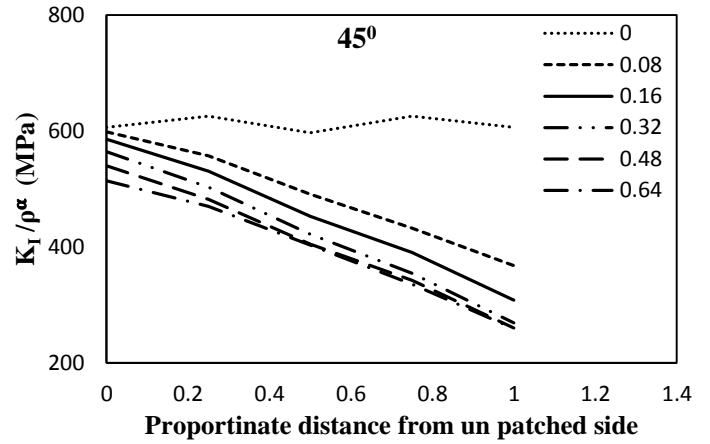


(d)

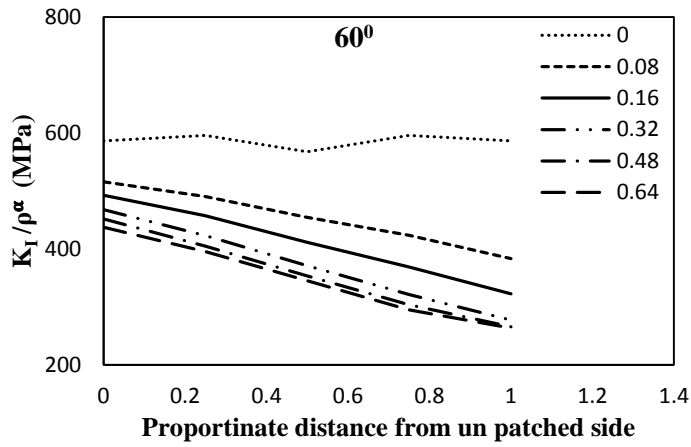
Figure 3.23:  $K_I/\rho^\alpha$  versus SR on unpatched side for  $60^\circ$  inclined crack, 2 inch Crack Length at different loads (a) 41.2 MPa, (b) 62 MPa, (c) 82.7 MPa and (d) 103.4 MPa



(a)

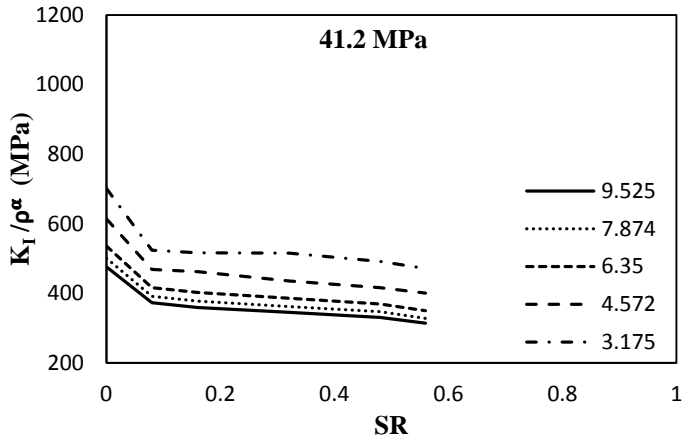


(b)

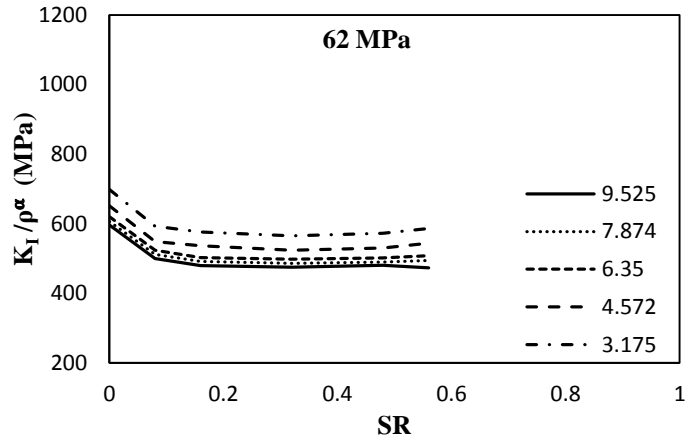


(c)

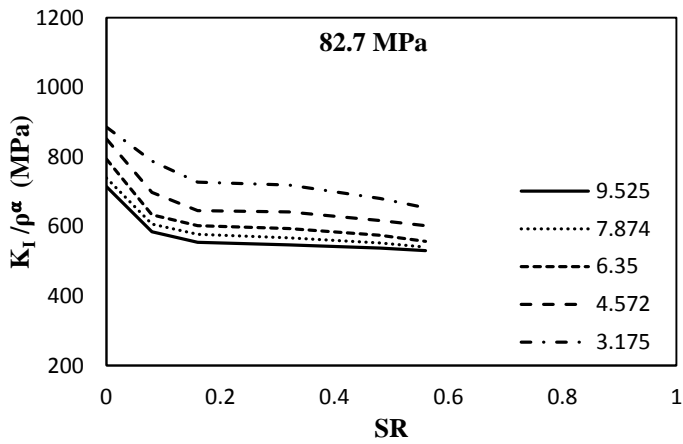
Figure 3.24: Through thickness variation of  $K_I/\rho^\alpha$  of the specimen for different SR having a crack of 50.8 mm (2 inch), 9.525 mm (0.375 inch) crack stop hole radii and for an applied load of 62 MPa load having different crack inclination (a)  $15^\circ$ , (b)  $45^\circ$ , (c)  $60^\circ$



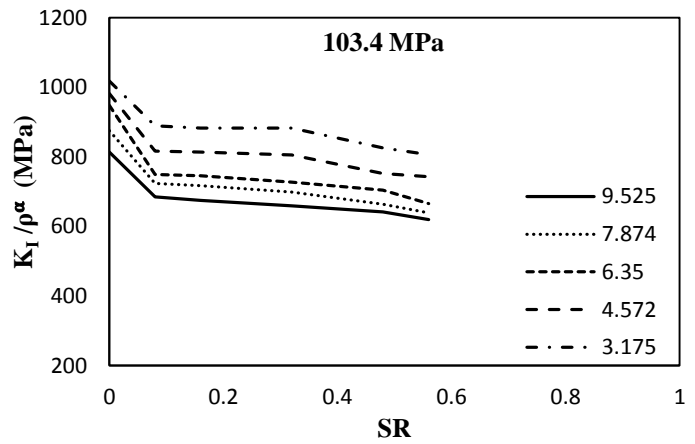
(a)



(b)

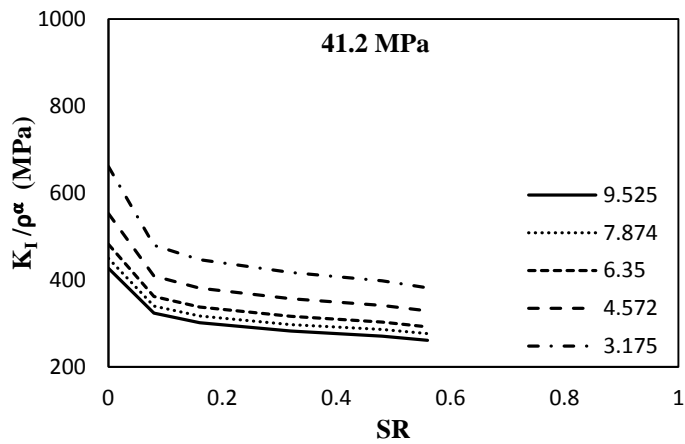


(c)

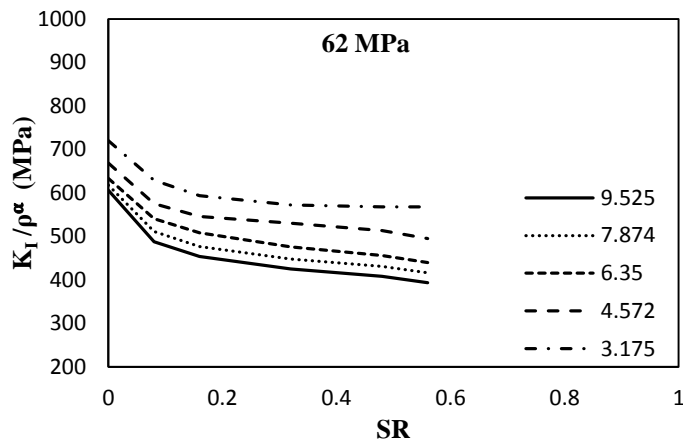


(d)

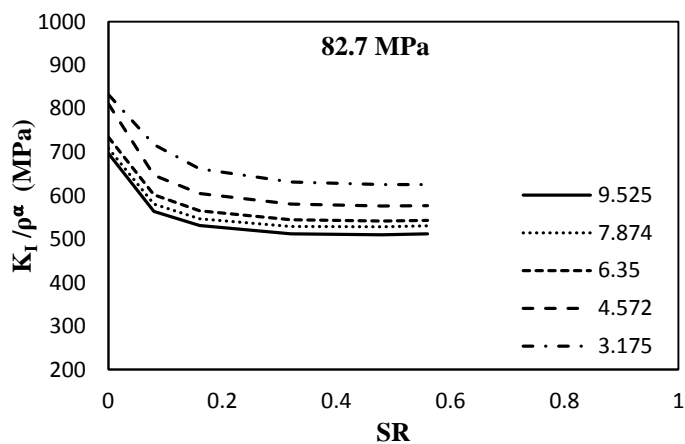
Figure 3.25:  $(K_I / \rho^\alpha)_{rms}$  versus SR for  $15^\circ$  inclined crack having 2 inch crack length at different loads (a) 41.2 MPa, (b) 62 MPa, (c) 82.7 MPa and (d) 103.4 MPa



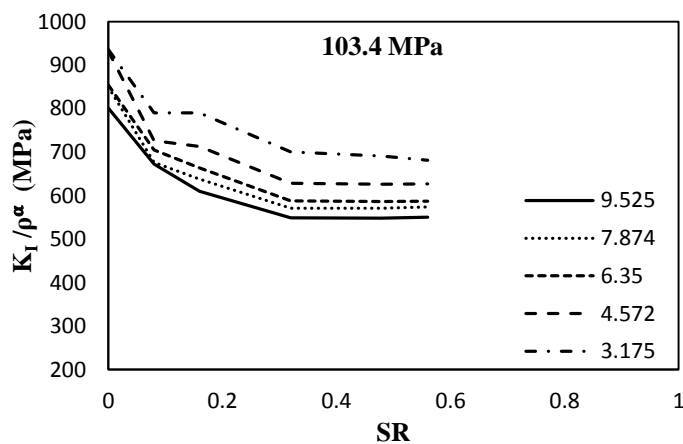
(a)



(b)

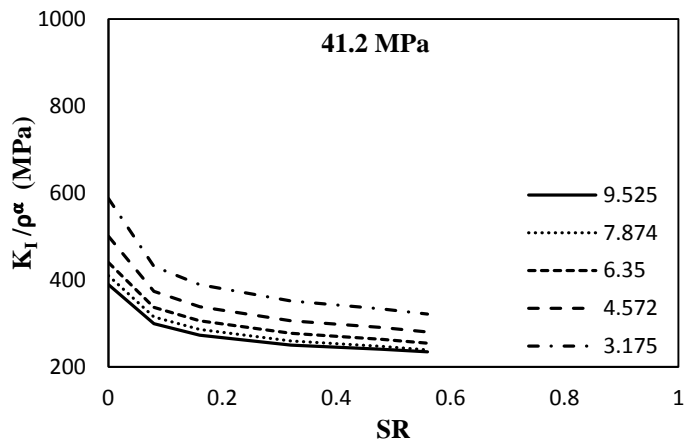


(c)

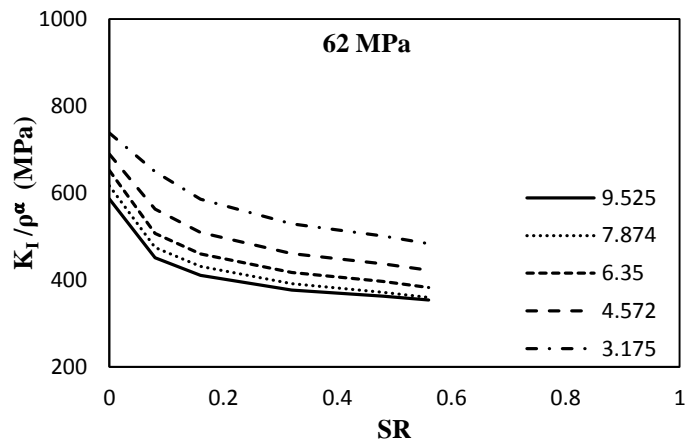


(d)

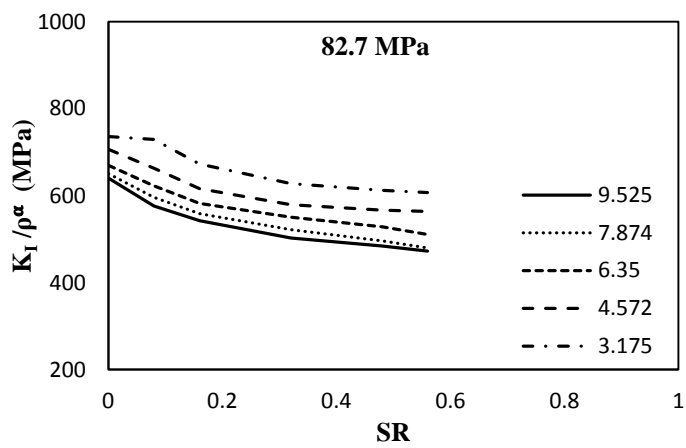
Figure 3.26:  $(K_I / \rho^\alpha)_{rms}$  versus SR for  $45^\circ$  inclined crack having 2 inch crack length at different loads (a) 41.2 MPa, (b) 62 MPa, (c) 82.7 MPa and (d) 103.4 MPa



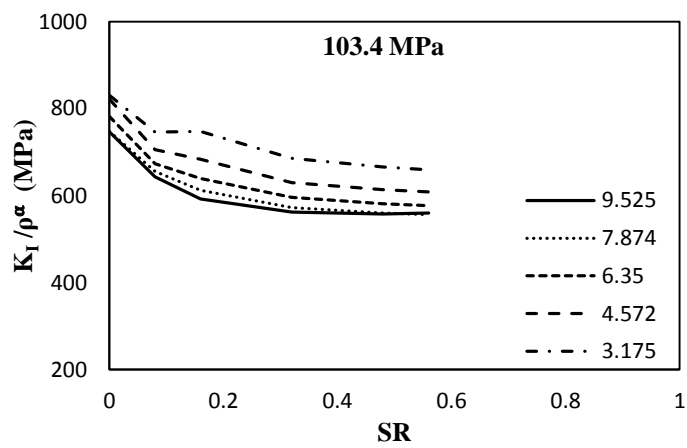
(a)



(b)



(c)



(d)

**Figure 3.27:  $(K_I / \rho^\alpha)_{rms}$  versus SR for  $60^\circ$  inclined crack having 2 inch crack length at different loads (a) 41.2 MPa, (b) 62 MPa, (c) 82.7 MPa and (d) 103.4 MPa**

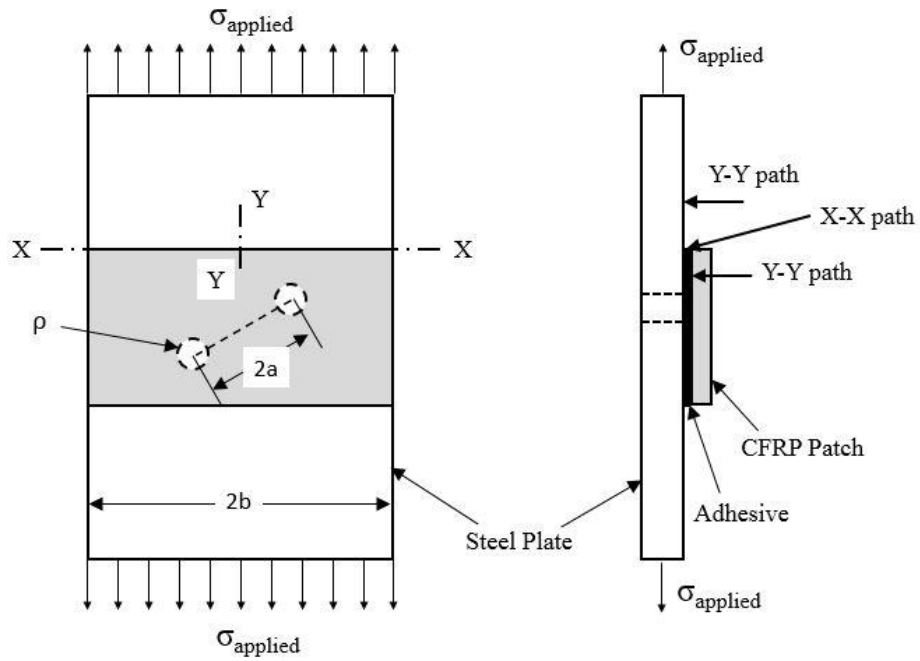


**Figure 3.28: Schematic representation of the lines considered for peel stress distribution**

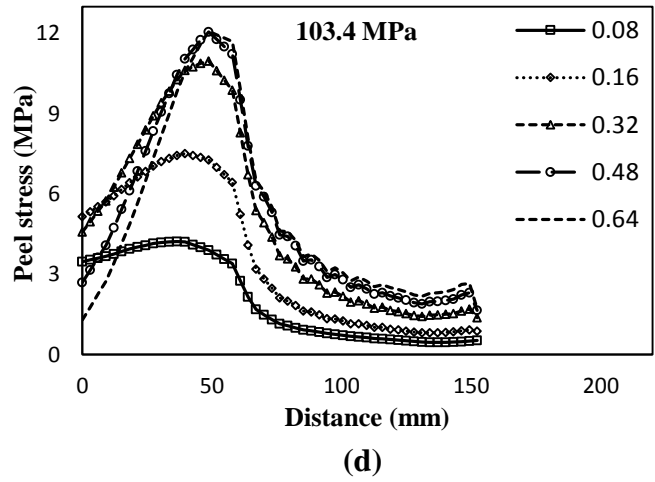
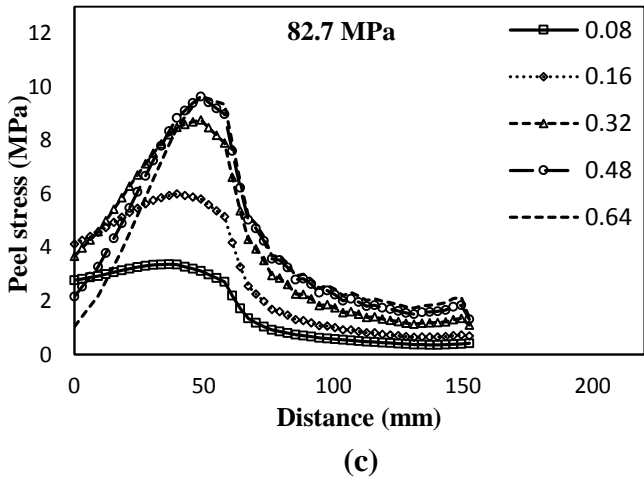
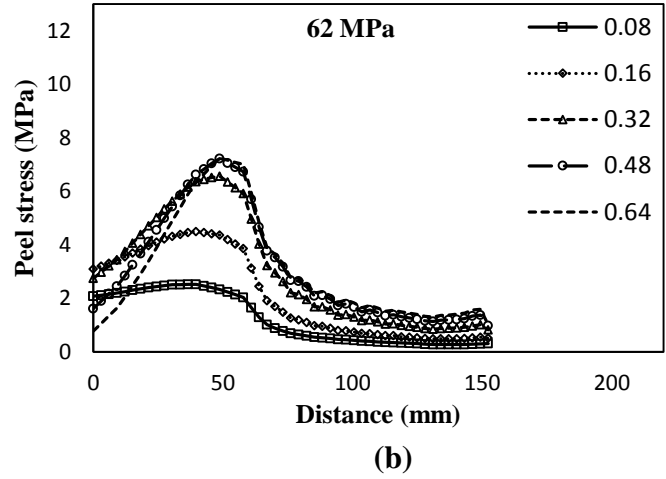
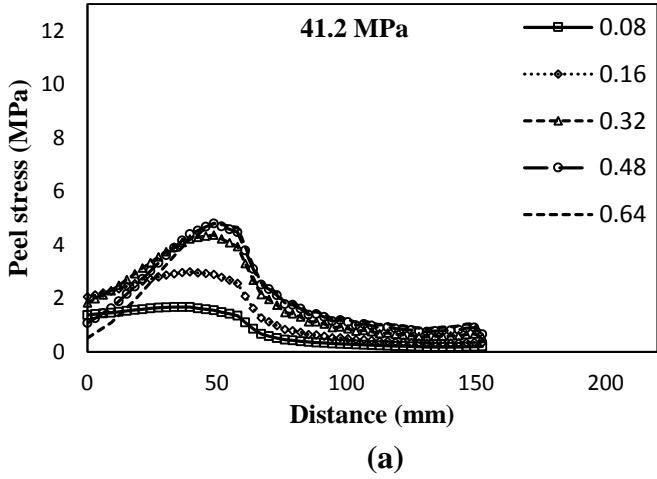
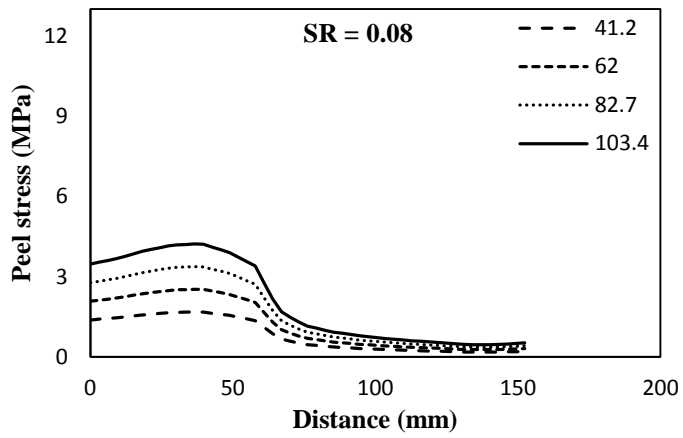
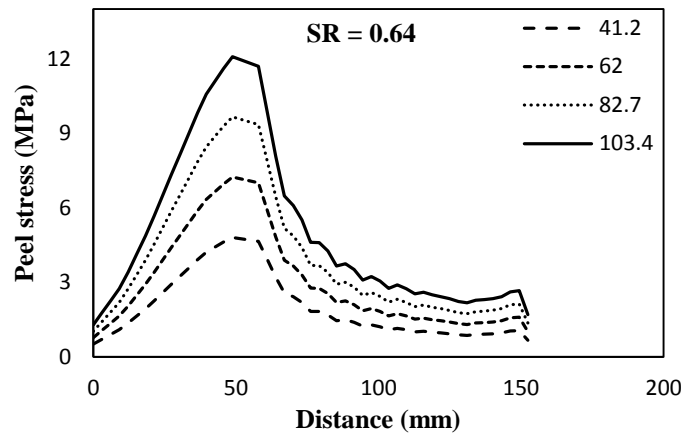


**Figure 3.29: Variation of peel stress in X-X direction for 45° inclined crack, 2 crack length at different loads (a) 41.2 MPa, (b) 62 MPa, (c) 82.7 MPa and (d) 103.4 MPa**



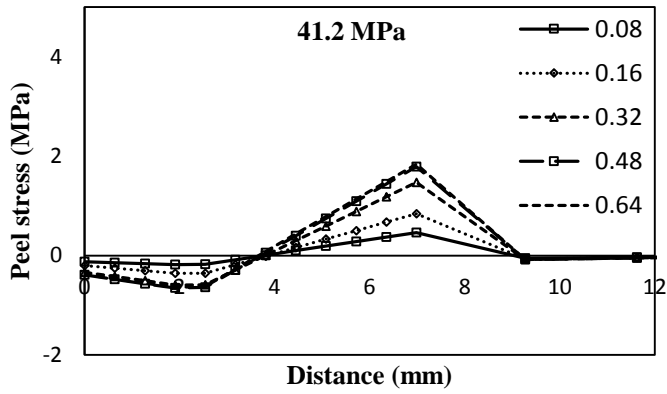


(a)

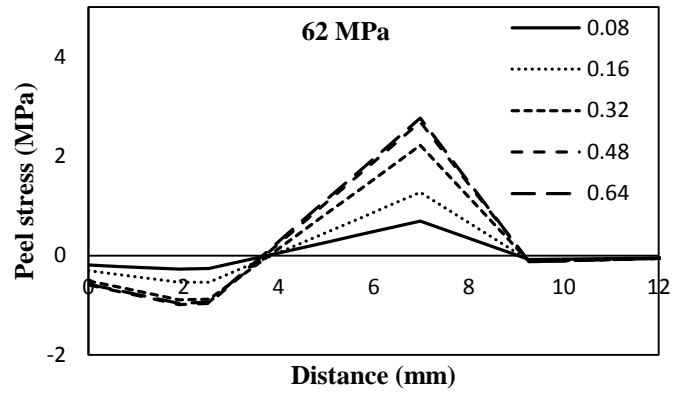


(b)

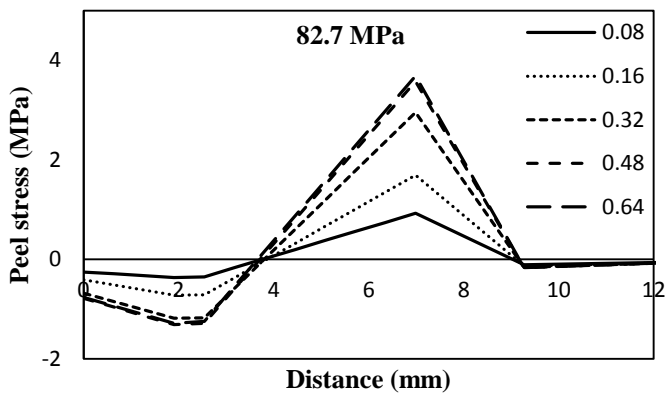
**Figure 3.30: Variation of peel stress in X-X direction for 45° inclined crack, 2 crack length at different SR (a) 0.08 and (b) 0.64**



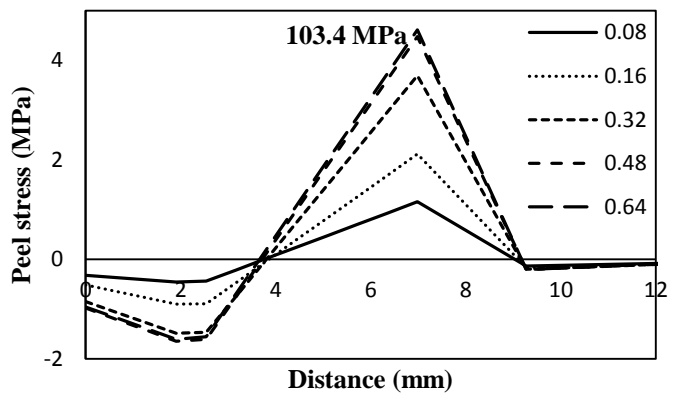
(a)



(b)

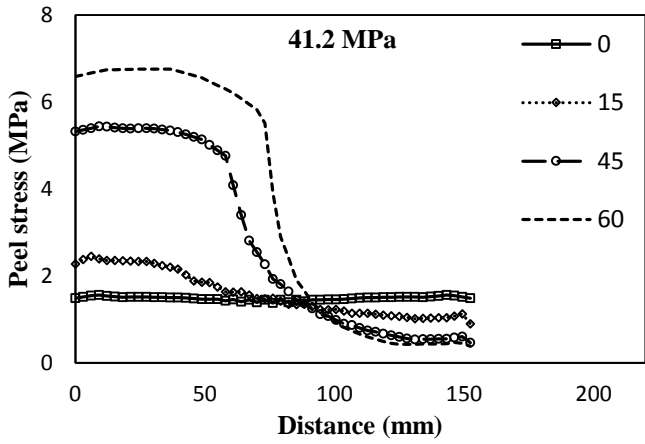


(c)

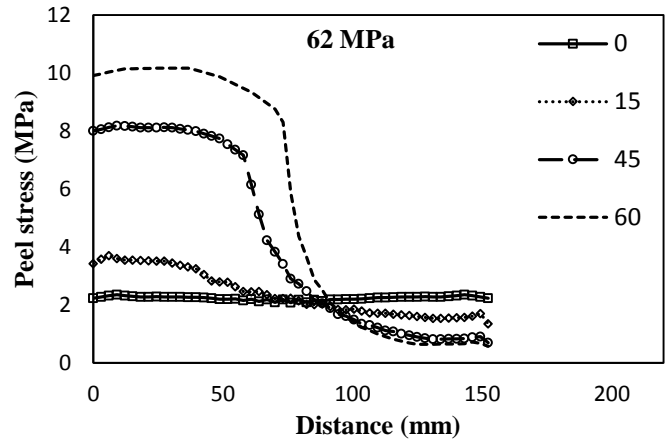


(d)

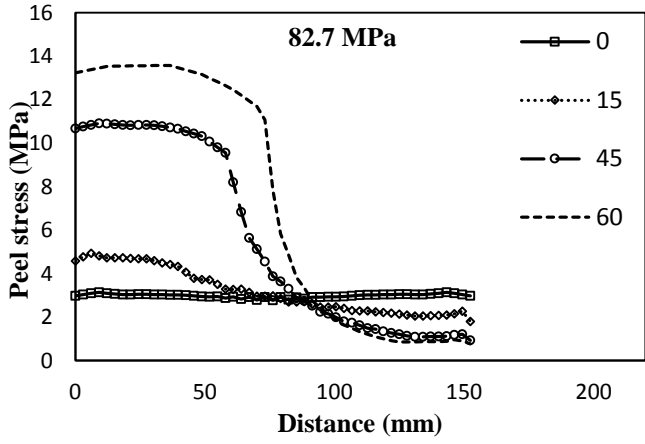
Figure 3.31: Variation of peel stress along Y-Y direction for  $45^\circ$  inclined crack, 2 crack length at different loads (a) 41.2 MPa, (b) 62 MPa, (c) 82.7 MPa and (d) 103.4 MPa



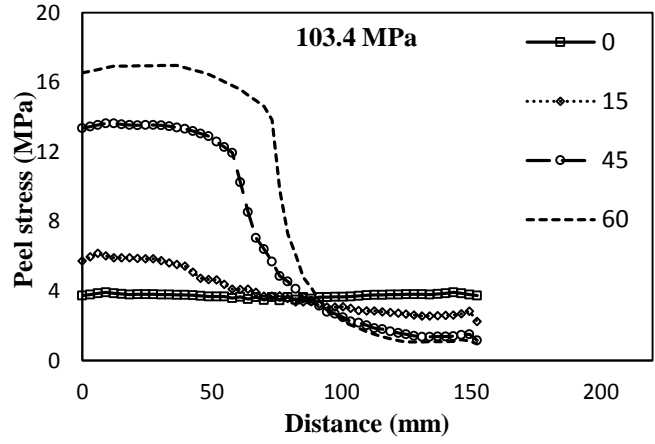
(a)



(b)

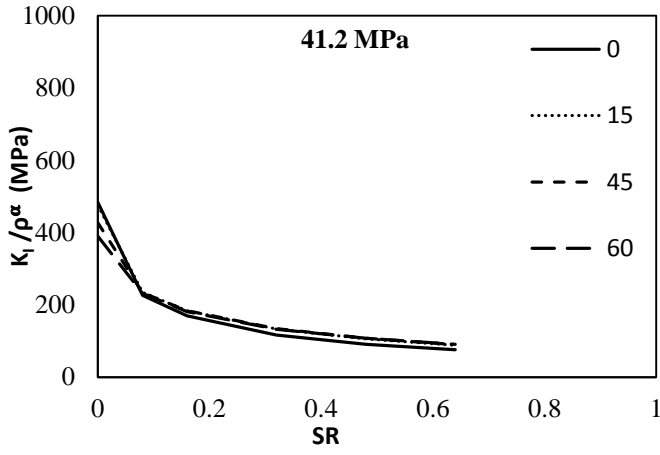


(c)

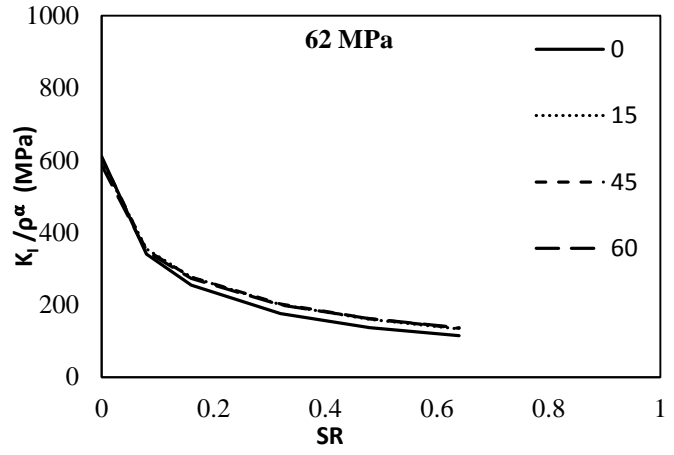


(d)

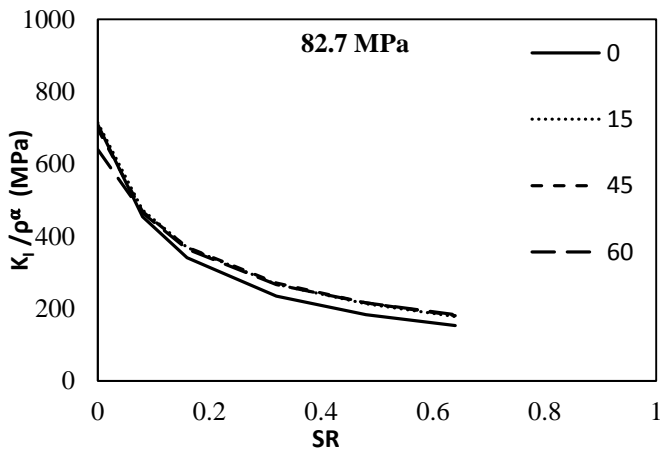
**Figure 3.32: comparison of peel stress for different inclination of crack having 2 inch crack length, 0.375 inch crack stop hole radii of double sided repaired panel for different applied loads (a) 41.2 MPa, (b) 62 MPa, (c) 82.7 MPa and (d) 103.4 MPa**



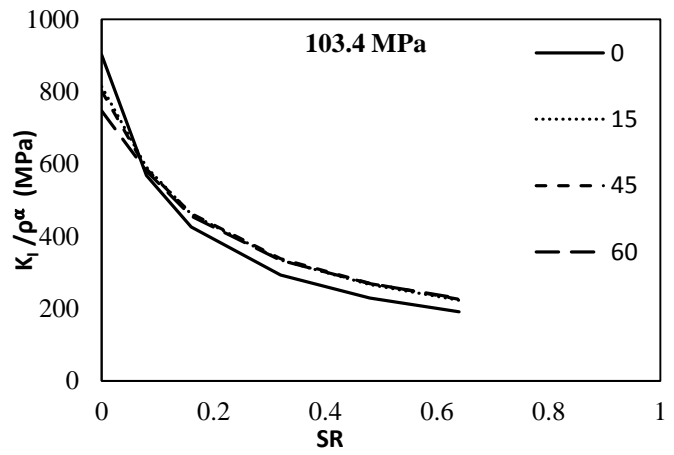
(a)



(b)



(c)



(d)

Figure 3.33: comparison of  $K_I / \rho^\alpha$  for different inclination of crack having 2 inch crack length, 0.375 inch crack stop hole radii of double sided repaired panel for different applied loads (a) 41.2 MPa, (b) 62 MPa, (c) 82.7 MPa and (d) 103.4 MPa

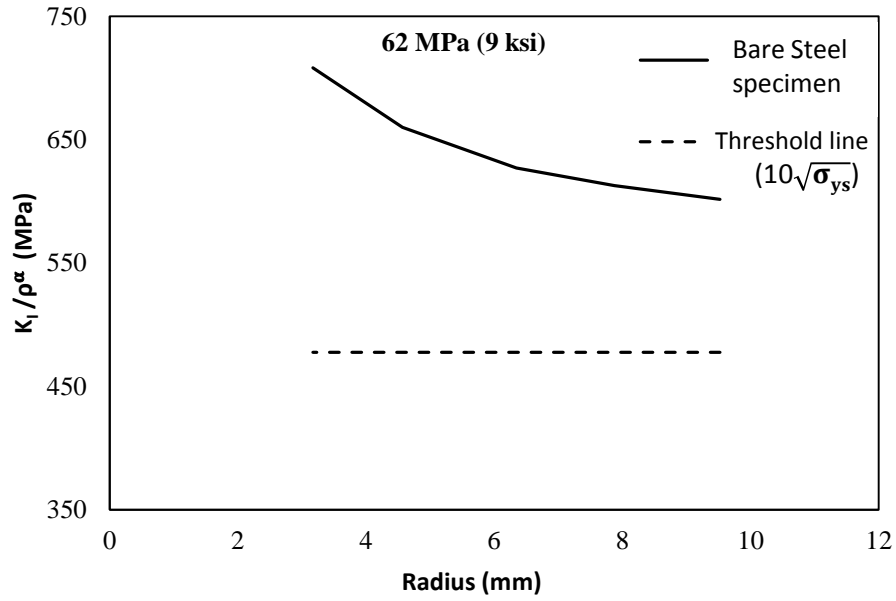


Figure 3.34:  $K_I / \rho^\alpha$  versus crack stop hole radius of bare steel specimen having a crack of 2 inch length and  $30^\circ$  inclination for 62 MPa load

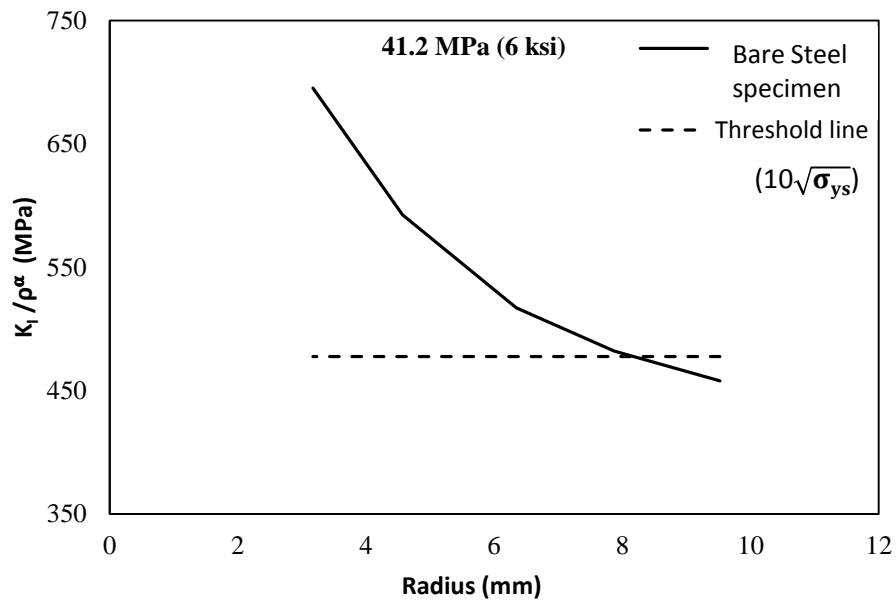


Figure 3.35:  $K_I / \rho^\alpha$  versus crack stop hole radius of bare steel specimen having a crack of 2 inch length and  $30^\circ$  inclination for 41.2 MPa load

<b>Sl. no.</b>	<b>Title</b>
3.1	Specimen details
3.2	CFRP and Adhesive Material Properties
3.3a	RF Values at 41.2 MPa Load for different Crack Inclination, Crack Stop Hole Radius and SR (Symmetrically bonded CFRP Patch)
3.3b	RF Values at 62 MPa Load for different Crack Inclination, Crack Stop Hole Radius and SR (Symmetrically bonded CFRP Patch)
3.3c	RF Values at 82.7 MPa Load for different Crack Inclination, Crack Stop Hole Radius and SR (Symmetrically bonded CFRP Patch)
3.3d	RF Values at 103.4 MPa Load for different Crack Inclination, Crack Stop hole Radius and SR (Symmetrically bonded CFRP Patch)
3.4a	RF Values at 41.2 MPa Load for different Crack Inclination, Crack Stop Hole Radius and SR (Asymmetrically bonded CFRP Patch)
3.4b	RF Values at 62 MPa Load for different Crack Inclination, Crack Stop Hole Radius and SR (Asymmetrically bonded CFRP Patch)
3.4c	RF Values at 82.7 MPa Load for different Crack Inclination, Crack Stop Hole Radius and SR (Asymmetrically bonded CFRP Patch)
3.4d	RF Values at 103.4 MPa Load for different Crack Inclination, Crack Stop Hole Radius and SR (Asymmetrically bonded CFRP Patch)
3.5	Variation of p0 to p17 with Coefficients a, b, c, d and e (Symmetrically bonded CFRP Patch)
3.6	Variation of p0 to p17 with Coefficients a, b, c, d and e (Asymmetrically bonded CFRP Patch)

**Table 3.1: Specimen details**

Width of the specimen ( $B$ ) mm	152.4 (6")
Height of the specimen ( $L$ ) mm	294.2 (11.5")
Length of the crack( $2a$ ) mm	25.4 (1"),38.1(1.5"), 50.8(2"), 63.5(2.5")
Thickness of the steel plate ( $T$ ) mm	3.175
Radius of the hole( $\rho$ ) mm (in.)	9.525 (3/8) 7.874 (5/16) 6.35 (2/8) 4.572 (3/16) 3.175 (1/8)

**Table 3.2: CFRP and Adhesive Material Properties**

<b>Material</b>	<b>Adhesive</b>	<b>CFRP</b>
$E_x$ (Gpa)	4.97	135
$E_y$ (Gpa)	-	9
$E_z$ (Gpa)	-	9
$G_{xy}$ (Gpa)	-	5
$G_{zy}$ (Gpa)	-	8
$G_{zx}$ (Gpa)	-	5
$\nu_{xy}$	0.47	0.3
$\nu_{zy}$	-	0.02
$\nu_{zx}$	-	0.3

**Table 3.3a. RF Values at 41.2 MPa Load for different Crack Inclination, Crack Stop Hole Radius and SR (Symmetrically bonded CFRP Patch)**

Crack Inclination	SR	41.2 MPa				
		Radius (mm)				
		9.525	7.874	6.35	4.572	3.175
0°	0	1.00	1.00	1.00	1.00	1.00
	0.08	0.47	0.48	0.48	0.43	0.45
	0.16	0.35	0.38	0.38	0.34	0.35
	0.32	0.24	0.28	0.28	0.25	0.26
	0.48	0.19	0.22	0.22	0.20	0.21
	0.64	0.16	0.18	0.18	0.17	0.17
15°	0	1.00	1.00	1.00	1.00	1.00
	0.08	0.49	0.49	0.47	0.46	0.45
	0.16	0.39	0.38	0.37	0.36	0.35
	0.32	0.28	0.28	0.27	0.27	0.26
	0.48	0.22	0.22	0.22	0.21	0.21
	0.64	0.19	0.19	0.18	0.18	0.18
45°	0	1.00	1.00	1.00	1.00	1.00
	0.08	0.55	0.54	0.53	0.51	0.48
	0.16	0.43	0.43	0.42	0.40	0.38
	0.32	0.32	0.31	0.31	0.29	0.28
	0.48	0.25	0.25	0.25	0.24	0.22
	0.64	0.21	0.21	0.21	0.20	0.19
60°	0	1.00	1.00	1.00	1.00	1.00
	0.08	0.59	0.60	0.59	0.56	0.54
	0.16	0.47	0.47	0.47	0.45	0.43
	0.32	0.34	0.35	0.35	0.33	0.31
	0.48	0.28	0.28	0.28	0.26	0.25
	0.64	0.23	0.24	0.23	0.22	0.21



**Table 3.3b. RF Values at 62 MPa Load for different Crack Inclination, Crack Stop Hole Radius and SR (Symmetrically bonded CFRP Patch)**

Crack Inclination	SR	62 MPa				
		Radius (mm)				
		9.525	7.874	6.35	4.572	3.175
0°	0	1.00	1.00	1.00	1.00	1.00
	0.08	0.56	0.59	0.61	0.60	0.67
	0.16	0.42	0.47	0.48	0.46	0.52
	0.32	0.29	0.34	0.35	0.34	0.38
	0.48	0.22	0.27	0.28	0.27	0.31
	0.64	0.19	0.23	0.23	0.23	0.26
15°	0	1.00	1.00	1.00	1.00	1.00
	0.08	0.59	0.61	0.62	0.64	0.68
	0.16	0.46	0.48	0.48	0.51	0.53
	0.32	0.34	0.35	0.35	0.38	0.39
	0.48	0.27	0.28	0.28	0.30	0.32
	0.64	0.22	0.23	0.24	0.25	0.27
45°	0	1.00	1.00	1.00	1.00	1.00
	0.08	0.58	0.59	0.61	0.63	0.66
	0.16	0.46	0.47	0.48	0.50	0.52
	0.32	0.33	0.34	0.35	0.37	0.38
	0.48	0.27	0.28	0.28	0.29	0.31
	0.64	0.22	0.23	0.24	0.25	0.26
60°	0	1.00	1.00	1.00	1.00	1.00
	0.08	0.59	0.60	0.60	0.62	0.65
	0.16	0.47	0.47	0.48	0.49	0.51
	0.32	0.34	0.35	0.35	0.36	0.38
	0.48	0.28	0.28	0.28	0.29	0.30
	0.64	0.23	0.24	0.24	0.24	0.26

**Table 3.3c. RF Values at 82.7 MPa Load for different Crack Inclination, Crack Stop Hole Radius and SR (Symmetrically bonded CFRP Patch)**

Crack Inclination	SR	82.7 MPa				
		Radius (mm)				
		9.525	7.874	6.35	4.572	3.175
0°	0	1.00	1.00	1.00	1.00	1.00
	0.08	0.64	0.66	0.67	0.61	0.72
	0.16	0.48	0.52	0.52	0.48	0.57
	0.32	0.33	0.38	0.38	0.35	0.41
	0.48	0.26	0.30	0.31	0.28	0.33
	0.64	0.22	0.25	0.26	0.24	0.28
15°	0	1.00	1.00	1.00	1.00	1.00
	0.08	0.66	0.67	0.65	0.66	0.72
	0.16	0.52	0.52	0.51	0.52	0.56
	0.32	0.37	0.38	0.37	0.38	0.41
	0.48	0.30	0.30	0.30	0.31	0.33
	0.64	0.25	0.25	0.25	0.26	0.28
45°	0	1.00	1.00	1.00	1.00	1.00
	0.08	0.67	0.69	0.70	0.69	0.76
	0.16	0.53	0.54	0.55	0.55	0.60
	0.32	0.39	0.40	0.41	0.40	0.44
	0.48	0.31	0.32	0.33	0.32	0.36
	0.64	0.26	0.27	0.27	0.27	0.30
60°	0	1.00	1.00	1.00	1.00	1.00
	0.08	0.73	0.75	0.78	0.80	0.87
	0.16	0.57	0.60	0.62	0.63	0.68
	0.32	0.42	0.44	0.46	0.47	0.50
	0.48	0.34	0.35	0.37	0.38	0.41
	0.64	0.29	0.30	0.31	0.32	0.34

**Table 3.3d. RF Values at 103.4 MPa Load for different Crack Inclination, Crack Stop Hole Radius and SR (Symmetrically bonded CFRP Patch)**

Crack Inclination	SR	103.4 MPa				
		Radius (mm)				
		9.525	7.874	6.35	4.572	3.175
0°	0	1.00	1.00	1.00	1.00	1.00
	0.08	0.63	0.71	0.75	0.69	0.68
	0.16	0.47	0.56	0.59	0.54	0.57
	0.32	0.32	0.41	0.43	0.39	0.42
	0.48	0.25	0.32	0.34	0.32	0.34
	0.64	0.21	0.27	0.29	0.27	0.28
15°	0	1.00	1.00	1.00	1.00	1.00
	0.08	0.73	0.71	0.68	0.71	0.72
	0.16	0.57	0.55	0.53	0.57	0.61
	0.32	0.41	0.41	0.39	0.42	0.45
	0.48	0.33	0.32	0.31	0.34	0.36
	0.64	0.27	0.27	0.26	0.28	0.30
45°	0	1.00	1.00	1.00	1.00	1.00
	0.08	0.73	0.72	0.75	0.75	0.80
	0.16	0.58	0.57	0.59	0.59	0.67
	0.32	0.42	0.42	0.44	0.44	0.49
	0.48	0.34	0.34	0.35	0.35	0.39
	0.64	0.28	0.28	0.29	0.30	0.33
60°	0	1.00	1.00	1.00	1.00	1.00
	0.08	0.78	0.82	0.84	0.86	0.91
	0.16	0.61	0.65	0.66	0.68	0.76
	0.32	0.45	0.48	0.49	0.50	0.56
	0.48	0.36	0.38	0.39	0.40	0.45
	0.64	0.31	0.32	0.33	0.34	0.38

**Table 3.4a. RF Values at 41.2 MPa Load for different Crack Inclination, Crack Stop Hole Radius and SR (Asymmetrically bonded CFRP Patch)**

Crack Inclination	SR	41.2 MPa				
		Radius (mm)				
		9.525	7.874	6.35	4.572	3.175
0°	0	1.00	1.00	1.00	1.00	1.00
	0.08	0.47	0.49	0.50	0.43	0.45
	0.16	0.39	0.43	0.43	0.37	0.40
	0.32	0.38	0.41	0.42	0.38	0.38
	0.48	0.41	0.42	0.42	0.41	0.39
	0.64	0.44	0.42	0.44	0.42	0.40
15°	0	1.00	1.00	1.00	1.00	1.00
	0.08	0.50	0.50	0.49	0.46	0.45
	0.16	0.43	0.43	0.42	0.40	0.40
	0.32	0.40	0.41	0.40	0.39	0.39
	0.48	0.41	0.41	0.41	0.40	0.40
	0.64	0.42	0.42	0.42	0.42	0.42
45°	0	1	1	1	1	1
	0.08	0.57	0.57	0.57	0.55	0.53
	0.16	0.48	0.48	0.48	0.47	0.45
	0.32	0.42	0.43	0.42	0.42	0.40
	0.48	0.40	0.42	0.41	0.40	0.38
	0.64	0.40	0.42	0.41	0.40	0.38
60°	0	1.00	1.00	1.00	1.00	1.00
	0.08	0.65	0.66	0.65	0.63	0.61
	0.16	0.55	0.55	0.55	0.52	0.51
	0.32	0.47	0.46	0.46	0.44	0.43
	0.48	0.45	0.43	0.43	0.41	0.40
	0.64	0.45	0.41	0.41	0.39	0.38

**Table 3.4b. RF Values at 62 MPa Load for different Crack Inclination, Crack Stop Hole Radius and SR (Asymmetrically bonded CFRP Patch)**

Crack Inclination	SR	62 MPa				
		Radius (mm)				
		9.525	7.874	6.35	4.572	3.175
0°	0	1.00	1.00	1.00	1.00	1.00
	0.08	0.56	0.61	0.63	0.59	0.65
	0.16	0.46	0.52	0.55	0.52	0.58
	0.32	0.45	0.50	0.53	0.53	0.56
	0.48	0.50	0.51	0.54	0.56	0.58
	0.64	0.53	0.52	0.54	0.58	0.59
15°	0	1.00	1.00	1.00	1.00	1.00
	0.08	0.60	0.62	0.64	0.65	0.68
	0.16	0.51	0.54	0.55	0.57	0.60
	0.32	0.49	0.51	0.52	0.55	0.58
	0.48	0.50	0.51	0.53	0.56	0.60
	0.64	0.51	0.52	0.54	0.60	0.64
45°	0	1.00	1.00	1.00	1.00	1.00
	0.08	0.61	0.63	0.65	0.69	0.73
	0.16	0.51	0.53	0.55	0.58	0.62
	0.32	0.44	0.47	0.49	0.52	0.55
	0.48	0.43	0.46	0.47	0.50	0.53
	0.64	0.43	0.46	0.47	0.50	0.53
60°	0	1.00	1.00	1.00	1.00	1.00
	0.08	0.65	0.66	0.66	0.68	0.73
	0.16	0.55	0.55	0.56	0.57	0.61
	0.32	0.47	0.46	0.47	0.48	0.51
	0.48	0.45	0.43	0.43	0.44	0.47
	0.64	0.45	0.41	0.42	0.43	0.46

**Table 3.4c. RF Values at 82.7 MPa Load for different Crack Inclination, Crack Stop Hole Radius and SR (Asymmetrically bonded CFRP Patch)**

Crack Inclination	SR	82.7 MPa				
		Radius (mm)				
		9.525	7.874	6.35	4.572	3.175
0°	0	1.00	1.00	1.00	1.00	1.00
	0.08	0.65	0.67	0.68	0.64	0.73
	0.16	0.56	0.58	0.60	0.54	0.64
	0.32	0.56	0.56	0.58	0.57	0.58
	0.48	0.60	0.57	0.59	0.60	0.61
	0.64	0.62	0.58	0.60	0.62	0.62
15°	0	1.00	1.00	1.00	1.00	1.00
	0.08	0.67	0.68	0.66	0.69	0.75
	0.16	0.57	0.59	0.57	0.57	0.65
	0.32	0.54	0.55	0.55	0.55	0.60
	0.48	0.56	0.56	0.56	0.57	0.62
	0.64	0.57	0.57	0.57	0.61	0.67
45°	0	1.00	1.00	1.00	1.00	1.00
	0.08	0.70	0.73	0.74	0.75	0.85
	0.16	0.59	0.62	0.63	0.64	0.71
	0.32	0.51	0.55	0.56	0.57	0.63
	0.48	0.50	0.54	0.54	0.55	0.61
	0.64	0.50	0.54	0.54	0.54	0.61
60°	0	1.00	1.00	1.00	1.00	1.00
	0.08	0.80	0.83	0.86	0.89	0.98
	0.16	0.67	0.70	0.73	0.75	0.81
	0.32	0.58	0.58	0.61	0.62	0.68
	0.48	0.55	0.54	0.56	0.58	0.63
	0.64	0.55	0.52	0.54	0.56	0.62

**Table 3.4d. RF Values at 103.4 MPa Load for different Crack Inclination, Crack Stop Hole Radius and SR (Asymmetrically bonded CFRP Patch)**

Crack Inclination	SR	103.4 MPa				
		Radius (mm)				
		9.525	7.874	6.35	4.572	3.175
0°	0	1.00	1.00	1.00	1.00	1.00
	0.08	0.63	0.68	0.71	0.64	0.63
	0.16	0.62	0.68	0.71	0.66	0.63
	0.32	0.61	0.65	0.70	0.68	0.66
	0.48	0.63	0.65	0.70	0.70	0.65
	0.64	0.68	0.65	0.70	0.70	0.66
15°	0	1.00	1.00	1.00	1.00	1.00
	0.08	0.71	0.67	0.66	0.65	0.67
	0.16	0.68	0.67	0.65	0.65	0.67
	0.32	0.64	0.63	0.62	0.66	0.71
	0.48	0.63	0.63	0.62	0.67	0.69
	0.64	0.63	0.60	0.62	0.70	0.73
45°	0	1.00	1.00	1.00	1.00	1.00
	0.08	0.77	0.74	0.76	0.74	0.79
	0.16	0.64	0.64	0.70	0.71	0.79
	0.32	0.56	0.57	0.60	0.61	0.71
	0.48	0.54	0.56	0.58	0.59	0.69
	0.64	0.54	0.56	0.58	0.59	0.67
60°	0	1.00	1.00	1.00	1.00	1.00
	0.08	0.87	0.89	0.87	0.87	0.90
	0.16	0.72	0.76	0.78	0.81	0.91
	0.32	0.62	0.63	0.65	0.67	0.75
	0.48	0.59	0.59	0.60	0.62	0.70
	0.64	0.59	0.57	0.58	0.60	0.68

**Table 3.5. Variation of p0 to p17 with Coefficients a, b, c, d and e  
(Symmetrically bonded CFRP Patch)**

<b>Coefficients</b>	<b>Coefficients</b>				
	<b>a</b>	<b>b</b>	<b>c</b>	<b>d</b>	<b>e</b>
<b>p0</b>	-1284.480	2149.181	-1300.527	345.8833	-38.4163
<b>p1</b>	4.9025	-8.1691	4.8942	-1.2647	0.1263
<b>p2</b>	33.7372	-55.8325	33.1349	-8.4659	0.8376
<b>p3</b>	45.2432	-79.1179	51.1830	-15.0689	1.9018
<b>p4</b>	-0.1855	0.3097	-0.1863	0.0487	-0.0050
<b>p5</b>	0.3271	-0.5544	0.3420	-0.0933	0.0102
<b>p6</b>	-2.2648	3.7904	-2.2907	0.6038	-0.0632
<b>p7</b>	-0.0069	0.0114	-0.0068	0.0018	-0.0002
<b>p8</b>	0.0038	-0.0063	0.0040	-0.0013	0.0002
<b>p9</b>	3.4367	-5.2493	2.6790	-0.4793	0.0053
<b>p10</b>	-0.2254	0.3700	-0.2165	0.0540	-0.0051
<b>p11</b>	-0.0020	0.0034	-0.0022	0.0006	-0.0001
<b>p12</b>	0.0006	-0.0011	0.0007	-0.0002	0.0000
<b>p13</b>	0.0119	-0.0195	0.0116	-0.0031	0.0004
<b>p14</b>	-0.0490	0.0737	-0.0365	0.0061	0.0000
<b>p15</b>	0.0014	-0.0024	0.0014	-0.0004	0.0000
<b>p16</b>	0.0209	-0.0341	0.0198	-0.0048	0.0004



**Table 3.6. Variation of p0 to p17 with Coefficients a, b, c, d and e  
(Asymmetrically bonded CFRP Patch)**

Coefficients	Coefficients				
	a	b	c	d	e
<b>p0</b>	-2411.076	3967.636	-2330.847	584.6299	-57.0876
<b>p1</b>	16.7257	-26.9940	15.3726	-3.6388	0.3172
<b>p2</b>	63.7723	-104.5456	60.8558	-14.8863	1.3404
<b>p3</b>	204.6701	-332.5459	192.3257	-47.4175	4.5377
<b>p4</b>	-0.3469	0.5708	-0.3327	0.0809	-0.0071
<b>p5</b>	-1.3029	2.0268	-1.0878	0.2338	-0.0182
<b>p6</b>	-5.6529	9.2182	-5.3436	1.3082	-0.1198
<b>p7</b>	0.0142	-0.0215	0.0109	-0.0020	0.0001
<b>p8</b>	-0.0319	0.0459	-0.0223	0.0041	-0.0004
<b>p9</b>	-2.3953	3.7637	-2.1599	0.5881	-0.0813
<b>p10</b>	-0.4130	0.6784	-0.3953	0.0964	-0.0085
<b>p11</b>	0.0040	-0.0056	0.0026	-0.0004	0.0000
<b>p12</b>	0.0007	-0.0012	0.0007	-0.0002	0.0000
<b>p13</b>	0.0092	-0.0185	0.0137	-0.0049	0.0009
<b>p14</b>	0.0481	-0.0745	0.0412	-0.0101	0.0011
<b>p15</b>	0.0017	-0.0029	0.0017	-0.0004	0.0000
<b>p16</b>	0.0332	-0.0547	0.0321	-0.0079	0.0007

# CHAPTER 4

## Further Study

In this study plate with centre crack repaired with crack stop hole, CFRP under tensile loading condition is considered. This study further can be extended to the following conditions.

1. Mixed loading conditions such as tensile plus torsional loading.
2. Experimental study is needed to validate the results obtained from finite element study.
3. In this study effect of weld attachments on repair technique is not considered. Further study is needed to find the effect of weld attachments on repair methods.
4. Effect of crack stop hole and CFRP on cracks emanating from notches under cyclic loading needs to be studied.
5. Effect of prestressed CFRP patches.
6. Studying real life structural elements.